TEXAS TRANSPORTATION INSTITUTE

INVESTIGATION OF THE MICROSTRUCTURAL MECHANISMS OF RELAXATION AND FRACTURE HEALING IN ASPHALT

PREPARED FOR THE AIR FORCE OFFICE OF SCIENTIFIC RESEARCH

FINAL REPORT
GRANT NO. AFOSR-89-0520

APRIL 12, 1993

TEXAS TRANSPORTATION INSTITUTE
THE TEXAS A&M UNIVERSITY SYSTEM
COLLEGE STATION, TEXAS

UNCLASSIFIED

SECURITY CLASSIFICATION OF THIS PAGE

REPORT DOCUMENTATION PAGE

1a. REPORT SECURITY CLASSIFICATION: N/A	1b. RESTRICTIVE MARKINGS: N/A
2a. SECURITY CLASSIFICATION AUTHORITY: N/A	3. DISTRIBUTION/AVAILABILITY OF REPORT: Approved for public release, distribution unlimited
2b. DECLASSIFICATION/DOWNGRADING SCHEDULE: N/A	
4. PERFORMING ORGANIZATION REPORT NUMBER(S):	5. MONITORING ORGANIZATION REPORT NUMBER(S):
6a. NAME OF PERFORMING ORGANIZATION: Texas Transportation Institute, Texas A&M University; 6b. OFFICE SYMBOL (If applicable):	7a. NAME OF MONITORING ORGANIZATION: AFOSR/NA, Bolling AFB DC 20332-6448
6c. ADDRESS (City, State and ZIP Code): Texas A&M University, Suite 508, TTI/CE Building, College Station, Texas 77843-3135	7b. ADDRESS (City, State and ZIP Code): AFOSR/NA, Bolling AFB DC 20332-6448
8a. NAME OF FUNDING/SPONSORING ORGANIZATION: AFOSR; 8b. OFFICE SYMBOL (If applicable): NA	9. PROCUREMENT INSTRUMENT IDENTIFICATION NUMBER: AFOSR-89-0520
8c. ADDRESS (City, State and ZIP Code): Bolling AFB, Washington, D.C.	10. SOURCE OF FUNDING NOS. — PROGRAM ELEMENT NO.: 61102F; PROJECT NO.: 2302; TASK NO.: CS; WORK UNIT NO.:
11. TITLE (Include Security Classification): Investigation of the Microstructural Mechanism of Relaxation and Fracture Healing in Asphalt	
12. PERSONAL AUTHOR(S): Dallas N. Little, S. Prapnnachari, Allen Letton and Y. R. Kim	
13a. TYPE OF REPORT: FINAL; 13b. TIME COVERED: FROM 8-15-90 TO 4-12-93	14. DATE OF REPORT (Yr., Mo., Day): 4-12-93; 15. PAGE COUNT: 173
16. SUPPLEMENTARY NOTATION: This is the third year of a three year grant.	
17. COSATI CODES — FIELD / GROUP / SUB. GR.	18. SUBJECT TERMS (Continue on reverse if necessary and identify by block number): Fracture healing, FTIR, asphalt, micromechanisms of fracture, asphalt modification, viscoelastic correspondence principle.

19. ABSTRACT (Continue on reverse if necessary and identify by block number)

Two major research issues are addressed. The first issue is the microstructural components of asphalt cement which influence and/or control relaxation and creep under mechanical loading. The second and allied issue is the identificaiton and evaluation of asphalt cement and asphalt concrete microstructural components that influence and/or control the microdamage (microfracture) healing of asphalt concrete mixtures.

A unique approach, for the study of asphalt cement, is used to evaluate the mechanism of relaxation and creep and the microstructural components controlling this mechanism within asphalt cement. This approach involves the study of infrared spectral peak shifts and peak geometry changes due to the application of mechanically-induced stress. This approach is demonstrated to be successful and determines that the primary microstructural

(continued)

20. DISTRIBUTION/AVAILABILITY OF ABSTRACT: UNCLASSIFIED/UNLIMITED ☐ SAME AS RPT. ☐ DTIC USERS ☐	21. ABSTRACT SECURITY CLASSIFICATION: UNCLASSIFIED
22a. NAME OF RESPONSIBLE INDIVIDUAL: MARTIN LEWIS, Maj, USAF	22b. TELEPHONE NUMBER (Include Area Code): 202-767-6963 — 22c. OFFICE SYMBOL: AFOSR/NA

DD FORM 1473, 83 APR EDITION OF 1 JAN 73 IS OBSOLETE

UNCLASSIFIED

SECURITY CLASSIFICATION OF THIS PAGE

19. ABSTRACT (continued).

component of the asphalt cement related to creep and relaxation deformation is aliphatic appendages to the various molecular species. The nature of these appendages, i.e., shape and length, are strongly related to equilibrium modulus, zero shear viscosity and microdamage healing.

The shape and length of the aliphatic substituents within the asphalt are also shown to be keenly related to the microdamage or microfracture healing index. In fact as the average lengths of the chains increase, the healing index increases. This is true for every asphalt binder tested and evaluated in this manner.

The strong correlation between methylene-methyl ratio and aliphatic chain length and relaxation and creep properties and microdamage healing is discussed in light of the latest asphalt microstructural models, such as the dispersed polar fluids model (DPF) and the older colloidal and micellar models.

TABLE OF CONTENTS

LIST OF TABLES

LIST OF FIGURES

LIST OF FIGURES (Continued)

LIST OF FIGURES (Continued)

CHAPTER 1

INTRODUCTION

RESEARCH OBJECTIVES

This research addresses two major issues. The first is to establish the mechanism controlling the process of relaxation and creep deformation in asphalt cement. The second issue is to establish the mechanism by which chemical healing of microcracks occurs within the process zone preceding the macrocrack in asphalt concrete mixtures.

The microstructural components of asphalt cement which control creep and relaxation responses are logically tied to the mechanisms leading to frequency shifting and band distortions which can be detected using FTIR analysis of asphalts under conditions of stress and relaxation. These stress-induced frequency shifts can be interpreted in terms of changes in potential energy, functions due to deformed primary carbon-carbon bonds, valence angles, torsion angles and non-bonded interactions. These molecular deformation processes (inter and intra-molecular) occurring during the creep and relaxation mode were identified in this research using dynamic infrared analysis.

A technique has been developed at Texas A&M University by which fracture healing in asphalt concrete samples can be measured. This process allows one to separately analyze the time-dependent, viscoelastic effects of the asphalt binder on microdamage healing and those effects not related to mechanical time dependency but which are related to chemical and diffusion effects. This technique was used in this research to quantify microdamage (microfracture) healing and to help identify the component or components of the asphalt cement microstructure that control chemical healing.

REPORT ORGANIZATION

Chapter 2 addresses the first research issue: evaluation of the microstructural components of asphalt cement which contribute to and control relaxation and creep. This chapter discusses the development of the procedure used to measure and evaluate infrared spectral changes in asphalt cement while the asphalt cement specimen is subjected to mechanically-induced stress. This chapter discusses the findings of this study and the microstructural components of asphalt cement determined to have the strongest influence on the relaxation and creep properties of the asphalt cement.

Chapter 3 addresses the second research issue: evaluation of the microstructural components of asphalt cement which contribute to and control the microdamage (or microfracture) healing within asphalt concrete mixtures. Fifteen different asphalt concrete mixtures were evaluated in this study to determine the influence of binder type, aggregate type, modifier, etc. on the microdamage healing potential of asphalt concrete mixtures.

Chapter 3 discusses the findings of this experimental study and the implications of these findings on the microstructural model responsible for microdamage healing in asphalt cements and asphalt concrete mixtures. Chapter 3 also addresses the importance of the findings from chapter 2, regarding microstructural effects on relaxation and creep of asphalt cements, on microdamage healing.

This report contains one appendix entitled "Characterization of Damage Growth in Asphalt Concrete." This appendix supports the work discussed in chapter 3.

CHAPTER 2

RHEOLOGICAL AND RHEO-OPTICAL CHARACTERIZATION OF ASPHALT CEMENT AND EVALUATION OF RELAXATION PROPERTIES

INTRODUCTION

The rheological properties of asphalt depend on its molecular structure and chemical composition. The widely used Corbett fractions provide the chemical composition of asphalt but lack the detailed structure/property relationships needed to accurately design asphalt systems. Depending on the proportions of the generic fractions, an asphalt is either a dispersed type asphalt or a solution type (Monismith, 1961). The dispersion type is also termed micellar or colloidal; the solution type is termed "polymer type". It is unclear as to which structure accurately represents the mechanical behavior of an asphalt system. In this work, material science tools were used to elucidate information as to the structure of a "typical" asphalt molecule. In particular, a rheo-optical technique was developed to probe changes in molecular vibrations, via fourier transform infrared spectroscopy (FTIR) during shear deformation. The objective was to identify the important chemical aspects of an asphalt molecule that are related to the deformation properties of the asphalt. To clarify this relationship, detailed viscoelastic characterization of the asphalt was conducted to insure an understanding of the asphalt's rheological properties. The FTIR results suggest an important link between rheological performance and linear structures in the asphalt cement complex. This concept was further probed via small angle x-ray scattering. Fractal analysis was used to determine the Porod scattering dimension which is a measure of the dimensionality of the tested structure (i.e. is it linear or branched, or three dimensionally branched?).

Asphaltenes are colloids (or micelles) dispersed in the oily medium peptized by resins. The peptizing ability of resins keeps asphaltenes, the highly associated component of asphalt, dispersed in the oily phase. The asphaltene fraction is the solute and the other fractions combined (called maltenes) make the solvent. There is limited consensus among researchers as to whether the asphaltene or the maltene contributes most to the overall physical behavior of an asphalt. Corbett described asphaltenes as solution thickeners which raise the asphalt's viscosity, and the other fractions were described as being responsible for the ductility and fluidity of asphalt (Corbett, 1970). Dealy (1979) found asphaltenes to be the structuring component of asphalt and to play a key role in the rheological behavior of asphalt. Conversely, Boduszynski et al. (1980) found that asphaltenes lacked an independent rheological identity. They indicated that, due to the presence of the solvents, asphaltenes conglomerate as a highly associated phase; their study also indicated similarity in the molecular weights of asphaltenes and saturates (Boduszynski, et. al. 1980). Petersen (1984), referring to the work of Boduszynski et al. (1980), emphasized the role of compatibility among the four generic fractions of an asphalt. Halstead (1985) reviewed the work of Boduszynski et al. and Petersen and found that it is the inter component relationship among the generic fractions that controls the overall physical properties of an asphalt and not simply the quantity of any single component. The functionality, and the molecular structure are two main factors that hold the balance among the components of an asphalt (Petersen, 1984). The microstructural model under study by Strategic Highway Research Program (SHRP) researchers is progressing on the hypothesis of a dispersed polar fluid (DPF) (Binder, 1991). The role of the molecular structure responsible for the observed mechanical

performance of asphalt is hardly addressed in this SHRP study (Binder, 1991).

To predict the long term properties of the asphalt, the microstructure of the whole asphalt, containing all the fractions together, should be known. Monismith (1961) proposed two physical models to explain the chemical composition of asphalt. The first was the colloid or the micellar model, presented above, where the asphaltenes are held as discrete lumps by the peptizing ability of the resins (polar aromatics and naphthene aromatics) in the oil (saturates) medium. In the solution model, it was proposed that asphaltenes are dissolved in the oil-resin phase. The colloidal model was more popular than the solution model as asphalt was shown to deviate from true solution behavior (Halstead, 1985).

Recently, SHRP announced its findings on the microstructure of asphalt studied using NMR and chromatography techniques. The DPF (dispersed polar fluid) model pictures asphalt as a continuous, three-dimensional association of polar molecules dispersed in a fluid of non-polar or relatively low-polarity molecules. Sulfur, nitrogen, and oxygen are incorporated in asphalt molecules in the form of polar functional groups which are attached to hydrocarbon molecules. Many of the polar functional groups will behave as either acids or bases, and all are capable of forming dipolar, intermolecular bonds of varying strength with functional groups of opposite polarity. In this model, the viscoelastic properties of the asphalt and its response to load and temperature induced stresses, result directly from the making and breaking of bonds between polar molecules. When the asphalt is subjected to stress, these secondary bonds are broken and reformed continuously. (This would suggest the existence of a yield stress).

Information from the SHRP NMR data gives an account of the relative amounts of carbon and hydrogen present in asphalt fractions. It is not known whether or not the DPF model proposed by SHRP has been validated by any quantitative measurement at the molecular level. The proposition of a network of molecules floating in a non-polar fluid and was investigated in this effort.

The DPF model proposed by SHRP differs from the older micellar model in several important ways. First, the micellar model postulates that asphalt is a collodial system with particles that are very large on a molecular scale - representing an agglomeration of many individual asphalt molecules. By contrast, the DPF model postulates no large assemblages of molecules. Rather, micro-structural interactions depend on the wide variety of polar molecules dispersed in the asphalt. NMR analysis fails to find any large-scale assemblages.

Second, in the micellar model, collodial particles are considered to be relatively permanent assemblages suspended in a dispersing medium. The DPF model, conversely, proposes a structure which is continually forming and reforming as energy flows to and from the asphalt through media of external loading and temperature fluctuations.

Finally, the DPF model stresses the importance of polar asphalt molecules in mediating performance to a larger degree than the micellar model. A major component of the DPF model - producing a major influence over the formation of the molecular matrix - is the amphoteric. These molecules act as both an acid and a base and can then associate extensively due to the fact that they can fasten to other molecules at two or more sites instead of one.

VISCOELASTIC CHARACTERIZATION

Overview

Usually, strain controlled static tests are used to study the viscoelastic relaxation of a material. This test is particularly suitable for materials which are more elastic than viscous. For materials showing considerable viscous behavior, use of a strain controlled static test may be limited by long experiment times. Dynamic mechanical tests overcome this constraint, and therefore were used to characterize the asphalts studied here. Interconversions between viscoelastic functions are well documented in the literature and were employed to predict performance.

To facilitate interconversion between time and frequency dependent linear viscoelastic functions, master curves of the storage (G′) and loss (G") modulus were constructed and used to calculate the discrete relaxation spectrum for each asphalt. The discrete function is related to the master curve through the expressions below:

$$G(t) = \sum_{i=1}^{z} G_i \, e^{\frac{-t}{\tau_i}} \tag{1}$$

$$G'(\omega) = \sum_{i=1}^{z} \frac{G_i \omega^2 \tau_i^2}{1 + \omega^2 \tau_1^2} \tag{2}$$

$$G''(\omega) = \sum_{i=1}^{z} \frac{G_i \omega \tau_i}{1 + \omega^2 \tau_i^2} \tag{3}$$

The G_i′s and corresponding τ_i′s make up the discrete relaxation spectra. If the G_i′s and τ_i′s are known from the G′ and G" master curves, then G(t), the relaxation modulus, can be calculated straight-forwardly. The number of discrete nodes is selected to provide a good fit to G′ and G".

The relaxed modulus, G_R, and the zero shear viscosity, η_0, are synonymous in characterizing the long term behavior of a material. The

relaxed modulus or equilibrium modulus is the stiffness of a material, under a sustained state of deformation, at an infinitely long time. The relaxed modulus is indeed the long-term resistance of a material against flow. For the range of frequencies and temperatures employed in this study, the asphalts' equilibrium modulus was not obtainable. For this reason, the study of zero shear viscosity was an essential alternative to evaluate the long-term resistance against flow. The zero shear viscosity is approximated as follows:

$$\eta_0 = \sum_{i=1}^{Z} G_i \tau_i \qquad (4)$$

Prapnnachari (1992) provides more detailed information about the viscoelastic characterization performed in this study.

Dynamic Mechanical Measurements

Eleven types of asphalts representing different sources were tested (Prapnnachari, 1992) using a Rheometrics® mechanical spectrometer (RMS®). The commercial names of the asphalts were replaced by representative names for the purpose of this study. For purposes of simplification in identification of data, asphalts studied are referred to as type A, B, C, D, E, F, G, H, I, J, and K. The identification key for these asphalts in as follows:

Asphalt Type

A = AAA (AC-20)
B = AAG (AC-20)
C = AAM (AC-20)
D = Conoco AC-20
E = Frontier AC-20
F = Conoco AC-10
G = Frontier AC-10
H = Sinclair AC-10
I = Exxon AC-20
J = Santa Maria AC-10
K = Coastal AR-4000

Since the procedure for dynamic measurements on the Rheometrics mechanical spectrometer is well established, discussion is limited to the analysis of the dynamic data only (Walter, 1975; Barnes et al., 1989).

To completely characterize the asphalts, the test was conducted in two temperature regions. High temperature tests were performed from 25°C to 65°C, while low temperature tests were performed below 25°C down to -25°C. Twenty five millimeter diameter parallel plates were used for the high temperature test; for the low temperature, the rectangular torsion configuration was used. The frequency range used for both high and low temperature was from 0.1 rad/sec to 100 rad/sec. Before performing the temperature frequency sweep, linear viscoelastic strain levels were determined using strain sweeps and noting the point at which G' and G" obtained strain dependence. For temperature frequency sweeps, the high temperature test was performed in three stages: 65°C to 55°C, 55°C to 40°C, and 40°C to 25°C. The low temperature test was also performed in two stages: 25°C to 5°C, and 5°C to 25°C. The reason for dividing the test in to stages was to apply appropriate strain levels to the sample so that the RMS could generate enough torque to minimize the noise in the data. In general, a strain level of 25 percent was found suitable for testing between 55°C to 65°C; a 15 percent strain level was suitable for testing between 55°C to 40°C; and a strain level of 3 percent was found appropriate for testing from 40°C to 25°C. The strain level applied for the cold temperature range was 0.3 percent below 20°C down to 5°C, and 0.1 percent for the rest of the lower range. Overlap in each temperature range was selected to insure reproducibility. Values of G', G", G*, $\tan(\delta)$, ω and temperature were recorded.

Construction of the Master Curves

Time temperature superposition is valid for thermorheologically simple materials. The G′, G" and tan(δ) master curves were constructed by horizontal shifting of the isotherms on the frequency (or time) scale. Thus, the master curve is a log-log plot of shifted G′, G" and tan δ against reduced frequency. The reference temperature for all the master curves was selected as 25° C. Typical isotherms of G′, G", and tan(δ) for a representative asphalt (of the eleven studied) (type J) are shown separately in Figures 1, 2, and 3. The actual shifting of the isotherms of G′, G", and tan(δ) was done simultaneously to insure the condition that all viscoelastic functions have the same shift factors. However, they are reported separately. Horizontal shifting was checked using the tan(δ) curve since tan(δ) is independent of any geometry errors that may result in vertical shifts. Tan(δ) superposition insured, G′ and G" superposition. Sometimes vertical shifting of the moduli (G′, and G") was required to correct for geometry measuring errors and changes in density. Vertical shifting of the tan(δ) curves was not allowed. The marginal vertical shifting indicated the influence of temperature on density; however, for all practical purposes this was insignificantly low.

Construction of Discrete Relaxation Spectra

The resulting G′ and G" master curves were used to calculate the discrete relaxation spectrum as presented by Baumgaertel and Winter (1989). The calculated relaxation modulus, G(t) versus time, was verified by performing actual relaxation tests on three asphalt types: A, B, and C. The values of G(t) obtained from the experiment and the IRIS program are comparable; Figure 4 shows this comparison. In selected experimental time windows the values of G(t) for the three asphalts match with the

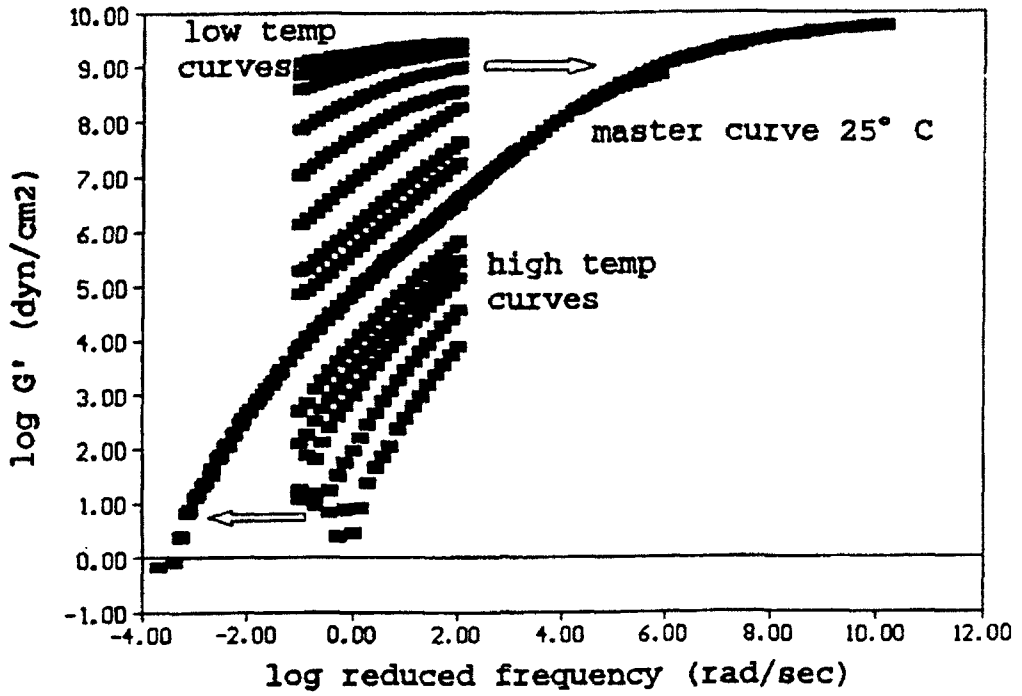

Figure 1. Shifting of G' isotherms to obtain master curve at 25°C.

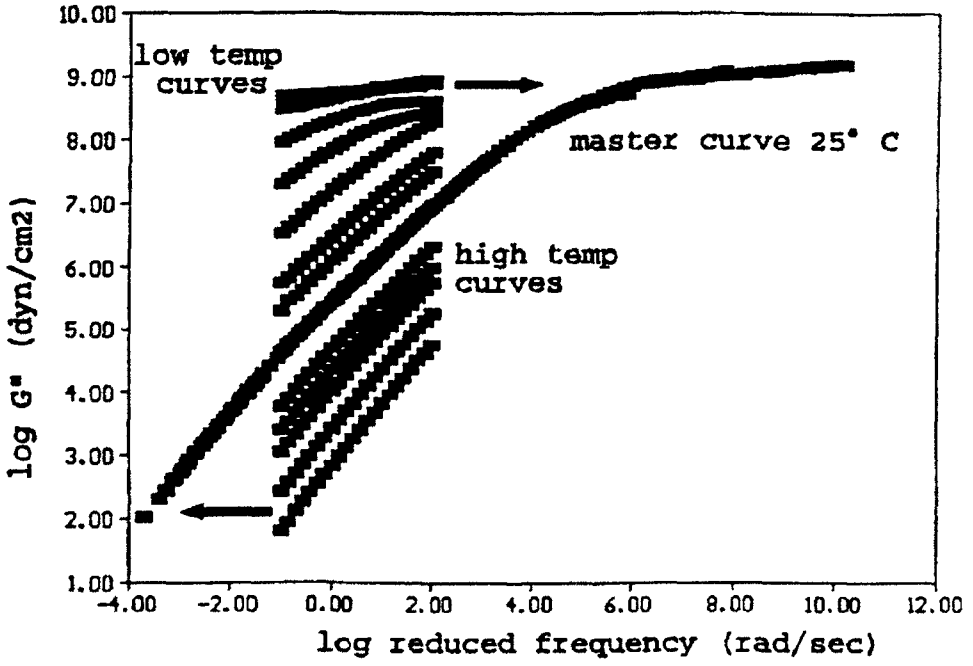

Figure 2. Shifting of G" isotherms to obtain master curve at 25°C.

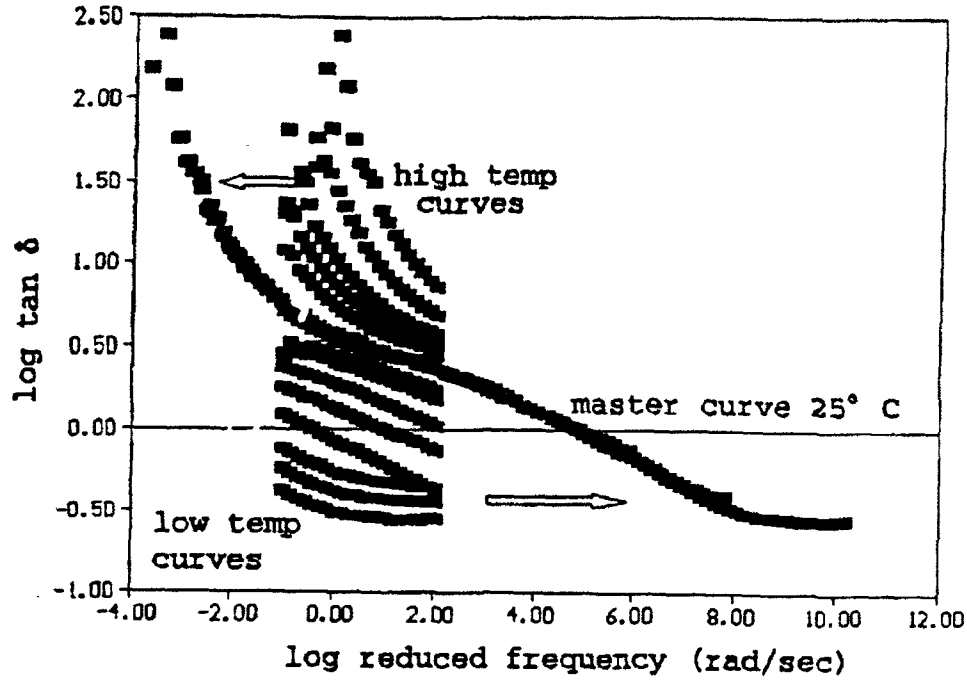

Figure 3. Shifting of tan(δ) isotherms to obtain master curve at 25°.

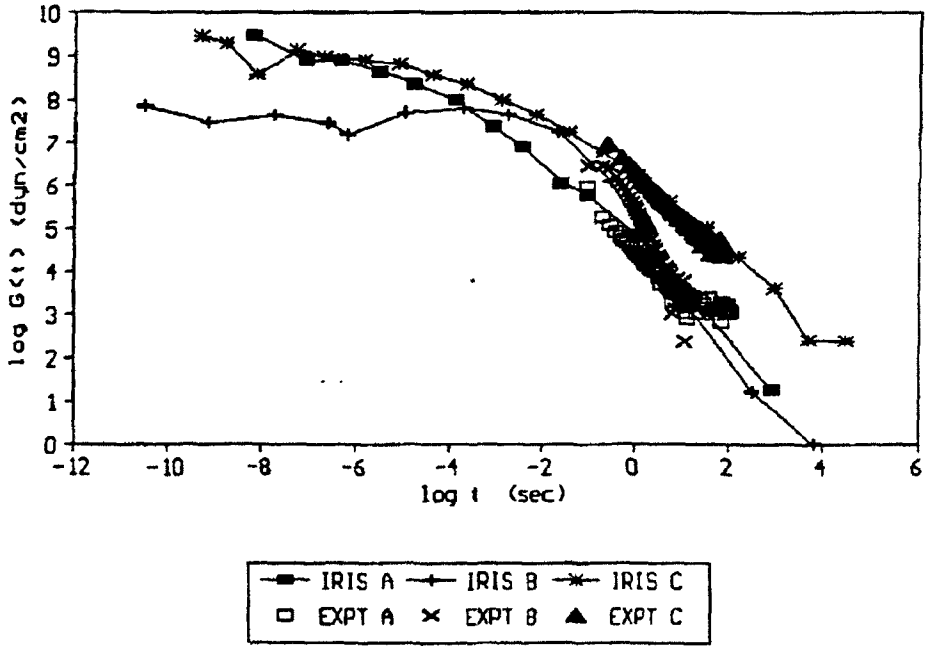

Figure 4. Verification of numerically calculated relaxation spectrum by experimental relaxation test.

values obtained from prediction. Figure 5 illustrates a typical relaxation modulus for an asphalt (type A).

Computation of Relaxation Strength

Baumgaertel and Winter (1989) used the discrete relaxation spectrum to calculate the steady shear or zero shear viscosity. The steady shear viscosity, equation 4, is a measure of the long term resistance of the material against flow. Table 1 presents zero shear viscosity for the asphalts studied.

MICROSTRUCTURAL MECHANICS BY RHEO-OPTICAL/FTIR STUDIES

Overview

Infrared (IR) is widely used to study the influence of mechanical stress on the molecular structure of polymers. This study employed IR spectroscopy to evaluate the influence of stretching (mechanically induced shearing) on the molecular structure of asphalt. Although the detailed chemical knowledge of the interconnectivitity of asphalt systems is not known and cannot be determined by this techniques, information as to the importance of specific bond or group types on mechanical properties can be extracted using rheo-optical techniques. The coupling of IR spectroscopy and controlled shear deformation is introduced in this report. A detailed introduction to and discussion of analysis through IR spectroscopy is presented by Prapnnachari (1992).

Experimental Setup

The IR experimental set up included two main units; the IR spectrometer, a Nicolet model 60SXR, and the asphalt shear deformation stage (Minimat® marketed by Polymer Laboratory of Massachusetts) which

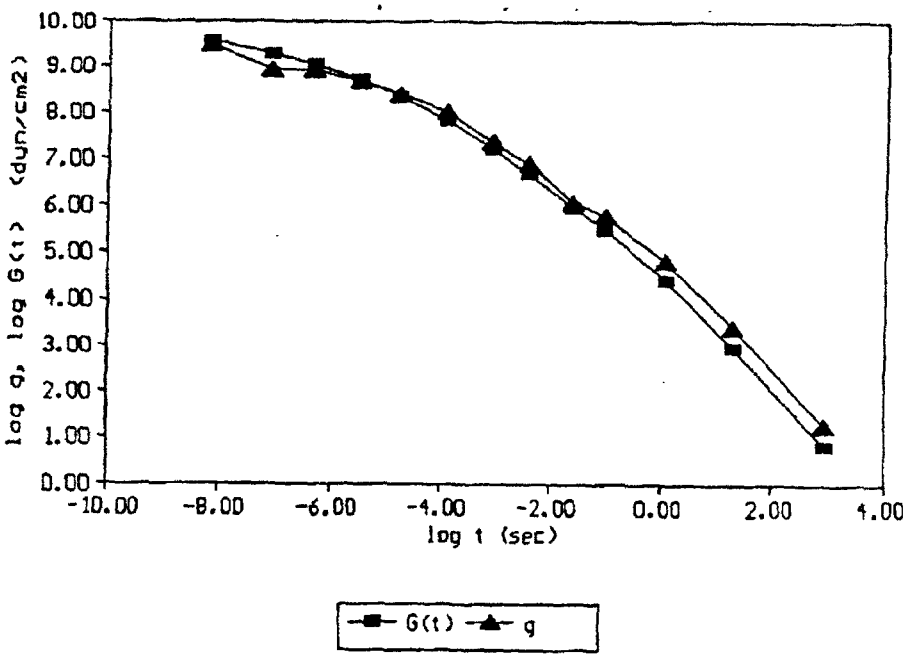

Figure 5. Relaxation spectrum at 25°C for asphalt type A.

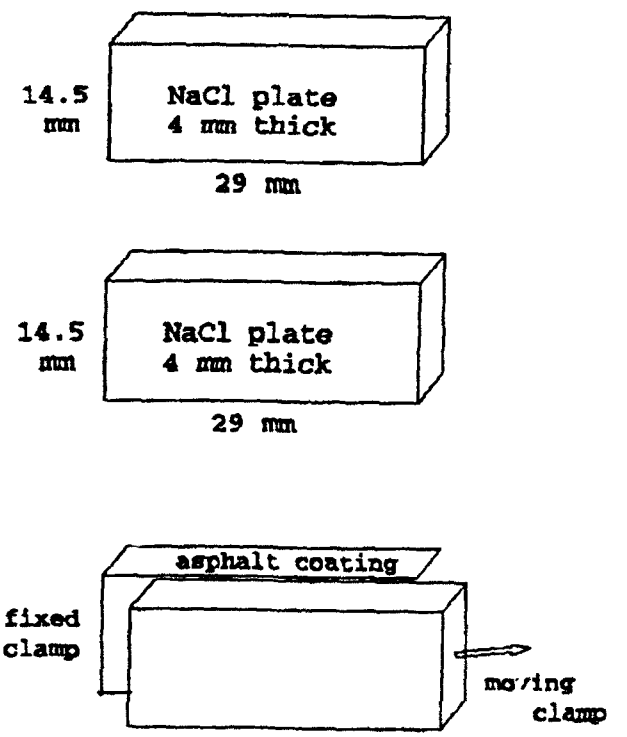

Figure 6. A schematic diagram of the NaCl plate arrangement used to shear the asphalt.

Table 1. The relaxation parameter of zero shear viscosity, η_o, as obtained from the relaxation spectra of the eleven asphalts tested.

Asphalt Type	Zero Shear Viscosity (Poises)
A	2.95e+05
B	9.16e+05
C	1.78e+07
D	3.14e+06
E	4.23e+06
F	1.17e+06
G	1.19e+06
H	2.59e+06
I	1.89e+06
J	0.49e+06
K	3.76e+06

fits in the sample chamber of the Nicolet IR spectrometer and is used to shear the asphalt in a thin film, similar to how the asphalt exists in a mixture. While being stretched, the asphalt film is penetrated with an IR beam.

In order to establish a transmission IR spectrum, selection of a proper window material was a key consideration. The first criterion to consider in selecting a window material was the frequency range over which the spectrum must be measured. Other important considerations included solubility, reactivity, and refractive index of the window material with respect to the sample. Mechanical and thermal characteristics of the window materials also played a major role in their selection for this test. Hygroscopic materials such as potassium bromide (KBr) and sodium chloride (NaCl) are used most frequently, primarily because they do not react with organic compounds. Although potassium bromide (KBr) has a slightly wider spectral range than sodium chloride (NaCl), it is too brittle to withstand significant mechanical shocks. Besides, KBr is more hygroscopic and less resistant to thermal fluctuations than NaCl. In this study, NaCl was selected as a window material.

Due to width limitations in the space available for sample holding, a 29 mm x 14.5 mm x 4 mm NaCl plate was selected for use. In sample preparation, two such rectangular NaCl plates were coated with a thin layer of asphalt and then sandwiched together, Figure 6. Only one end of each NaCl plate was clamped. The plates remained together under the adhesive influence of the asphalt. In order to insure full adhesion to the sodium chloride plates, a small quantity of asphalt was smeared over one face at a temperature between 60°C to 93°C. The second NaCl plate was pressed firmly by hand over the first, still hot, NaCl plate. This

sandwich arrangement was kept at a temperature of between 60°C to 93°C in an oven for a few minutes to insure uniformity. After cooling the system was placed and clamped in sample holders. Obviously, the portion of NaCl plates under the clamp grip was not coated with asphalt. Subsequently, the entire set was mounted in the sample box of the IR spectrometer.

The maximum available overlap between the two plates, through which the IR beam could pass, was 13 mm. The number of reproducible IR scans per minute was not greater than six. In order to optimize the number of IR scans obtained during shearing, a 6 mm/min rate of shear was used. The IR spectral changes below a 4 mm/min shearing rate were hardly perceptible and the spectral changes from 4 mm/min to 6 mm/min rate of shearing were identical. The IR spectrometer was programmed so that the first IR scan collected was for the unstretched (no shear induced) sample. Subsequently the Minimat shearing and IR scanning was triggered simultaneously. Figure 7 and 8 illustrate the set-up of the IR experiment. Figure 7 is a view of the entire experiment setup (IR spectrometer and minimat). Figure 8 is a view of the minimate device which fits within the chamber of the IR spectrometer and actually shears the asphalt between the NaCl plates while the IR spectra is used to analyze changes in absorbance bands during stretching. Prapnnachari (1992) provides a much more complete discussion of the experimental setup and the evolution of the approach used.

Infrared Spectral Analysis

IR spectra of asphalts have nine main absorbance bands which are summarized in Table 2. The absorbance bands in IR spectrum are characteristic of a specific molecular structure and its mode of vibration. Asphalt is composed of hydrocarbons, and the band assignments

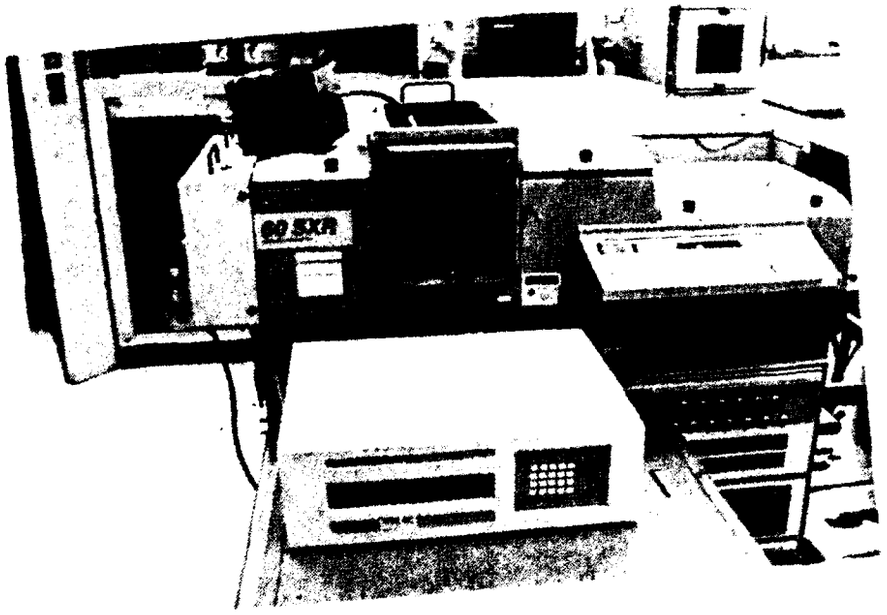

Figure 7. Photograph of Minimat in FTIR chamber.

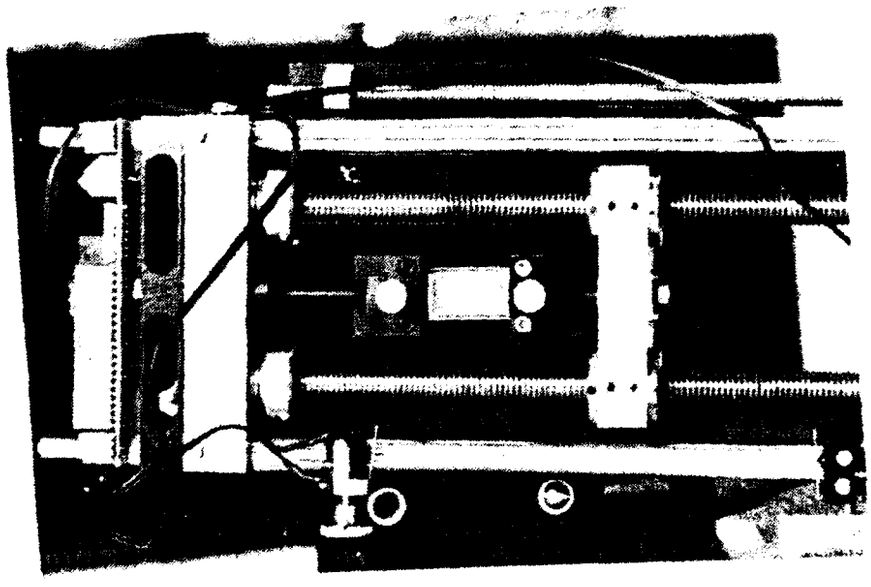

Figure 8. Photograph of Minimat deformation stage.

Table 2. IR band assignments for asphalt.

Wave Numbers (cm^{-1})	S-Strong M-Med. W-Weak	Methyl Groups CH_3 Saturated Aliphatic	Methylene Groups CH_2 Saturated Aliphatic	Aromatic
2950	s	asymmetric stretch	asymmetric stretch	
2860	m	symmetric stretch	symmetric stretch	
1600	w			aromatic ring modes, weak for nonpolar substituents υ (c - c)
1460	m	asymmetric bending	symmetric bending	
1376	m	symmetric bending		
*866	w			1,2,3,4/5 tetra/penta substituted δ (CH)
*813	w			1,4 disubstituted (para) δ (CH)
*745	w			1,2 disubstituted (ortho) or monosubstituted δ (CH)
*720	w		rocking mode $(CH_2)_{n>4}$	monosubstituted δ (CH)

* Aromatic frequencies are more characteristic of the position of the substituents than of their nature.

for hydrocarbons are well established in the literature. Primarily using the band assignments for hydrocarbons, Stewart (1957), and Beitchman (1959) characterized asphalt bands as summarized in Table 2. In general, the region between 3100 and 2800 cm^{-1} of IR spectrum indicates the nature of the hydrocarbon part of a molecule. This region was first examined since the position of the CH stretching bands suggests the structural feature of a hydrocarbon molecule. Absence of absorbence above 3000 cm^{-1} suggests that molecules are aliphatic and alicyclic with no ethylenic or aromatic structure. Figure 9, a typical IR spectrum of an asphalt, shows strong absorbence from 2950 to 2850 cm^{-1} which suggests the dominance of aliphatic and alicyclic hydrocarbon structures in all the asphalts tested. This does not mean that aromatics are absent in the asphalt molecules. Sometimes the closer frequencies develop coupled vibrations, shifting absorbence to unexpected regions of the spectrum. This might occur due to the complex structure of the asphalt molecules. Close examination of the absorbence in the 3000 to 2800 cm^{-1} region indicates the presence of two peaks for aliphatic and alicyclic CH stretching: one near 2850 cm^{-1} and the other near 2925 cm^{-1}. The steep shoulder near the 3000 cm^{-1} peak indicates weak absorbence due to the aromatics. This peak is obscured by the very strong CH_3 and CH_3 stretching bands of the aliphatics and alicyclics. Generally the aromatic structures in a hydrocarbon can be found (Lambart et. al. 1987) in five regions of the IR spectrum: 3100 to 3000 cm^{-1} for CH stretching, 1650 to 1430 cm^{-1} for C=C stretching, 1275 to 1000 cm^{-1} for in plane CH bending, 900 to 690 cm^{-1} for out of plane CH bending, and 2000 to 1700 cm^{-1} for overtones and combinations. In the IR spectrum of an asphalt, weak absorbence near 1600 cm^{-1} suggests C=C stretching of the aromatics, and small absorbence at

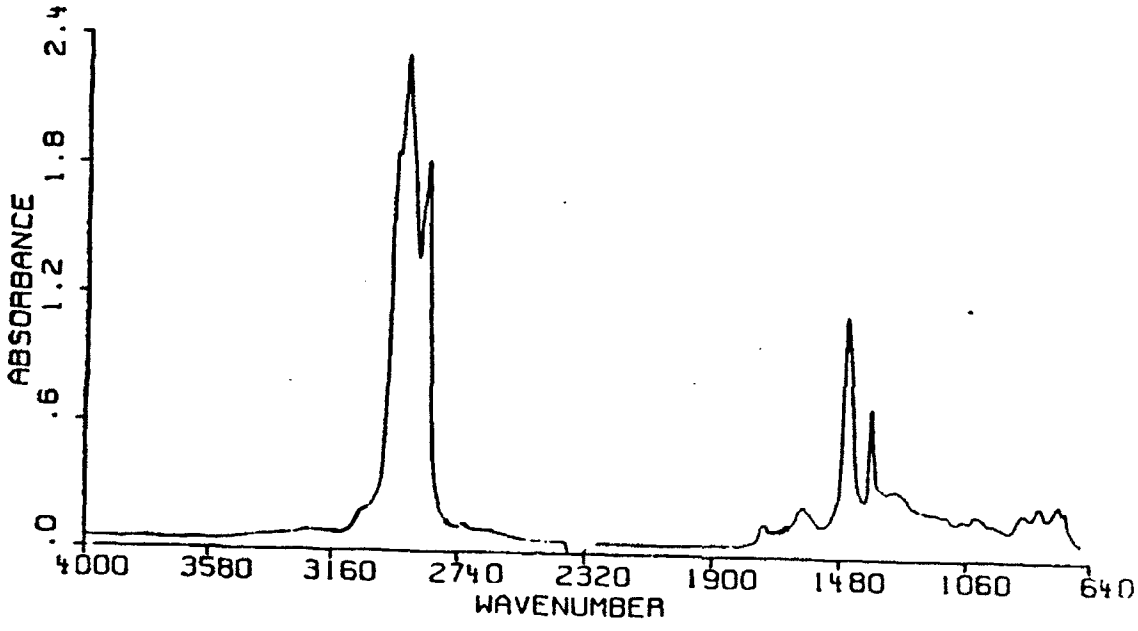

Figure 9. IR absorbance spectrum (650-4000 cm^{-1}) for unstretched asphalt type A.

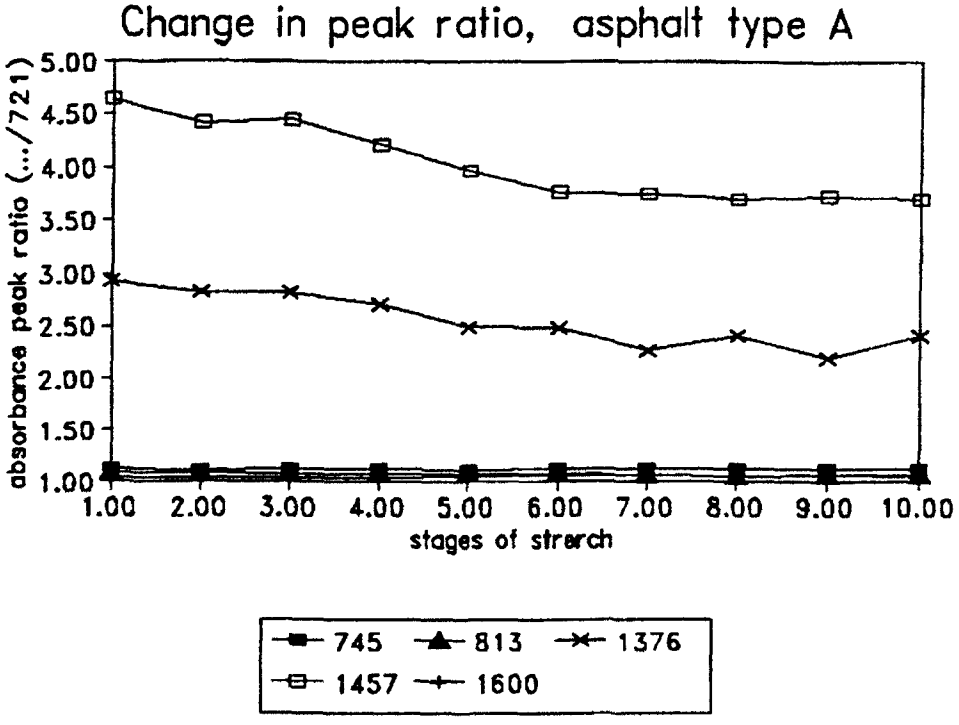

Figure 10. Plot of peak ratio versus stage of shearing (in mm) for asphalt type A.

863, 813, and 745 cm^{-1} is due to CH out of plane bending. The overtones and in-plane CH bending were not witnessed.

The region near 1460 and 1375 cm^{-1} reveals the presence of methylene and methyl groups. The band near 1460 cm^{-1} indicates the anti symmetric deformation of the HCH angle of a CH_3 molecule. The bending of methylene (CH_2) groups also gives rise to a band in the same region. The symmetric CH_3 bending gives a strong, sharp band near 1376 cm^{-1}. A small band near 720 cm^{-1} is indicative of a linear chain containing four or more CH_2 groups. The relative numbers of CH_2 and CH_3 groups are evaluated by the combined study of the 1460, 1376, and 720 cm^{-1} bands. When there are more CH_2 groups than CH_3 groups present, the 1460 cm^{-1} band will be stronger (Lambart, et al. 1987) than the 1376 cm^{-1} band. A greater relative intensity of the band near 1460 cm^{-1} than 1376 cm^{-1} was found in general in the IR spectra of all the asphalts. This shows the dominance of CH_2 groups over CH_3 groups in the asphalt molecules. The relative length of CH_2 chains among asphalts can be evaluated by the study of absorbance near 720 cm^{-1}, in particular by studying the change in ratio of the CH_2 and CH_3 absorbencies.

Absorbance Peaks

The height of an absorbance peak indicates the concentration of a particular molecular component in the sample. For a given asphalt the ratio of any two absorbance peaks provides the ratio of two representative molecular components present in asphalt. For an identical chemical and mechanical environment, the ratio between two peaks is always reproducible irrespective of the number of IR scans and the change

in thickness of the sample. The spectral changes under the influence of mechanical stress on the asphalt sample can thus be quantified by study of the change in the ratio of the absorbence peaks. For a number of spectra, ratios of the peak area were also compared as suggested by Keonig et. al., (1991). In all cases, the peak area ratios verified the results obtained from the evaluation of peak absorbance ratios.

The ratio of any two peaks can be used to study spectral changes. Table 3 shows the absorbence peak ratio of all other bands of the IR spectrum of asphalt type A with respect to its 721 cm^{-1} peak for various stages of shearing. As shown in Figure 10, the 1376 to 1457 cm^{-1} bands ratioed with respect to the 721 cm^{-1} band, changed appreciably. This is an obvious indication of the key role the chain length plays in asphalt during mechanically-induced shear. Figure 11 is a typical illustration of the collective spectra obtained during the stages of shearing for an asphalt (type K). The change in the shape of the bands and shoulders, mostly near the 745 cm^{-1} band, results from the interaction of substituent CH_2 molecules.

The study of changes in absorbence peak ratios (Figure 10) and changes in band shapes and shoulders (Figures 11) is complementary. The most affected peak ratios, 1457 and 1376 cm^{-1} bands ratioed with respect to the 721 cm^{-1} band, indicate that CH_2 and CH_3 molecules forming the chains attached to the asphalt molecules are most active in resisting stretching. The change in band shapes and shoulders in the region of the aromatic out-of-plane CH bending absorbence suggests the interaction of the CH_2 chains with the aromatics. This suggests that the network of CH_2 chains forming the substituents to the aromatics also contributes to resisting mechanically-induced stress.

Table 3. Absorbance peak ratios, asphalt type A.

Stretch Stages	Peak ratio with respect to 721 cm^{-1} band				
	745 cm^{-1}	813 cm^{-1}	1376 cm^{-1}	1457 cm	1600 cm^{-1}
1	1.119	1.086	2.924	4.633	1.033
2	1.109	1.082	2.820	4.415	1.037
3	1.120	1.071	2.810	4.447	1.034
4	1.118	1.072	2.703	4.211	1.036
5	1.113	1.069	2.492	3.971	1.046
6	1.122	1.068	2.480	3.772	1.060
7	1.121	1.064	2.273	3.750	1.058
8	1.122	1.057	2.412	3.710	1.056
9	1.124	1.063	2.207	3.734	1.060
10	1.116	1.062	2.412	3.698	1.057

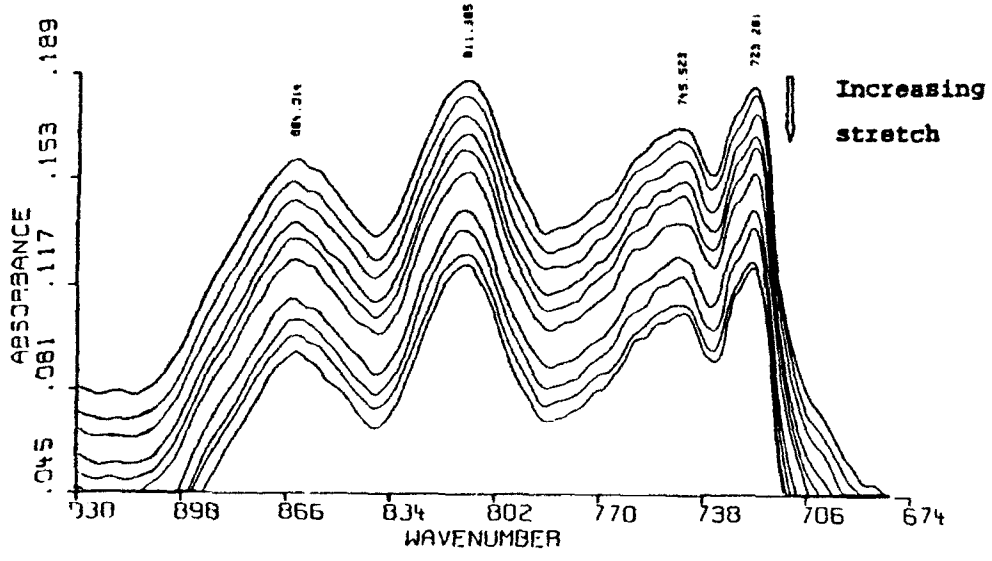

Figure 11. Collective IR absorbance spectra (680-930 cm^{-1}) for the stages of stretching for asphalt type K.

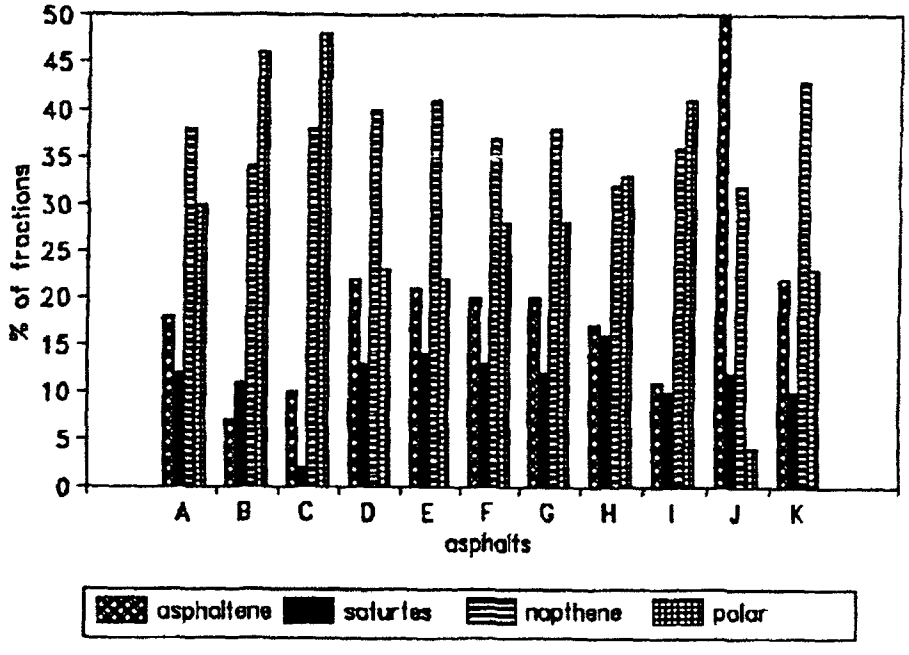

Figure 12. Corbett fractions of the asphalts studied.

Rheo-optical Measurements for Asphalt Factions

According to Corbett (1970), there are four generic fractions of an asphalt: asphaltenes, polar aromatics, naphthene aromatics, and saturates. The Corbett fractions obtained for asphalts A, B, C, D, E, F, G, H, I, J, and K are presented in Table 4 and Figure 12. The asphaltene and polar aromatics could not be sheared because of their solid physical state. The undeformed spectra of the naphthene aromatics and saturates of an asphalt (type K) are shown in Figures 13, and 14. The ratios of peak absorbence are plotted against the stages of deformation, and Figures 15 and 16 illustrate the effect of shearing on naphthene aromatics and saturates, respectively. It is evident that the behavior of these fractions is consistent with the observations on the neat, un-fractionated asphalt.

WIDE ANGLE AND SMALL ANGLE X-RAY DIFFRACTION

Principles of Diffraction

X-ray diffraction is a tool for the investigation of the fine structure of matter. Early x-ray use was limited to the determination of crystal structure. Today, x-rays are used not only for crystal structure determination, but are also applied to problems in chemical analysis, stress measurement, study of phase equilibrium and the measurement of particle size.

Diffraction is produced by the interference of waves scattered by an object. When the x-rays strike the object at angle = 2θ, every electron becomes the source of a scattered wave. If an x-ray beam of intensity I_0 irradiates a free electron, the intensity I is expressed as,

Table 4. Corbett fractions of the asphalts studied.

Asphalts	% of Asphaltene	% of Saturates	% of Naphthene Aromatic	% of Polar Aromatic
A	17.77	12.30	38.05	30.12
B	6.80	10.91	33.97	45.70
C	9.75	1.97	37.91	47.95
D	22.01	12.93	39.89	22.73
E	20.76	13.79	40.76	22.20
F	19.70	12.73	36.77	27.78
G	19.89	12.32	37.80	27.98
H	14.61	17.46	33.99	32.12
I	10.91	10.18	35.96	41.04
J	50.34	12.90	32.40	2.99
K	22.01	9.59	43.16	23.27

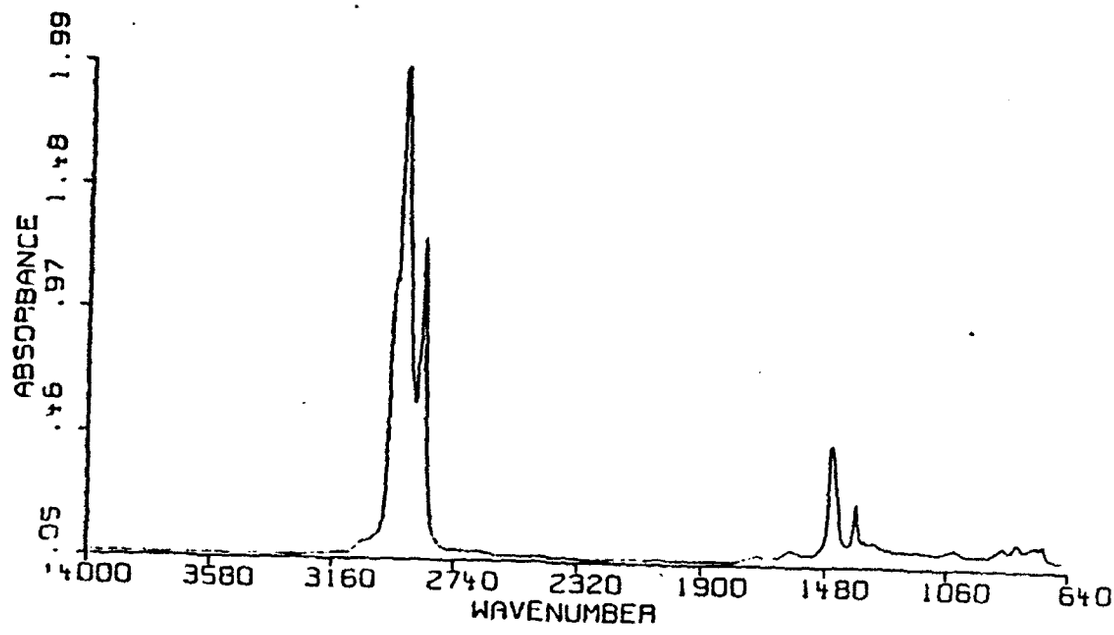

Figure 13. IR absorbance spectrum (650-4000 cm^{-1}) of the unsheared napthenic fraction of asphalt type K.

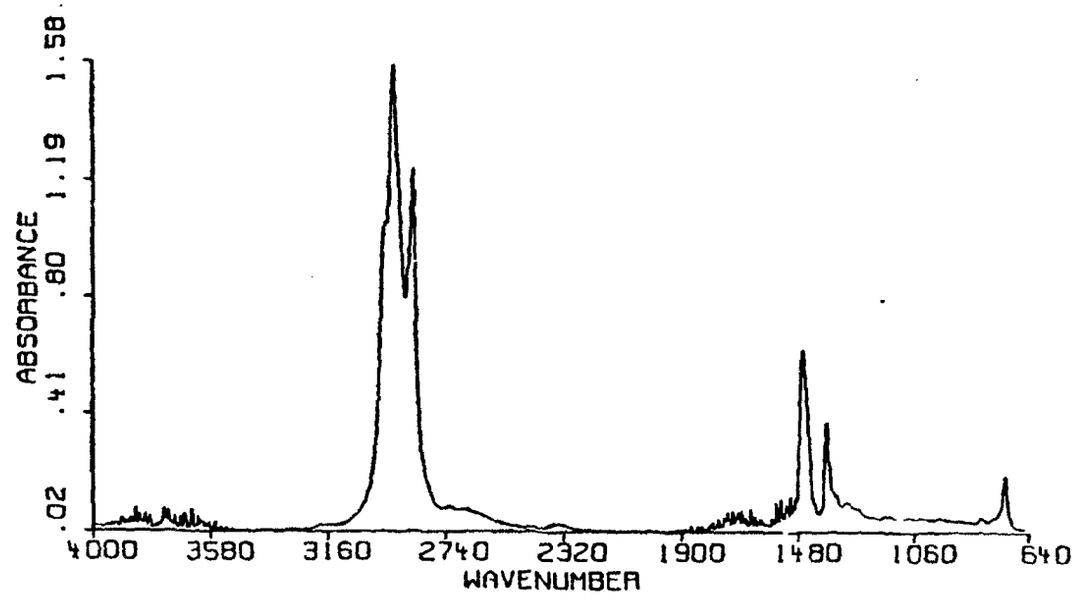

Figure 14. IR absorbance spectrum (650-4000 cm^{-1}) of the unsheared saturate fraction of asphalt type K.

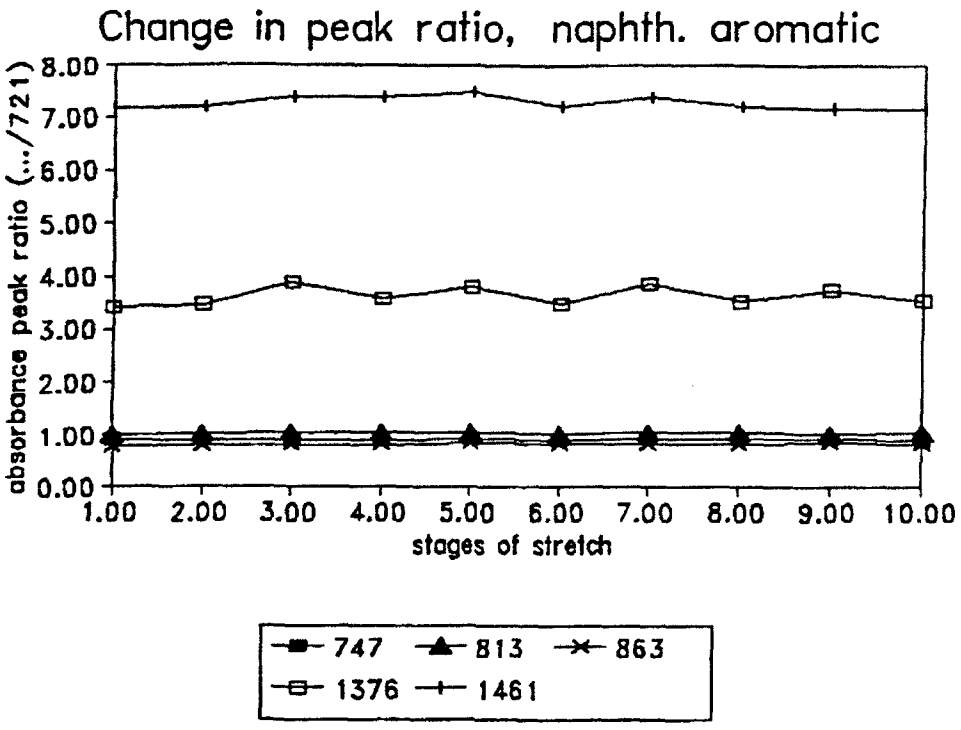

Figure 15. Plot of peak ratios versus shear stages of the napthene aromatics of asphalt type K.

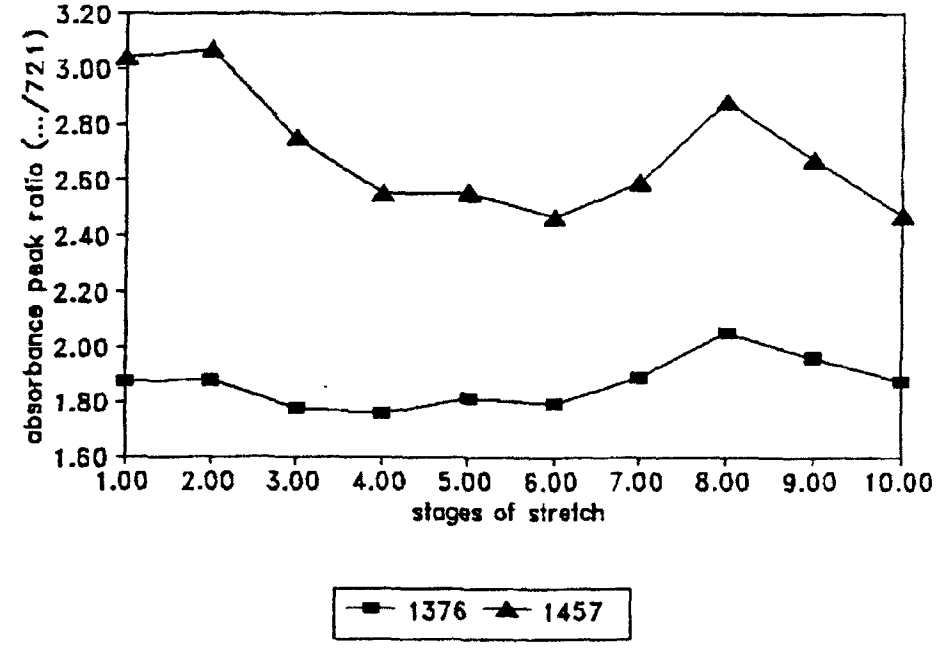

Figure 16. Plot of peak ratio versus shear stages of the saturates of asphalt type K. Stages of shear (stretch) are in mm.

$$I = I_0 \frac{K}{R^2} \left[\frac{1 + \cos^2 2\theta}{2} \right] \tag{5}$$

Here the constant K is defined by e^4/m^2c^4, where e and m are charge and mass of an electron and c is the velocity of light. R is the scattering vector.

For a noncrystalline material consisting of a single type of atom, the spatial distribution of atoms can be expressed conveniently by means of a radial distribution function $\rho(r)$, which is described as the number density of atoms to be found at a distance r from the center of any one of the atoms. The intensity I(s) of x-rays scattered from the material can be represented as,

$$I(s) = Nf^2 \left(1 + \int \rho(r)\, e^{-2\pi i s r}\, dr \right) \tag{6}$$

where f is the atomic scattering factor and N is the number of atoms in the scattering volume and the integration with respect to r is expressed throughout the scattering volume. The function $\rho(r)$ approaches the average density ρ_0 of atoms at $r \to \infty$ and hence,

$$I(s) = N r^2 \left(1 + \int [\rho(r) - \rho_0]\, e^{-2\pi i s r}\, d r\right) \tag{7}$$

If the material is isotropic, then equation (7) can be simplified to

$$I(s) = N f^2 \left[1 + \int_0^\infty 4\pi r^2 [\rho(r) - \rho_0] \frac{\sin 2\pi s r}{2\pi s r}\, dr \right] \tag{8}$$

Using the inversion theorem for Fourier integral,

$$4\pi r^2 \rho(r) = 4\pi r^2 \rho_0 + 8\pi r \int_0^\infty s\, i(s) \sin 2\pi r s\, d s \tag{9}$$

where $i(s) = (I(s)/Nf^2) - 1$

Here the radial distribution function $\rho(r)$ can be determined from the experimental intensity I(s). If the material contains more than one kind

of atom, its amorphous structure can be characterized in principle completely by a generalized radial distribution function (Alexander, 1985). From the radial distribution function, the density of atoms or the frequency of separations between atoms can be obtained by analyzing the peaks in the data. This provides a quantitative information source regarding the different atoms such as carbon and hydrogen in asphalt.

X-ray scattering techniques are usually categorized into wide angle x-ray scattering (WAXS) and small angle x-ray scattering (SAXS). In WAXS, the structural information is obtained on a scale of 1 nm or smaller. The angle measured is between 3° and 90°. The inhomogeneities of atomic dimensions give rise to WAXS. In SAXS, fluctuations in electron density over large distances, typically 30Å to 1000Å, are determined. The inhomogeneities of colloidal dimensions generate x-ray scattering and interference effects at very small angles, typically less than 2°, with the wavelength of CuKα, 1.542Å.

Since WAXS probes atomic dimensions, different bands of x-ray beam diffracted from the lattice planes are obtained as intensity. Knowing the position of peaks, quantitative information regarding crystalline and amorphous structures can be obtained. Since SAXS identifies large structures, the intensity peaks are spaced according to the distance between large areas of contrasting density. This capability provides a tool by which to determine whether asphalt is a colloid or a network structure.

Instrumentation

The WAXS measurements were conducted using a Scintag PAD-V operated at 40kV and 45 mA. The SAXS measurements were conducted using a Rigaku-Denki generator (RU-2000) with a rotating anode source operated at

50kV and 150mA. In both instruments, Ni-filtered CuKα radiation was used as an incident x-ray source, and the intensity was measured by a scintillation counter with a pulse height analyzer. The x-ray diffraction data were collected on-line on a VAX computer running under DMAXB Rigaku software. The correction for the non-uniformity of the detector efficiency along its window length was applied first before other corrections for background, slit smearing, etc. were made. The intensity data were scaled to unit by comparison with scattering from a calibrated Lupolen sample.

For WAXS, the sample is mounted on an aluminum plate and diffraction of x-ray occurs by reflection. The 2θ range of measurement is from 2° to 60°. In SAXS, the sample is fixed vertically in the aluminum plate and the diffraction mode is transmission. The range of measurement is 0.1° to 7°. The samples used for WAXS study were pure and modified Santa Maria AC-10 asphalts and four SHRP asphalts: AAA-1, AAF-1, AAG-1 and AAM-1. Modification of the Santa Maria AC-10 was made by adding 5 percent polyethylene by means of a high shear blending process. Two sources polyethylene were added: Muehlstein and Dow.

Determination of Crystallinity in Asphalt

X-ray diffraction is a definitive technique for estimating the degree of crystallinity in polymers. Many methods are available to calculate the crystallinity form x-ray diffraction (Alexander, 1969). All methods require that the intensity due to amorphous scattering be separated before one begins to evaluate the crystallinity. In this report crystalline peaks associated with the crystalline region of polymer modified asphalts were resolved using profile fitting of the diffraction pattern. In analyzing the data, no corrections were made for incoherent

scattering and for Lorentz and polarization factors. These corrections may not be important in calculating the relative crystallinity but are necessary in the calculation of absolute crystallinity. The deconvolution of peaks was done by fitting Gaussian profiles from which the peak positions and relative crystallinities were obtained. Relative crystallinity or crystalline index (CI) is calculated as,

$$CI = \frac{A_c}{(A_a + A_c)} \tag{10}$$

where A_c is the area under the crystalline diffraction peak and A_a is the area under the amorphous peak.

The WAXS pattern of pure PE (tested by Micheal Heaney of Dow Chemical) in Figure 17 shows two crystalline peaks at 20.5° ($\gamma 1$) and 23.9° ($\gamma 2$). Figure 18 shows that pure asphalt is completely amorphous and no regular pattern of the arrangement of asphalt molecules is present. Figure 19 and 20 show the WAXS pattern of Santa Maria asphalt modified with Muelstein and Dow variety of LDPE's. Through both have the same quantity of polymer, the crystalline content of Muelstein LDPE in the asphalt is higher than the crystalline content of Dow LDPE in the asphalt. This is observed by calculating the crystalline index of each type. The two crystalline peaks are denoted by $\gamma 1$ and $\gamma 2$. The CI for Muehlstein LDPE modified asphalt was calculated as 3.3 percent and 0.1 percent for the two peaks. The CI for Dow LDPE modified asphalt was calculated as 1.8 percent and 0.05 percent. Since the amount of crystalline matter in a material affects its physical properties, these results are very significant in the study of modified asphalts.

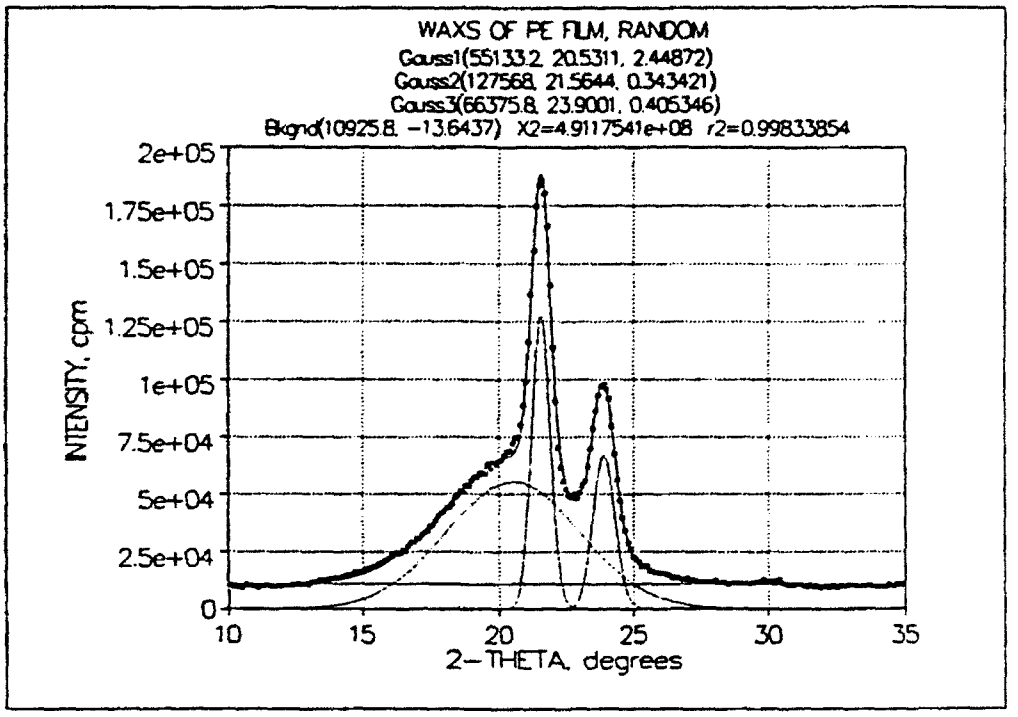

Figure 17. Profile fit of WAXS scan.

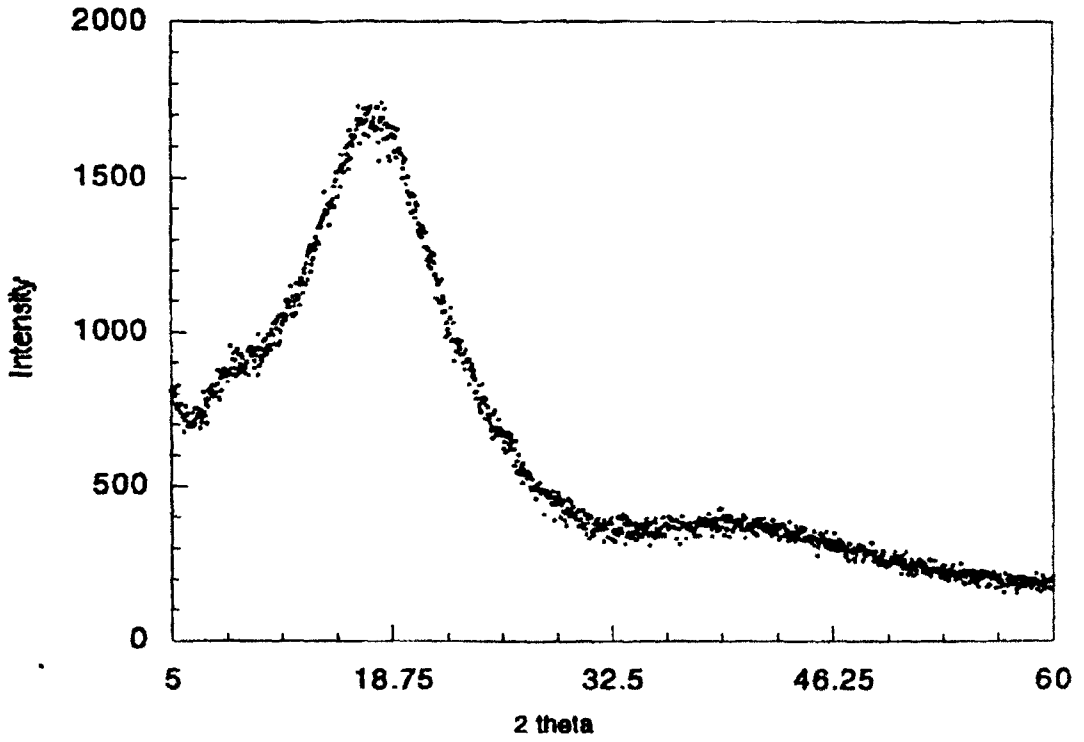

Figure 18. WAXS pattern of unmodified Santa Maria AC-10 asphalt.

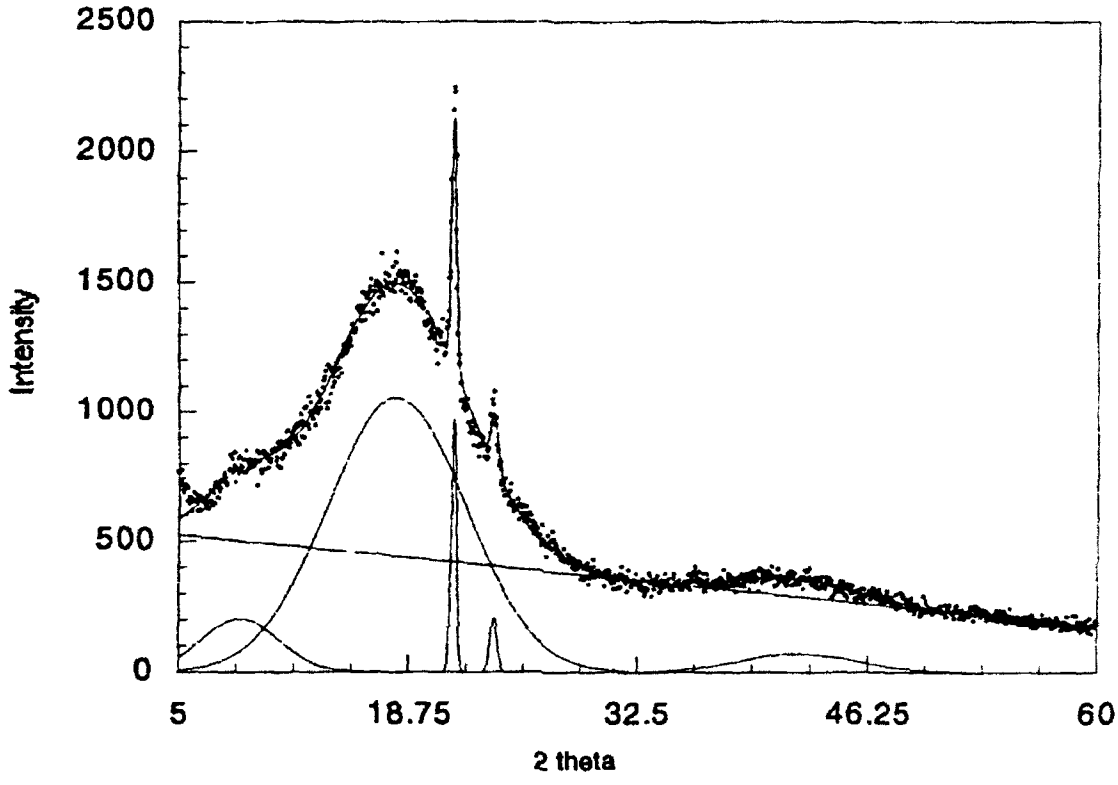

Figure 19. WAXS pattern of Muehlstein LDPE modified Santa Maria AC-10 asphalt.

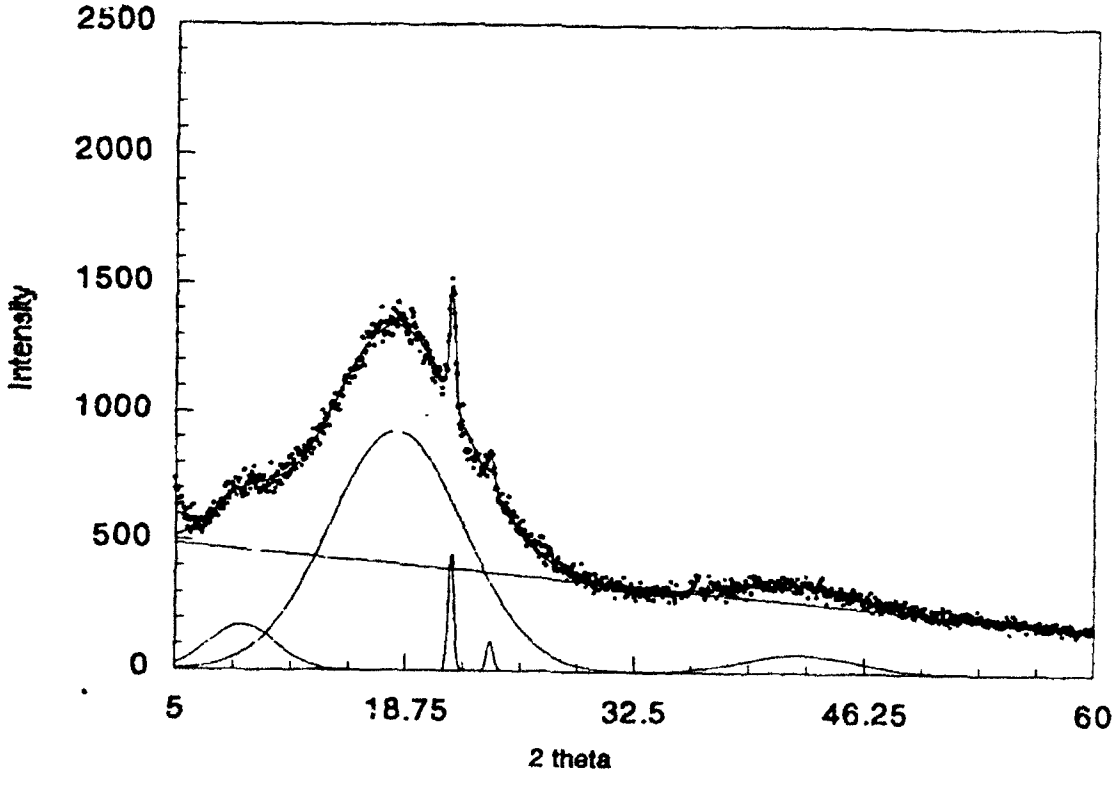

Figure 20. WAXS pattern of Dow LDPE modified Santa Maria AC-10 asphalt.

Use of Fractal Analysis to Determine Asphalt Molecular Topology

Fractal analysis can be used to characterize disordered objects ranging from macromolecules to the earth's surface (Mandebrot, 1982). These objects display "dilation symmetry", which means that they look geometrically self-similar under transformation of scale such as changing the magnification of a microscope. Complex structures such as Eden, Vold, Wittne-Sander, etc. (Schaefer, 1989), can be simply characterized with the single parameter D, the fractal dimension, which is defined as the exponent that relates the mass M of an object to its size R as

$$M \sim R^D \tag{11}$$

This equation also applies to simple objects such as rods, disks and spheres, for which the exponent D is equal to 1, 2 and 3 respectively. For fractal objects, however, the exponent need not be integral.

Polymers are described by equation 11 and are called 'mass fractals'. On the contrary, colloids are 'surface fractals' which are uniformly dense but have a rough surface. Surface fractals share the self-similarity property; however, if the surface is magnified, its geometric features do not change. Mathematically, surface self-similarity is represented by an analog of equation 11:

$$S \sim R^{Ds} \tag{12}$$

where S is the surface area and D_s is the surface fractal dimension. For a smooth object, $D_s=2$, consistent with the notion that a smooth surface is two-dimensional. For fractally rough surfaces, however, D_s varies between 2 and 3, so D_s is a measure of the surface roughness.

Fractals can be characterized by small angle x-ray scattering techniques. The asphalt sample was subjected to x-rays, and the angular dependence of the scattered intensity was measured. For fractal objects,

the intensity profile has a power-law dependence when plotted versus the magnitude of the wave vector K (Martin, 1987):

$$I \sim S^{-2D + D_s} \tag{13}$$

The quantity $P=-2D + D_s$ is called the Porod shape. Through Bragg's law, the parameter S can be related to a characteristic length L and the scattering angle θ ($S=2\pi/L=4\pi\lambda^{-1} \sin\theta$), where λ is the wavelength. By scanning θ, an object on different length scales can be studied effectively. Though there are exceptions to general rules (Martin, 1987), it is usually possible to distinguish structures by the exponent in equation 13. Polymeric (mass fractals where $D_s=D$) systems yield scattering curves with slopes between -1 and -3, whereas smooth colloids give slopes of -4. Rough colloids give slopes between -3 and -4 (Bale, 1984). The analysis of the Porod slopes of SAXS curves is shown in Figure 21 for polymeric and colloidal systems.

The method described above was employed on four of the SHRP asphalts. Figure 22 shows the raw data, empty cell and absorption data for asphalt AAF-1. Correction for the empty cell scattering and absorption was made as:

$$I_{cor} = I_{raw} - [I_{empty\ cell} - I_{abs}] \tag{14}$$

The background correction was made following the method of Ruland (Ruland, 1977). Figure 23 shows the corrected intensity I(s). The power law scattering, $I(s) \sim S^{-P}$ was observed in the range of -7 to -4 of ln s. The exponent P is determined to be 0.8 by the least square method (Figure 24). This is consistent for all asphalts studied.

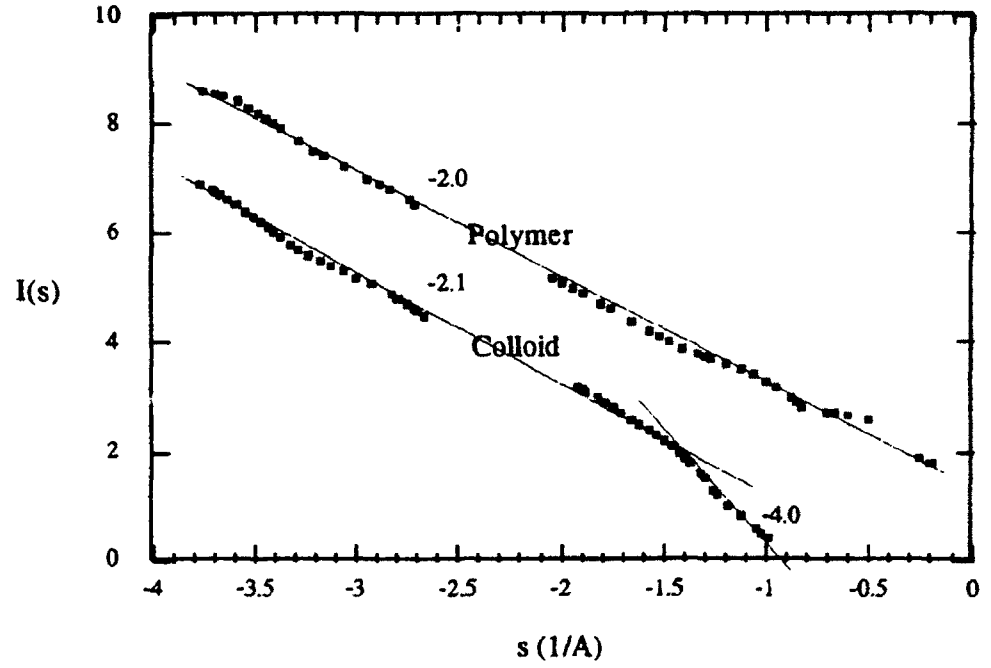

Figure 21. Contrasting SAXS profiles for polymeric and colloidal systems.

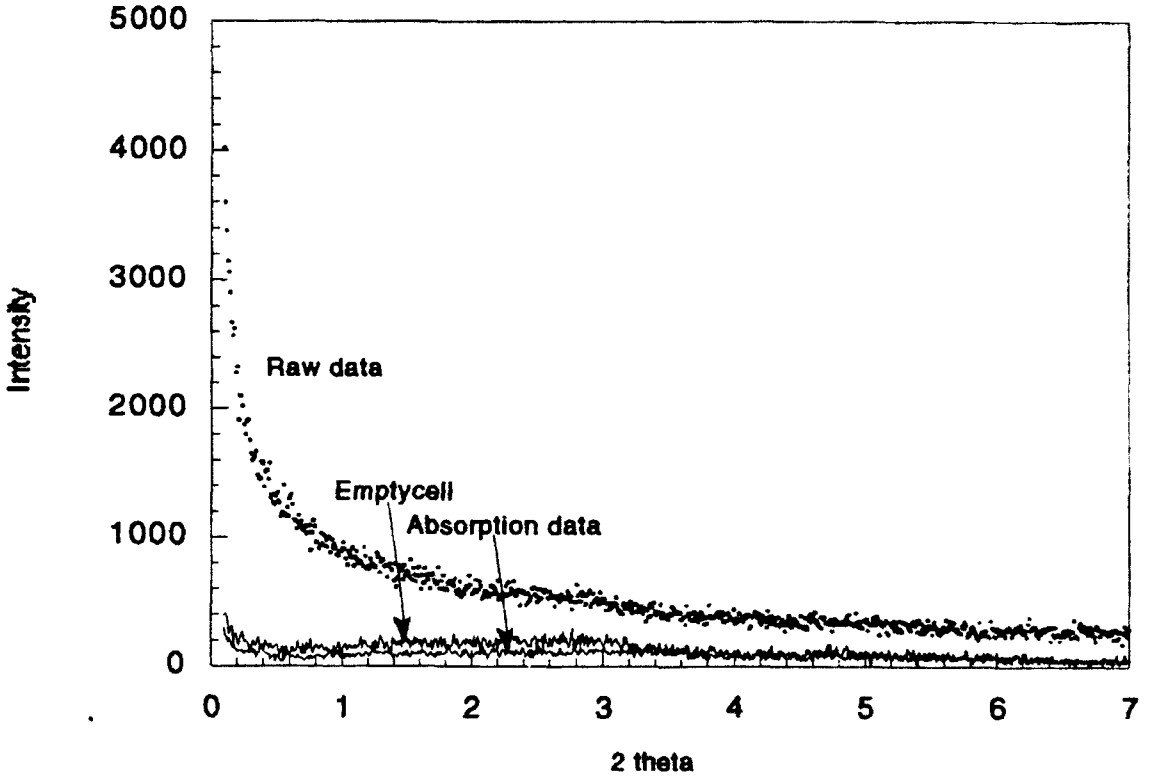

Figure 22. SAXS curves of AAM raw data, empty cell scattering and absorption data.

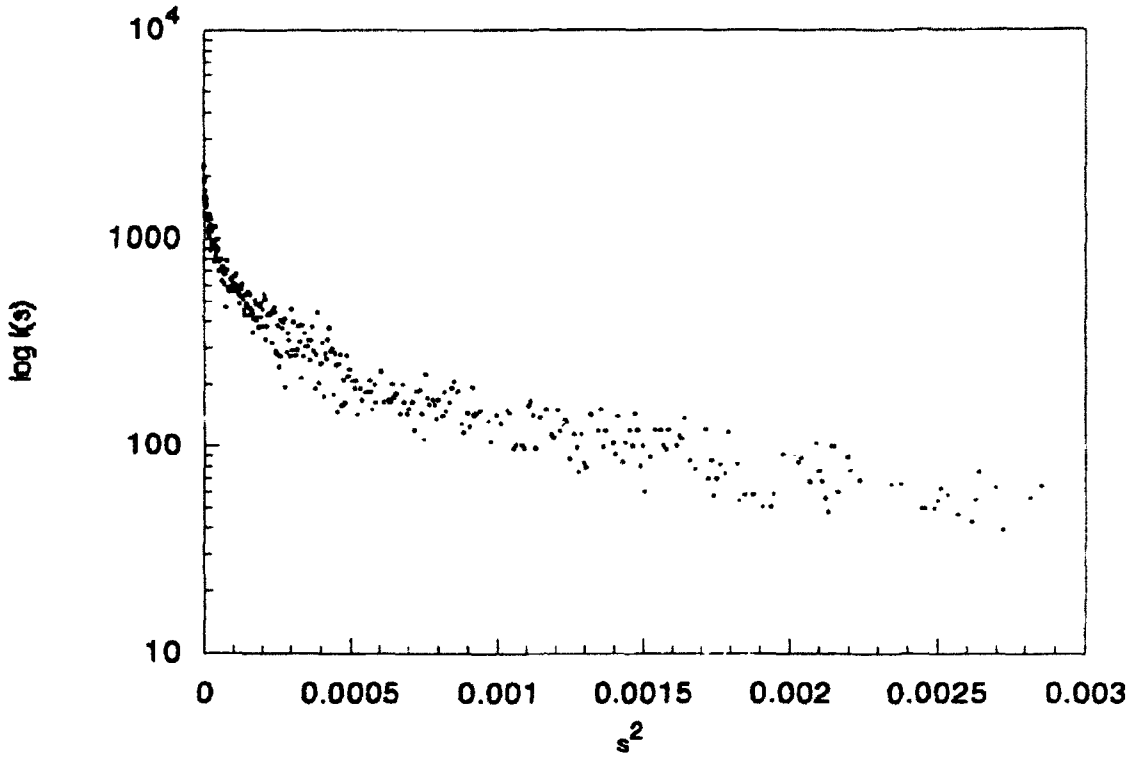

Figure 23. Log I versus s^2 plot of the SAXS curve for AAM asphalt.

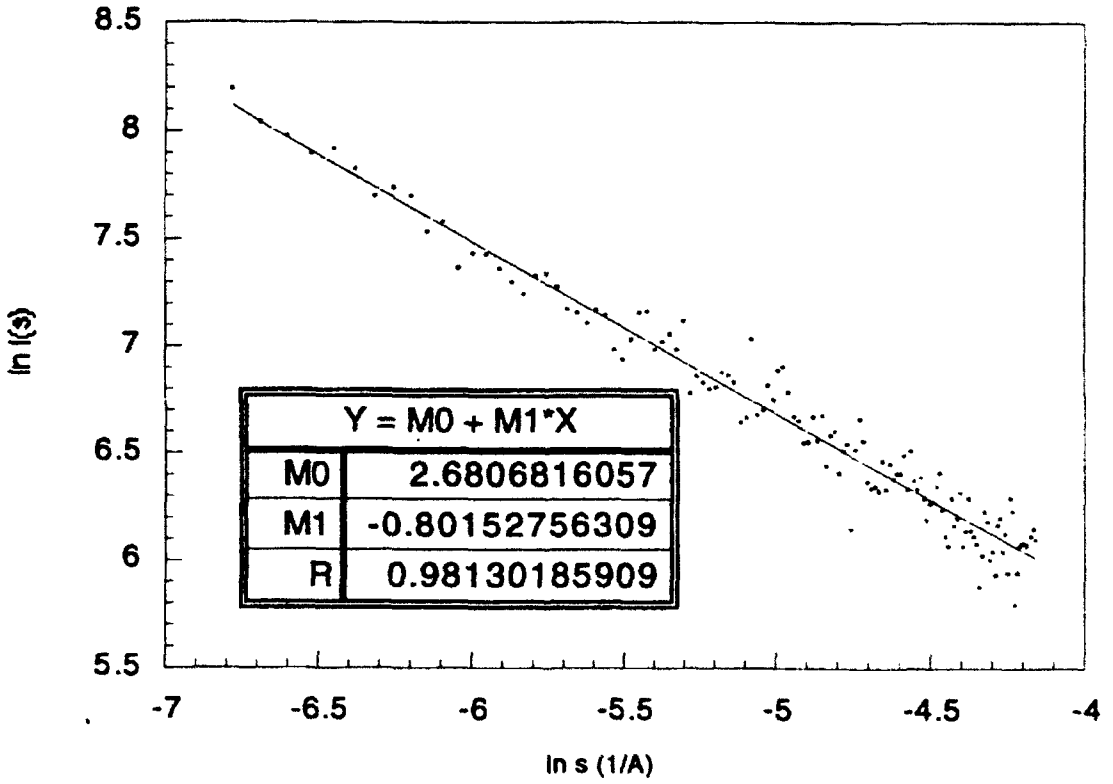

Figure 24. Log-log plot of the SAXS curve for AAM grade asphalt.

RESULTS and DISCUSSIONS

Evaluation of Relaxation Mechanism

The changes in the molecular structure of asphalts were observed in the collective IR absorbence spectra of their stretched state; the perturbations and shoulders at random frequencies indicative of the region of substituents to the aromatics demonstrate the conformational changes to the appendages of the aromatics, Figure 11. Figures 10 shows that most changes occur in the peak ratio of CH_2 and CH_3 bands (721, 1376, and 1457 cm^{-1}). The stretching of the asphalt sample in the IR beam indicated that the methylene structures, irrespective of their position in the molecule (Figure 10), were most active in resisting mechanically - induced stress. The band at 721 cm^{-1} is for skeletal rocking of CH_2 molecules; the band at 1376 cm^{-1} represents the symmetrical bending mode vibration of CH_3 molecules; the band at 1457 cm^{-1} represents the combined symmetrical and asymmetrical bending modes of vibration of CH_2 and CH_3 molecules, respectively.

The length of a methylene chain structure is represented by the ratio of CH_3 and CH_3 molecules present. The higher the ratio, the longer is the representative chain length. The changes observed in the ratio of the peaks of the absorbence bands offered qualitative information only. No fixed pattern or reproducibility was observed for each stage of the stretch on replicates of the asphalt samples. They showed random changes in the peak ratio which indicates high randomness in the orientation and length of asphalt chains. The observation illustrated by Figure 10 suggests that the changes under mechanically - induced stress are due to interactions among and within methyl and methylene molecules. The extent of these changes could not be quantified because the asphalts studied

possess random orientation of the short methylene chains. The representative chain length of the asphalt molecule represented by the ratio of CH_2 (721 cm^{-1}) and CH_3 (1376 cm^{-1}) absorbance of the undeformed sample is compiled in Table 5. Stewart (1957) suggested this absorbance as indicative of the presence of bulk assemblies of aliphatic hydrocarbon chains in an asphalt molecule.

The strength of the asphalts was evaluated by the relaxation spectrum obtained from the master curves of the storage and loss moduli. The master curves were constructed on analysis of the dynamic mechanical test data explained previously. The experiment was carried out in the temperature range of 25°C to 65°C, and the master curves were constructed at 25°C reference temperature. The absence of the rubbery plateau in the master curves of the asphalts suggests single relaxation transition for asphalts. This indicates that the asphalts demonstrate the polymeric solution type behavior.

The plot in Figure 25 demonstrates the dependence of the relaxation strength of asphalts on their representative chain length. The slope of the log zero shear viscosity and log CH_2/CH_3 plot is 4.2 with considerable scatter among the data. The reptation model (De Gennes 1990; Baumgaertel el. al. 1990; Doi and Edwards 1986; Aklonis 1983) of polymeric solutions established that the slope is 3.45 with almost no scatter of data. This suggests that the asphalts lack true similarity with the polymeric solutions. The polymer solution models are indeed for the high molecular weight chains. The asphalts are low molecular weight hydrocarbons, and, therefore, the polymer solution models would not truly apply to them. However, the dependence of the relaxation behavior of the asphalts on their chain length was observed. The deviation from the polymer solutions

Table 5. The values of the ratio of peak absorbance of CH_2 (721 cm^{-1}) and CH_3 (1376 cm^{-1}), and the relaxation strength of the asphalts.

Asphalt Type	Ratio of CH_2 (721 cm^{-1}) and CH_3 (1376 cm^{-1}) Absorbance	Zero Shear Viscosity (Poises)
A	0.342	2.95e+05
B	0.284	9.16e+05
C	0.624	1.78e+07
D	0.409	3.14e+06
E	0.412	4.23e+06
F	0.386	1.17e+06
G	0.406	1.19e+06
H	0.397	2.59e+06
I	0.384	1.89e+06
J	0.288	4.90e+05
K	0.376	3.76e+06

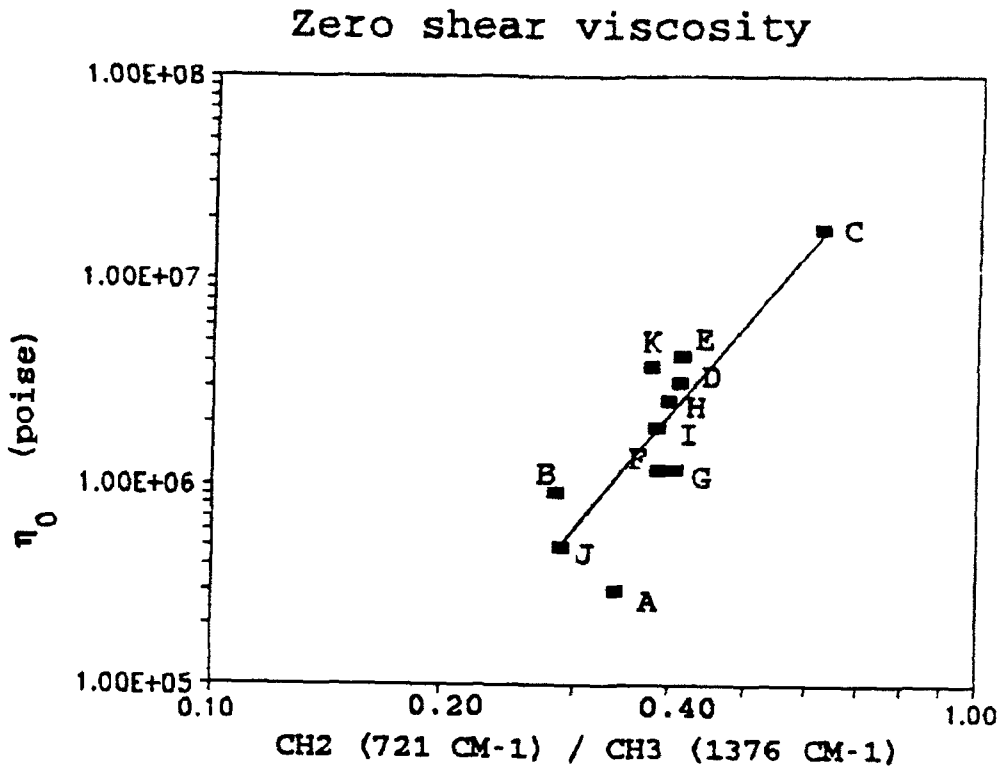

Figure 25. Chain length dependence of relaxation strength of the asphalts. η_o is the zero shear viscosity.

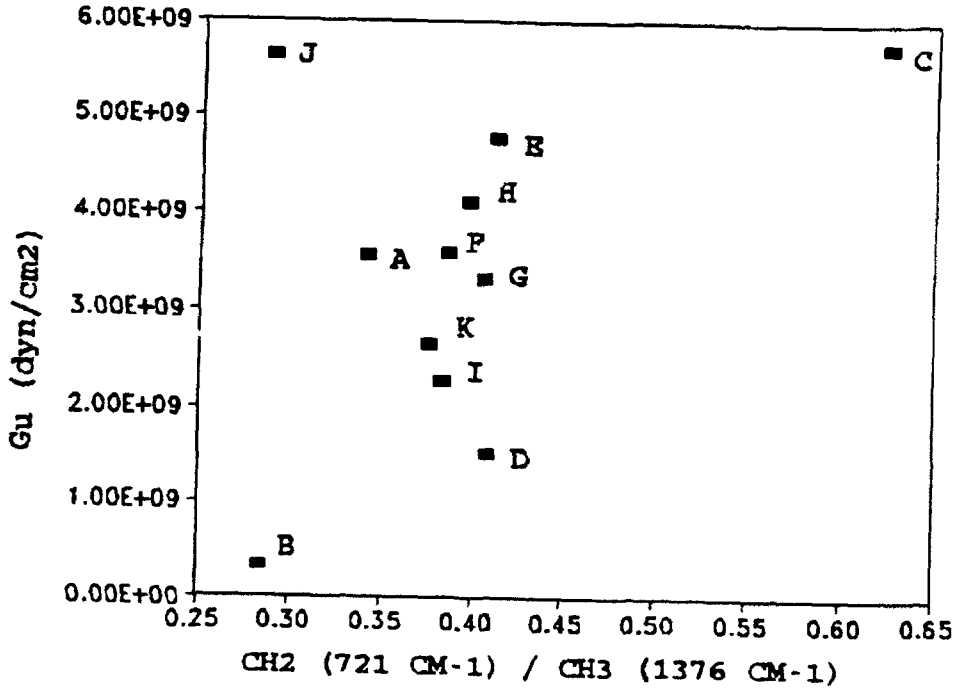

Figure 26. Unrelaxed relaxation strength versus chain length of the asphalts.

indicates that the asphalts are also strongly influenced by their dispersed structure.

The analysis of the generic fractions of the asphalts (Table 4 and Figure 12) with zero shear viscosity did not show any significant correlations. It suggests that no component of the Corbett fraction can by itself explain the physical property of asphalt. A plot of unrelaxed modulus of asphalts (unrelaxed modulus is obtained from discrete relaxation spectra at infinitely small time common to all the asphalts) shown in Figure 26 demonstrates correlation (except the asphalt type J) with their representative chain lengths. Asphalt type J, although having an abnormally high initial modulus, does not maintain the long term resistance against flow; its initial high modulus might be due to highly polar and interactive asphaltene fractions. Table 4, and Figure 12, showed that type J asphalt has the highest asphaltene percentage. But, since asphalt J has the smallest representative methylene chain length it lacks the long term potential of resistance against flow.

CONCLUSIONS FROM THE RHEOLOGICAL AND RHEO-OPTICAL STUDY

It was the objective of this effort to probe the relationship between asphalt's molecular structure and the viscoelastic properties observed for the asphalt. The bulk assemblies of the methylene chains in asphalts were observed to be most active in resisting mechanically-induced stress. This result is concluded from the rheo-optical studies in which specific IR bands were observed to change during shear deformation of the asphalt. The ratio of methylene to methyl absorbence in the IR spectrum offered a method of evaluating the representative length of the methylene chains in an asphalt. The methyl and methylene

absorbence bands used for the study were 1376, and 721 cm^{-1}, respectively. The methylene band, 721 cm^{-1}, represents aliphatic (CH_2) n>4 hydrocarbons in asphalts. Utilizing this information, a correlation between the asphalt's chain "length" and the viscoelastic properties of these materials was determined. In particular, the relaxation spectrum of asphalt was employed to evaluate zero shear viscosity which is a measure of long term resistance against flow. The study demonstrated the dependence of the asphalt's long term resistance against flow on the representative length of the methylene chains.

The plot of the log of the representative length of the methylene chains vs. log of the zero shear viscosity showed considerable scatter. However, the slope of the plot is 4.2. As reported in the literature, for the true polymeric solutions, the data do not show scatter and the slope of the plot is 3.45. This demonstrates the influence of the dispersed structure on the relaxation behavior of asphalts.

When comparing the two asphalt models in review today, this data would suggest that a model supporting a colloid type structure is unlikely. The x-ray data does not suggest the existence of colloid structures (in the range employed for x-ray analysis) but instead, suggests the exist of linear type structures. This is in agreement with the rheo-optical data, suggesting that "linear" structures control the viscoelastic deformation of these materials. These linear structures are interconnected through a virtual network providing the structure needed to justify the observed mechanical properties. This proposed organization is not unlike the DPF model. The polar interactions form the virtual network with a number of linear structures (appendages to the aromatic structures) thereby controlling the visocelastic nature of the asphalt. More work is needed to further investigate this phenomenon.

CHAPTER 3

MICRODAMAGE HEALING IN ASPHALT CONCRETE

BACKGROUND

General

Texas Transportation Institute has been studying the concept of fracture healing for almost ten years. The concept of healing was identified in the polymer literature by TTI researchers, and its application to asphalt cement and ultimately to asphalt concrete pavements was immediately realized. Based on the work of Balbissi (1983), Tseng and Lytton (1968) hypothesized the link between fracture healing and the substantial delay (shift) between the laboratory fatigue relationship and the time at which fatigue cracking actually occurs in the field. Lab-to-field shift factors which have been reported in the literature based on empirical correlations are in the range of from 3 to 100. One of the most reliable lab-to-field shift factors, and most widely used, was that developed by Finn et al. (1977) in an evaluation or AASHTO Road Test data. He found the shift between laboratory fatigue and field cracking (10 percent) to be approximately 13.

Lytton (1992), in his work in the Strategic Highway Research Program (SHRP) study stipulates that through the application of mechanics to pavement materials the fatigue shift factor can be defined as being composed of three principal components:

1. Residual stresses due to the plasticity of the pavement layers.
2. Dilatancy stresses due to expansion of paving materials under large confining pressures under passing wheel loads.
3. Healing of microcracks and macrocracks.

Healing is assisted by the pressure induced by dilatancy stresses as these pressures can aid in pushing microcrack close together. In keeping with the consensus in the literature, Lytton (1992) proposes that the composite shift factor ranges from 3 to 100+ and is composed of the three components discussed above in a multiplication form:

$$\underset{SF}{(\text{Overall})} = \underset{SF_r}{(\text{Residual Stress})} \times \underset{SF_d}{(\text{Dilatancy Stress})} \times \underset{SF_h}{(\text{Healing})}$$

(Range 3-100+) (Range = 1/3-3) (Range = 1-4) (Range = 1-10)

Lytton (1992) bases his predictions of range in shift factors on an extensive study of performance of SHRP pavement sections.

Historical Work on Healing in Asphalt and Polymeric Materials

Bazin and Saunier (1967) introduced rest periods to asphalt concrete beam samples which had previously been failed under uniaxial tensile testing. They reported that a dense graded asphalt concrete mix could recover 90 percent of its original tensile strength after 3 days of recovery at 25°C. The researchers then performed cyclic fatigue tests. In these tests an asphalt concrete beam was loaded cyclicly until fatigue failure occurred. The beam was then allowed to rest and recover, and a cyclic load was again applied until fatigue failure reoccurred. The ratio of number of cycles to failure after the rest period to number of cycles to failure before the rest period was evaluated. This ratio was over 50 percent after one day of rest and with a 0.213 psi pressure used to press the crack faces together. This research clearly showed the evidence of healing even though the rest periods and pressures were not necessarily realistic in terms of their ability to duplicate pavement conditions.

Despite the relatively small amount of historical research in the area of asphalt concrete healing, the mechanism of healing within polymeric materials has been intensely studied. Prager and Tirrell (1981) described the healing phenomenon:

> "When two pieces of the same amorphous polymeric material are brought into contact at a temperature above the glass transition, the junction surface gradually develops increasing mechanical strength until, at long enough contact times, the full fracture strength of the virgin material is reached. At this point the junction surface has in all respects become indistinguishable from any other surface that might be located within the bulk material - we say the junction has healed."

Wool and O'Connor (1981) identified stages of the healing process which influence mechanical and spectroscopic measurements: (a) surface rearrangement, (b) surface approach, (c) wetting, (d) diffusion and (e) randomization. Kim and Wool (1983) introduced the concept of minor chains and described the diffusion model. Later de Gennes (1971) explained the microscopic sequences in a reptation model related to the Kim and Wool diffusion and minor chains model. The term "reptation" was defined as a chain travelling in a snake-like fashion, due to thermal fluctuation, through a tube-like region created by the presence of neighboring chains in a three-dimensional network. de Gennes explained that the wiggling motions occur rapidly, that their magnitudes are small and that in a time scale greater than that of the wiggling motions, a chain, on average, moves coherently back and forth along the center line of the tube in a certain diffusion constant, keeping its arc length constant.

Macromechanically, the most common technique used to describe the healing properties of polymers is to measure fracture mechanics parameters of a specimen which has healed. The fracture properties often used to evaluate healing potential are: energy release rate, G_I; stress intensity factor, K_I; fracture stress, σ_f and fracture strain, ϵ_f. These properties are dependent on the duration of the healing period, temperature, molecular weight and pressure applied during the healing period.

Kim and Wool (1983) used the critical energy release rate, G_{IC}, to define the portion of a chain that escapes from the tube-like regions defined earlier and influence the healing process through reptation-type interaction. Their model predicted that:

$$G_{IC} \sim t^{0.5} M^{-0.5} \tag{15}$$

where t is the duration of the healing period, and M is the molecular weight. They also proposed the following experimental relationship:

$$\frac{\sigma_{fh}}{\sigma_o} \sim \frac{t^{0.25}}{M^{0.75}} \tag{16}$$

where σ_{fh} is the fracture healing strength, and σ_o is the original strength.

The temperature dependence of healing mechanisms has been reported by many researchers (Bonnaure et al. (1962), Balbissi (1982), Bazin and Saunier (1967) and Wool and O'Connor (1981)). An increase in the test temperature shifts the recovery response to shorter times. Wool and O'Connor (1981) have constructed master healing curves by time-temperature superposition. Researchers in the area of polymer healing have also reported on the restoration of secondary bonds between chains

of microstructural components and that van der Waals forces or London dispersion forces play a very important role in healing, Wool (1979). Surface forces, electrostatic forces and hydrogen bonding have been reported to induce adhesive healing Briscoe (1978). It has also been pointed out that adhesive forces and the bulk viscoelastic properties of the "hinterland" adjacent to the interface are the most important factors in the adhesion of elastomers, Briscoe (1978).

Other healing research, De Zeeuw and Potente (1977) and Buckrall (1980), touts the orientation and interpenetration of the flowing material as influencing the strength of the crack healing effect and that this flow is dependent on healing temperature, contact period and the extent of melt displacement.

In order to understand the healing mechanism of asphalt concrete, it is helpful to keep the healing models developed for polymers in mind. Petersen (1984) claims that the association force (secondary bond) is the main factor controlling the physical properties of asphalt. That is, the higher the polarity, the stronger the association force, and the more viscous is the faction, even if molecular weights are relatively low. Petersen (1984) also presented a vivid description of the effect of degree of peptization on the flow properties as follows:

> "Consider what happens when a highly polar asphaltene fraction having a strong tendency to self-associate is added to a petrolene fraction having a relatively poor solvent power for the asphaltenes. Intermolecular agglomeration will result, producing large, interacting, viscosity-building networks. Conversely, when an asphaltene fraction is added to a petrolene fraction having relatively high solvent power for the

asphaltenes, molecular agglomerates are broken up or dispersed to form smaller associated species with less inter-association; thus, the viscosity-building effect of the asphaltenes is reduced."

Traxler (1960) also suggested that the degree of dispersion of the asphalt components is inversely related to the complex (non-Newtonian) flow properties of the asphalt. Kim and Little (1988) offer a much more complete review of the literature on fracture healing.

Recent Developments in Research Affecting Fracture Healing

Work by Balbissi (1983) used extensive lab testing with a controlled displacement crack propagation device (called the "overlay tester") to determine values of a healing-based shift factor which was calculated based on the theoretical model of the shift factor developed by Lytton (1980). The shift factors calculated by Balbissi (1982) ranged from 3 to 17.

Following this work, Kim, Little and Benson (1990) performed more sophisticated testing and analysis of fracture healing using much improved testing equipment. They developed a concept called the healing index and found it to be highly sensitive to the binder used in the controlled displacement fracture healing test. They also found that the healing index was related to the chemical properties of the asphalt cement and not just to viscoelastic properties. This was determined by using a nonlinear viscoelastic correspondence principle which is able to separate the time dependency effects from "chemical healing" or re-bonding of microfractures. After separating these effects, the magnitude

of chemical healing was calculated as was the healing index which resulted from this chemical healing.

A very significant breakthrough in the understanding of the effect of the composition of the asphalt on the healing of asphalt was made by Kim, Little, and Benson, (1990). They found that healing was directly proportional to the amount of longer-chained aliphatic molecules in the saturates and long-chained aliphatic side chains in the napthene aromatics, polar aromatics and asphaltenes generic fractions. They used methylene to methyl ratio (MMHC) as a quantifier of the nature of the long-chained aliphatic molecules and side chains. The MMHC is defined as the ratio of the number of methyl and methylene carbon atoms in independent aliphatic molecules or aliphatic chains attached to cycloalkanes or aromatic centers. Benson (1988) also found indications that the L. E. T. C. settling test is a predictor of healing but did not have sufficient data to thoroughly investigate this hypothesis. However, this finding is in keeping with Petersen's view of the effects of peptization on flow properties.

The findings of Benson (1988) are significant for the following reasons:

1. Microcrack healing of polymers have been ascribed to reptating, wiggling, long-chain molecules moving across fracture faces and restoring original strength. The significance of Alkane chain length in microfracture healing of asphalt concrete is that it offers some commonality between polymer and asphalt healing as well as offers a credible explanation.
2. Aliphatic chains were not found to be limited to the Corbett saturate fraction in the work by Benson and Little (1988) but

were instead found to be present as appendages to naphthene aromatics, polar aromatics and asphaltene fractions. This is illustrated in Table 6 for the nine asphalts evaluated by Benson and Little (1988). The CH_2/CH_3 ratio in this table was determined from NMR spectra and is indicative of aliphatic chain length.

3. Using the data in Table 6 to approximate aliphatic chain lengths for each generic fraction indicates that the Shamrock asphalt should have the greatest fracture healing potential followed by the Texaco asphalt, the Fina asphalt and the Witco asphalt. This was indeed the case.
4. The MMHC ratio is the ratio of the numbers of methyl and methylene hydrogen atoms to methyl and methylene carbons in independent aliphatic chains attached to cyclic akane or aromatic centers. This ratio increases as the ratio of methyl hydrogen to methylene functional groups increases in increasingly branched chain alkane material. This parameter is calculated from IR absorbance or vibrations occurring in spectral areas 3 and 7. This MMHC ratio, indicating branching of aliphatic chains demonstrates a strong correlation to microfracture healing.
5. Estimates of n-alkane carbon numbers, C_T, can be made using the MMHC ratio and the IC absorbance peak ratios: a_{1380}/a_{2920}. Based on graphical relationships such as that shown in Figure 27, C_T values were computed for each asphalt fraction as summarized in Table 7.

Table 6. An overall comparison of estimated ^1H NMR methylene/methyl proton ratios for the four generic fractions for nine kinds of asphalt cement (n = 1) (After Benson, 1988).

Asphalt Cement Source/Grade	$-CH_2/-CH_3$ Ratios			
	Saturates	Napthene Aromatics	Polar Aromatics	Asphaltenes
Fina				
AC-5	3.2	2.9	3.0	2.9
AC-20	3.3	2.8	3.2	3.7
Shamrock				
AC-5	4.4	5.0	2.9	7.6
AC-20	3.9	3.4	3.6	3.4
Texaco				
AC-5	3.3	3.7	2.9	4.9
AC-20	3.8	4.7	4.0	4.2
Witco				
AR-1000	2.0	2.3	1.7	3.2
AR-2000	3.9	2.3	1.6	3.7
AR-4000	2.1	2.8	1.8	3.5

Table 7. Estimated average n-alkane carbon numbers, C_T, of aliphatic portions of asphalt cement generic fractions (After Benson, 1988).

Asphalt Cement	Saturate Molecules C_T	Napthene Aromatic Chains C^T	Polar Aromatic Chains C^T	Asphaltene Chains C^T
Fina AC-5	14	10	5	4
Fina AC-20	10	9	7	3
Shamrock AC-5	9	7	7	5
Shamrock AC-20	19	13	5	10
Texaco AC-5	7	6	5	8
Texaco AC-20	7	9	9	3
Witco AR-1000	7	8	4	3
Witco AR-2000	11	7	4	4
Witco AR-4000	7	7	4	3

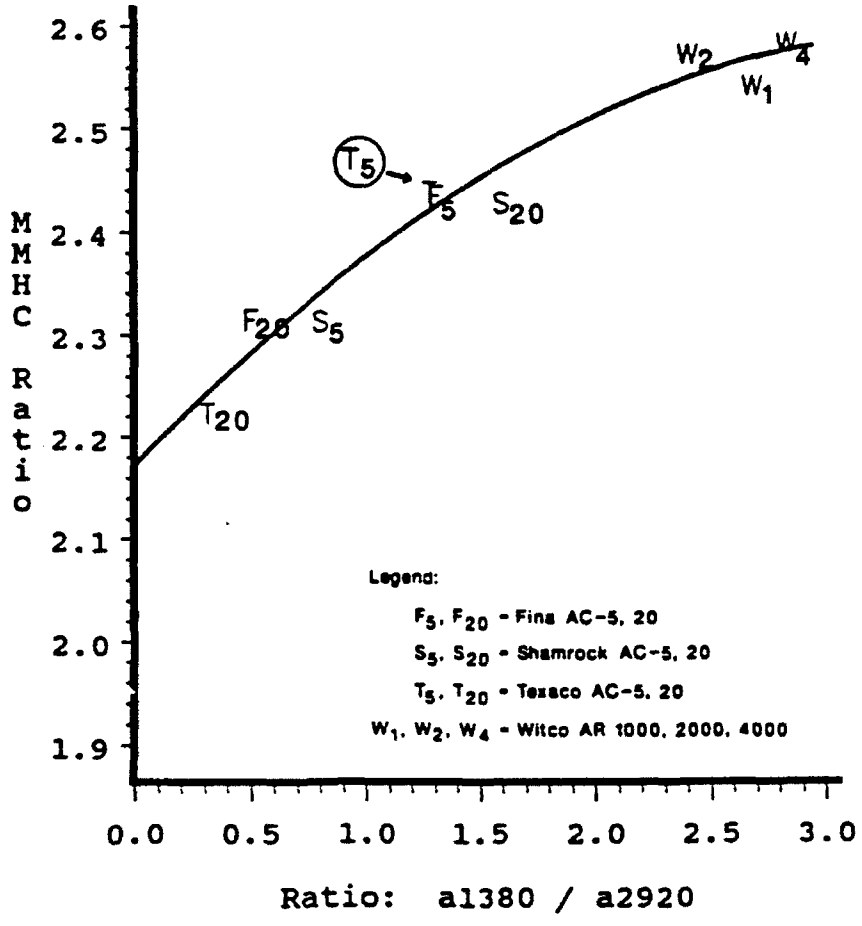

Figure 27. Best fit least squares line placed through data for MMHC ratio versus ratio of a_{1380} to a_{2920} for polar aromatics with 0.301 substituted (After Benson, 1988).

6. Figure 28 shows the approximate relationship between healing index and MMHC as developed by Benson and Little (1988).

The most statistically significant independent data variable defining chain length was found by Kim et al. (1990) to be the MMHC ratio from the FT-IR analysis of the generic fractions spectra. The most significant dependent variable for healing was the healing index, HI.

The equations or models for healing that arose from using MMHC data were as follows:

(1) $HI = -19.70 + 18.50\ (MMHC) - 4.248\ (MMHC)^2$, ($R^2 = 0.996$), where strain amplitude = 0.00674 units,

and

(2) $HI = -11.14 + 10.82\ (MMHC) - 2.529\ (MMHC)^2$, ($R^2 = 0.966$), where strain amplitude = 0.0092 units.

These curves are shown in Figure 29.

Based on the results of this research, Benson and Little (1988) stated that appendages of high methylene to methyl ratios on the various generic fractions significantly influence healing. However, how these appendages influence healing is not known. The healing mechanism is also related to asphalt flow properties which are, in turn, related to molecular interactions within the asphalt. The molecular interactions consist of secondary bonds or association forces that are one to two orders of magnitude weaker than the covalent chemical bonding forces that hold the atoms together in the molecule. The association forces are significantly different from covalent bonding forces in that they are generally reversible and are usually in dynamic equilibrium. That is,

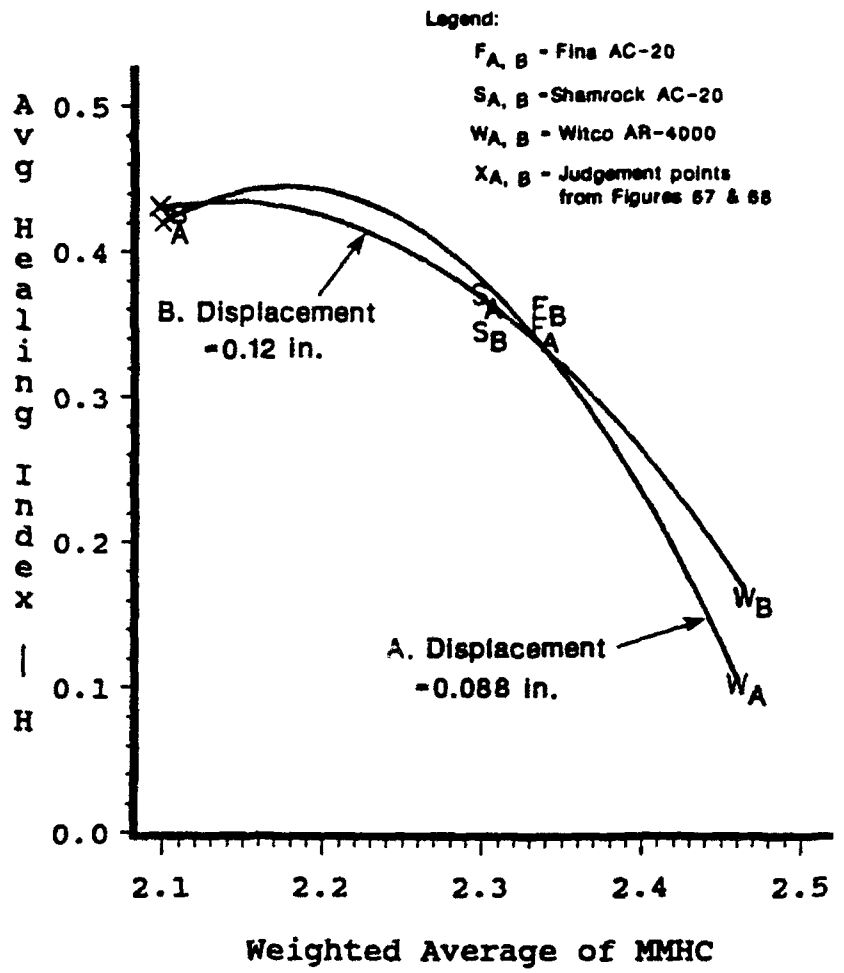

Figure 28. Proposed asphaltic concrete healing model of healing index, HI, versus weighted average aliphatic MMHC of asphalt cements (After Benson, 1988).

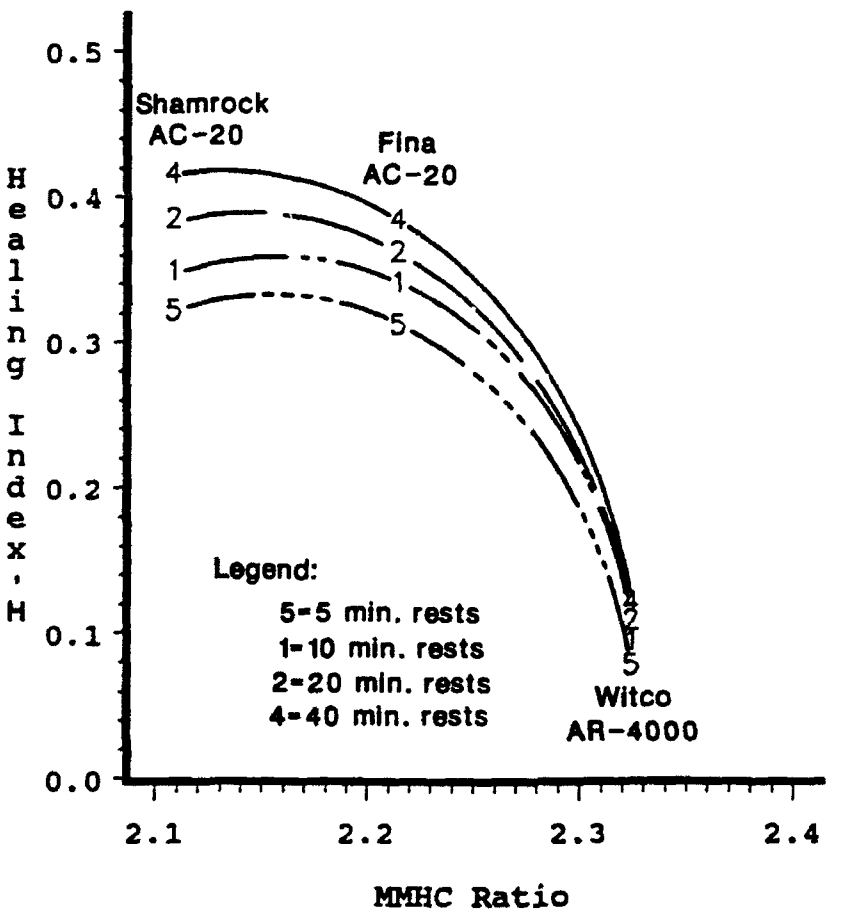

Figure 29. Healing index, HI, versus MMHC ratios for saturates generic fractions, with 0.301 substituted (After Benson, 1988).

they "make" and "brake" under forces induced by such factors as temperature and external stress.

It may be that after reassociation is established by association forces, the commingling of the aliphatic chains may contribute to healing. It also may be that longer aliphatic side chains on the various generic fractions help to maintain the dispersion necessary for flow and eventual microcrack healing.

Furthermore, a major reason for steric structuring in asphalt may occur within the asphaltene and other highly structured aromatic fractions (such as the polar aromatics). This may, in part, be due to association among the poly-nuclear aromatics due to interplaner bonding. This interplaner bonding is probably due to pie-bonds formed when the two-dimensional planes of polynuclear aromatic (such as anthracene) overlap closely enough. These pie-bonds are the result of the cumulative pie-sigma bonds in the benzene rings. Since these interplaner bonds can only occur if planes approach each other very closely, any appendages on the polynuclear aromatics, such as aliphatic chains, could prevent interplaner bonding and hence structuring. The result could be greater fluidity, better dispersion of molecular species and, thus, greater healing potential.

The work in this study continues to verify the importance of aliphatic appendages or "side chains" on the mechanical responses of asphalt concrete. This study concludes that for the asphalts studied, the structure is not comprised of large colloids but of a dispersed polar entities. These entities may be comprised of naphthenic or aromatic based structures, but these structures are apparently highly influenced by aliphatic appendages which play an important if not a dominate role in relaxation and microstructural damage healing.

The role of the aliphatic side chains in the mechanism of relaxation as discussed in Chapter 1 together with the importance of the aliphatic chain length in promoting microfracture healing as discussed by Benson and Little (1988) offers a separate and consistent verification of the importance of this species in the mechanistic performance of asphalt concrete. Perhaps these findings are verifications of Petersen's (1984) thoughts concerning the effects of association forces and dispersions on the flow and hence fracture healing properties of asphalt concrete.

Thus this "latest" model of the asphalt microstructure is most certainly one that accommodates the phenomenon of "healing". In this model, the viscoelastic properties of the asphalt, and its response to load and temperature-induced stress, result directly from the making and breaking of bonds between polar molecules. When the asphalt is subjected to stress, these secondary bonds are broken and reformed continuously. The result is that the molecules move relative to each other. This is an excellent description of "healing".

The latest SHRP studies do indeed offer encouragement that the healing phenomenon can be better understood by carefully considering the DPF model in an experimental matrix of mechanical healing tests.

USE OF NON-LINEAR VISCOELASTIC CORRESPONDENCE PRINCIPLE TO ANALYZE FRACTURE HEALING DATA

In his Ph.D. dissertation, Kim (1988) used the theory of non-linear viscoelasticity and the correspondence principle II to quantify healing. This principle states that using physical stresses with pseudo displacements one can reduce the nonlinear viscelastic problem to a nonlinear elastic case. The explicit form of the constitutive equation

between stresses and pseudo displacements is dependent on material type, sample geometry and loading history.

When a viscoelastic material is subjected to cyclic loading, a hysteresis loop is usually observed in the stress-strain diagram. According to correspondence principle theory for non-uniformly stressed bodies, such as a beam with a crack, the hysteresis loop will disappear in the nominal stress-pseudo strain plot if damage growth is negligible during the loading history. That is, the relationship between stress and pseudo strain is a single-valued function. Furthermore, even when the loading paths before and after rest periods are compared, this elastic-like behavior will be maintained, if negligible damage or healing has occurred. This is because the relaxation during the rest period is taken into account by integrating the convolution integral from the initial loading time to the present time.

When damage is large, the stress will decrease in displacement-controlled testing as the number of cycles increases. The difference in the stress at the same pseudo strain level is due to the damage growth in the sample. If rest periods are introduced in the loading history and relaxation is the only phenomenon occurring during the rest period, the stress after the rest period should be equal to or less than the stress before the rest period for the same pseudo strain, based on correspondence principle theory. If the stress after the rest period is larger than the stress before the rest period, at the same pseudo strain level, the increase in stress must logically be attributed to some chemical healing mechanism.

The concept outlined above was used by Kim and Little (1988) to evaluate the healing potential of different asphalt cements and different

asphalt concrete mixtures. In this evaluation the following types of tests were performed:

a. relaxation tests,
b. constant-strain-rate simple loading tests with rest periods. The magnitudes of displacements were within the linear viscoelastic range of the material (negligible permanent damage) and
c. constant-strain-rate simple loading tests with rest periods. The magnitudes of displacements in this test series resulted in crack growth.

The testing apparatus used in this testing protocol by Kim and Little is shown in Figure 30. The test applies a uniaxial tensile displacement, which is carefully controlled. The crack propagates from a pre-existing crack notched into the beam. The crack growth is monitored as shown in Figure 31. Here the macrocrack and the microcracks within the damage or process zone are clearly shown. It is the microcracks that are primarily affected by the healing process. The video of the process of crack propagation during the cyclic loading with rest period process clearly proved that the microcracks disappear after the rest period, visually confirming the healing process.

The loading history applied for test series b and c is shown in Figure 32. The numbers of initial simple loading cycles for tests b and c were 10 and 20, respectively. Then a set of four rest periods of 5, 10, 20 or 40 minutes duration was introduced in a random sequence. Five cycles of simple loading were applied after each rest period, and this loading pattern (rest period followed by five cycles of simple loading)

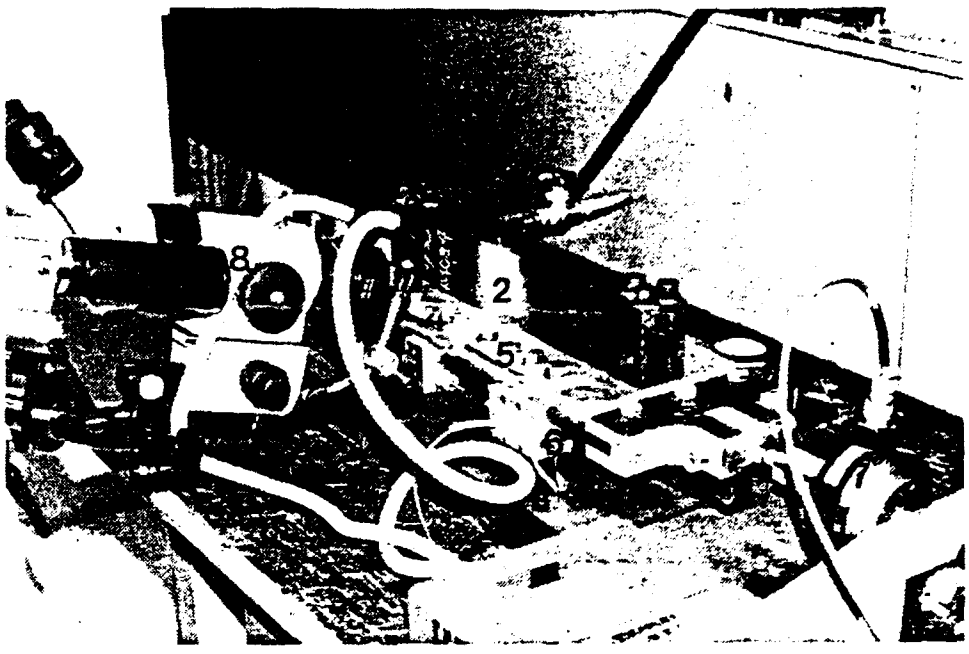

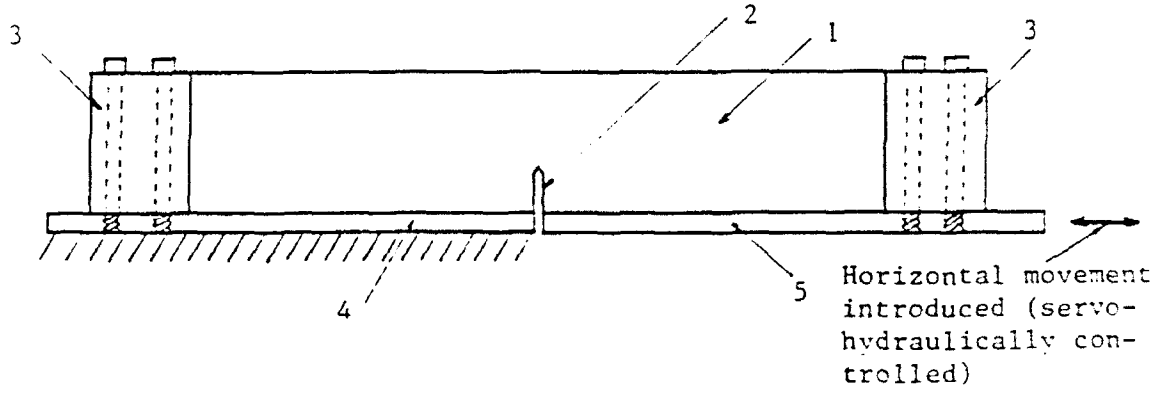

1. Beam epoxied to metal end support.
2. Sharp-tipped notch (introduced in some beams).
3. Metal end support.
4. Fixed platen.
5. Moving platen.
6. L.V.D.T. (connected to M.T.S. controller)
7. Load cell.
8. Microscopic video camera.

Figure 30. Picture and schematic presentation of uniaxial testing apparatus (After Kim, 1988).

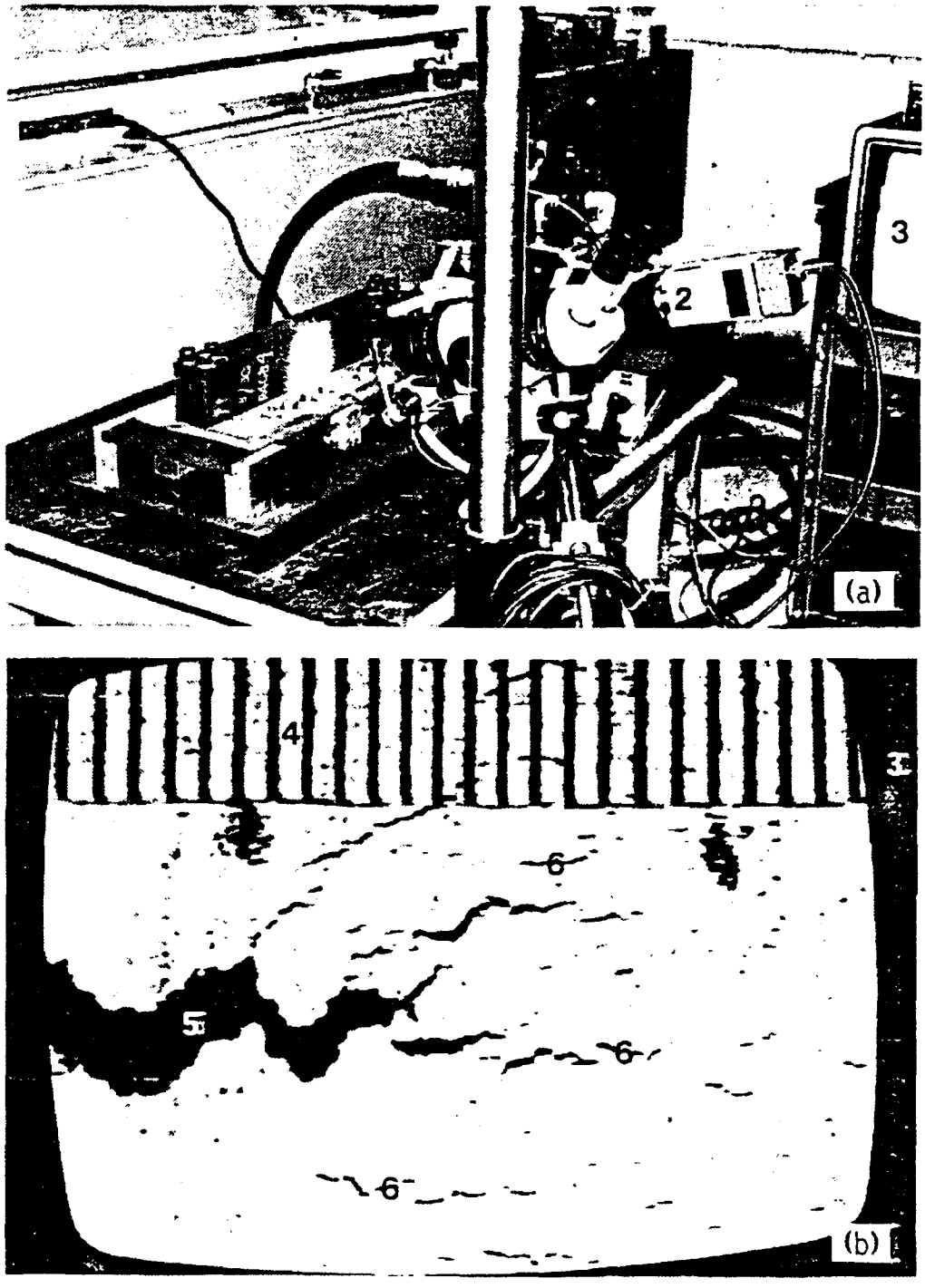

1. Beam sample with a sharp-tipped notch.
2. Microscopic video camera. 3. TV monitor.
4. Chartpak pattern film (0.02 in. between lines).
5. Macrocrack. 6. Microcracks.

Figure 31. (a) Microscopic video camera with testing apparatus. (b) Image of cracking area pictured from TV monitor. (After Kim, 1988).

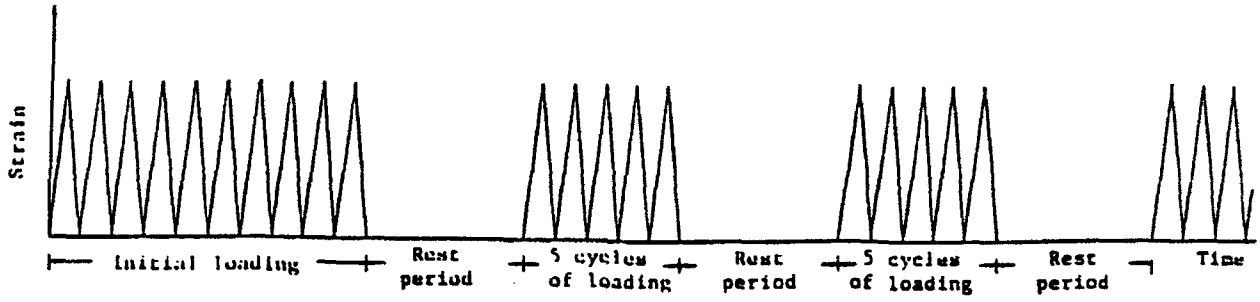

Figure 32. Strain history for tests "b" and "c" (After Kim, 1988).

was repeated until 3 repetitions for each rest period length were achieved.

The results of test series b demonstrated the applicability of the correspondence principle. The stress-pseudo strain plots of the first ten cycles and the cycles before and after the 40-minute rest period are presented in Figures 33 and 34, respectively. As shown in Figure 33, the loading and unloading paths of the first ten cycles practically fall on the same line. Also, in Figure 34, the stress-pseudo strain curves before and after the 40-minute rest period are practically the same.

Figure 35 shows loading and unloading paths for the initial 20 loading cycles. The stress-pseudo strain behavior before and after the 40-minute rest period is plotted in Figure 36. The first point to note in Figure 36 is that loading and unloading paths form a hysteresis loop which disappears after applying the correspondence principle to the test b series results. However, under the conditions of test c (i.e., damage accumulation through crack growth), visual dissipation of energy is due to the damage growth in the sample. Since the test was performed in a controlled strain mode with a constant strain amplitude, the stress at a selected pseudo strain level became smaller as cycling continued.

In Figures 35 and 36, the first loading path is different from the rest of the loading paths. The reason for this is that the largest pseudo strain in the loading history for the first loading is different from that in the remaining cycles. That is, the largest pseudo strain in the first loading is the current pseudo strain, while the largest pseudo strain in subsequent loading applications is a constant which is the largest pseudo strain during the first period. The effect of the largest pseudo strain on the constitutive relationship between stress and strain

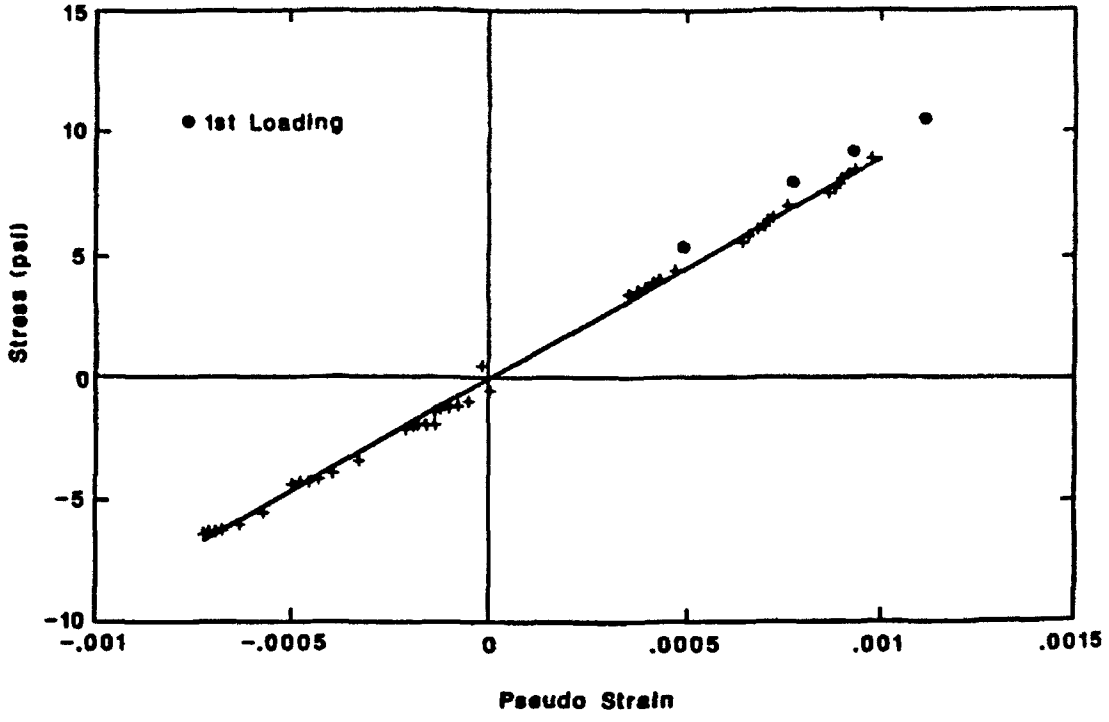

Figure 33. Stress versus pseudostrain of initial 10 cycles with negligible damage (After Kim, 1988).

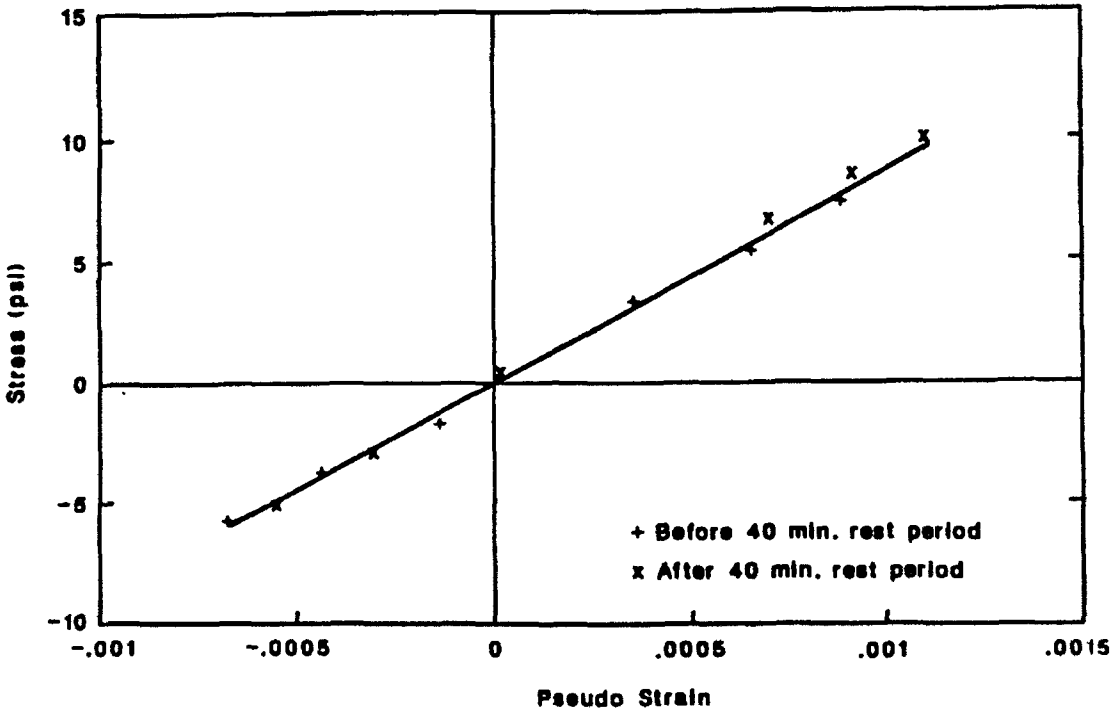

Figure 34. Stress versus pseudostrain before and after 40-min rest period with negligible damage (After Kim, 1988).

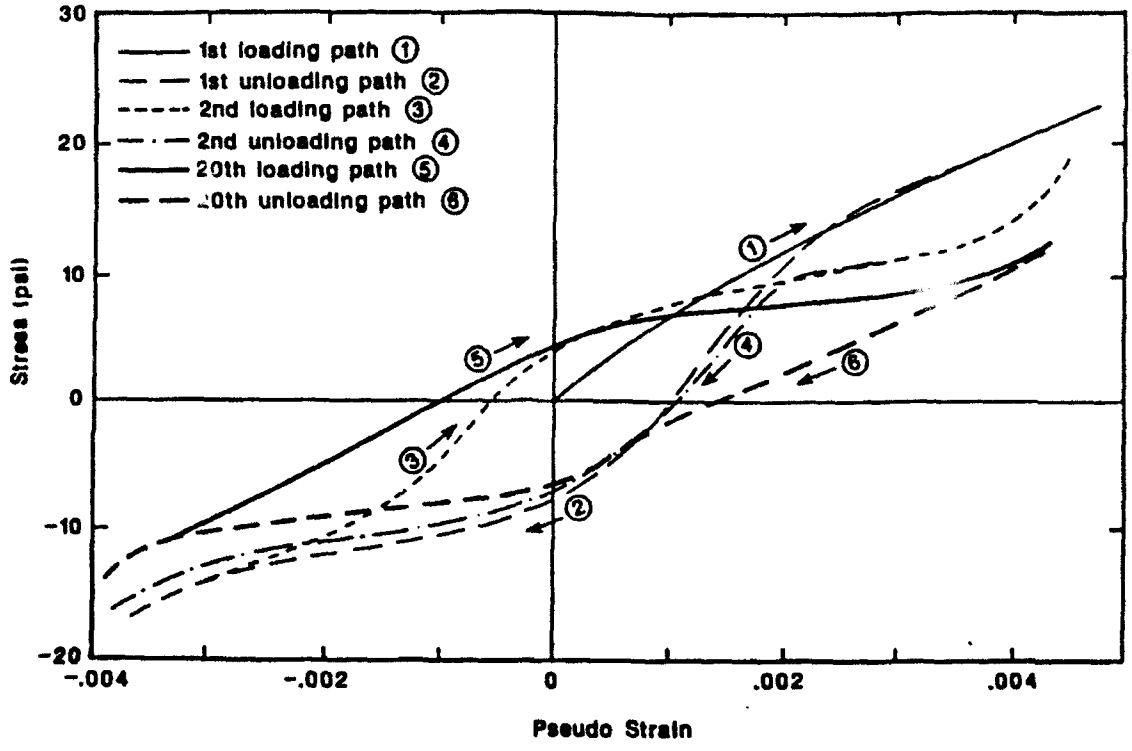

Figure 35. Stress versus pseudo strain of initial 20 cycles with strain amplitude of 0.0092 unit (Witco AR-4000 asphalt) (After Kim, 1988).

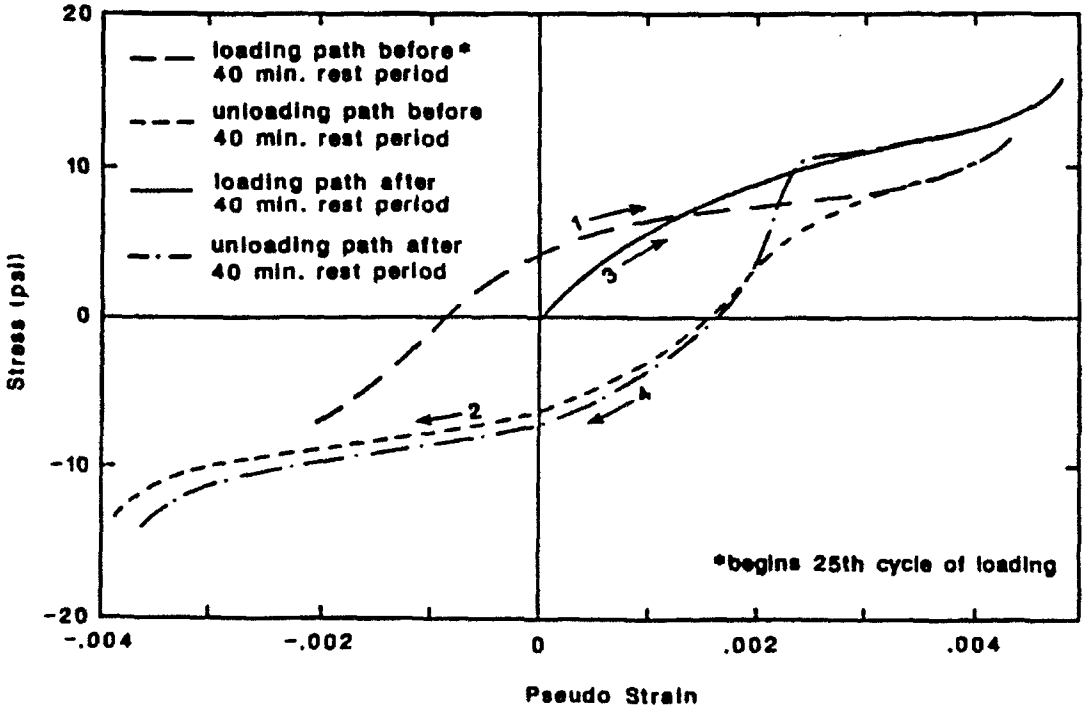

Figure 36. Stress versus pseudo strain before and after 40-min rest period with strain amplitude of 0.0092 units (Witco AR-4000) (After Kim, 1988).

was found to be very important and is discussed subsequently in damage modeling.

As discussed previously, the stress-pseudo strain curve after the rest period should be somewhat lower than the curve before the rest period if relaxation is the only mechanism influencing behavior during the rest period. However, as shown in Figure 36, there is a significant increase in the stress for the same pseudo strain following the rest period. This behavior was not observed in Figure 33 where damage was negligible. Therefore, Kim and Little (1988) concluded that during the rest period in a damaged asphalt concrete body, there exists a mechanism other than relaxation which provides a beneficial structural change.

Kim and Little (1988) defined the healing index as:

$$HI = \frac{\Phi^R_A - \Phi^R_B}{\Phi^R_A} \qquad (17)$$

where Φ^R_A is the pseudo energy density after the rest period and Φ^R_B is the pseudo energy density before the rest period. This calculation is illustrated in Figure 37.

In order to model the behavior of asphalt concrete under complicated, realistic loading, one needs to account for stress-induced damage along with the history-dependence of the material. By investigating the behavior of asphalt concrete under loading, one can establish a functional form of the stress-strain relationship, and discrepancies from the real response will be accounted for using a sufficient number of these internal state variables. The general form of

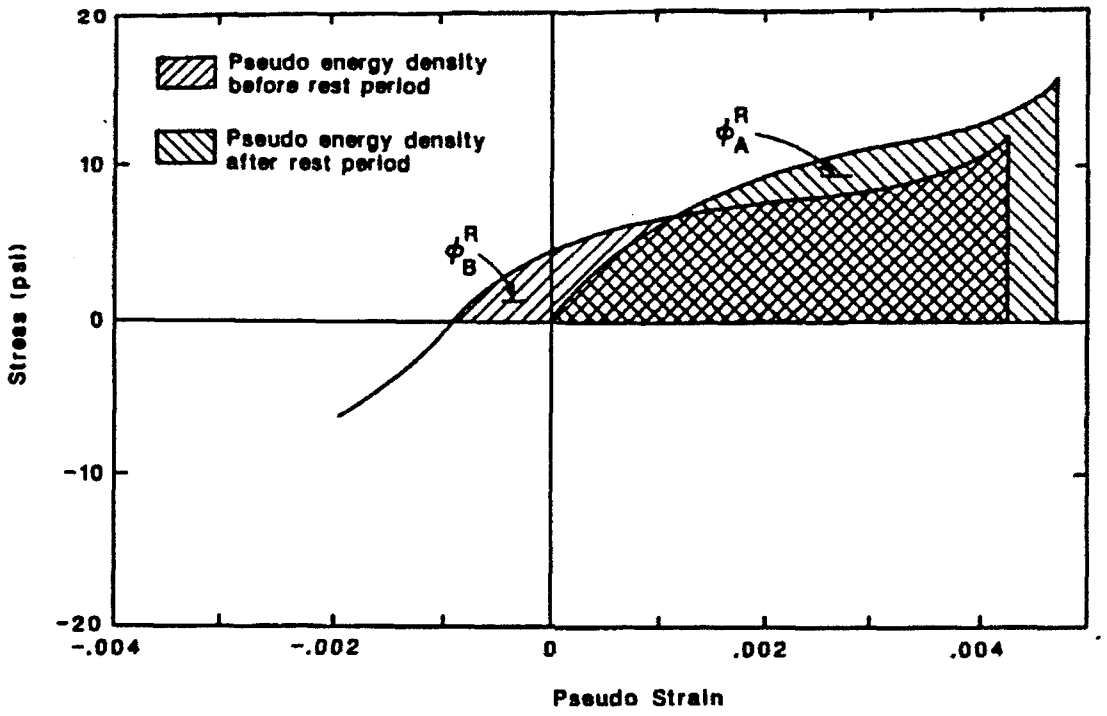

Figure 37. Illustration of pseudo energy densities before and after rest period (After Kim, 1988).

the constitutive model for asphalt concrete as proposed by Kim (1988) was as follows:

$$\sigma_{ij} = \sigma_{ij}\ (\epsilon_{kl},\ t,\ T,\ \frac{\delta T}{\delta x_n},\ \alpha_m) \tag{18}$$

where σ_{ij} is stress within the body, ϵ_{kl} is strain within the body, t is time, T is temperature, $\delta T/\delta x_n$ is the spatial temperature gradient within the body and α_m is the internal state variable.

Assuming that the temperature is constant spatially and that the effect of temperature on the stress-strain relationship can be included in the convolution integral using the thermologically simple behavior of asphalt concrete, the equation reduces to:

$$\sigma = \sigma(\epsilon^R,\ \alpha_m) \tag{19}$$

where

$$\epsilon^R = \frac{1}{E_R} \int_0^t E(t-\tau) \frac{d\epsilon}{d\tau}\, d\tau \tag{20}$$

From careful evaluation of stress versus pseudo strain plots with negligible damage growth, it became obvious that the largest pseudo strain in the loading history was an important internal state variable (ISV). Thus this ISV was added to the proposed constitutive equation as:

$$\sigma = \sigma(\epsilon_R,\ \epsilon^R{}_L,\ \alpha_m) \tag{21}$$

where ϵ_l^R is the maximum pseudo strain in the past history of loading.

However, equation 21 is not sufficient to model the constitutive behavior of asphalt concrete because it does not account for the damage accumulation in the asphalt concrete when the strain amplitude is high

enough to induce damage. To account for this damage Kim and Little used a damage parameter developed by Schapery (1988) which accounts for microcrack growth using a generalized J-integral which is valid for a failure zone in a continuum obeying power law relationships between stress and strain and between creep compliance and time, i.e., $\sigma \approx |\epsilon^R|^N$ and $D(t) = D_1\ t_m$. The basic form of the damage parameter was derived by first investigating the source of time dependence in the crack length expression and generalizing this analysis to microcrack growth from the fact that most of the failure time is consumed before the crack grows appreciably. Detailed steps in Schapery's analysis are reviewed by Kim (1988). The final form of the damage parameter proposed by Schapery is

$$S_p = \left(\int_0^t |\epsilon^R|^p\, dt\right)^{\frac{1}{p}} \tag{22}$$

where $p = (1 + N)k$.

The form of the constitutive model then becomes:

$$\sigma = \sigma(\epsilon^R,\ \epsilon^R{}_L,\ S_p) \tag{23}$$

Numerical integration was used to obtain S_p assuming that $d\epsilon^R/dt$ is constant within the range of the experimental data points. The value of p was calculated by assuming that p is equal to $2(1 + 1/m)$, where m is the exponent of the creep compliance versus time in the power creep compliance relationship. This approach, of course, assumes that the asphalt concrete being tested is linearly viscoelastic. This approach was selected as linearity was observed when induced damage was negligible. That is, the material itself is essentially linear, but the nonlinearity is due to the damage mechanism.

Kim used an experimental approach to find the explicit form of the constitutive equation for monotonic loading and for constant strain rate simple cyclic loading. Kim (1988) found the explicit form of the constitutive equation for cyclic loading to be:

$$\sigma = I\ F\ (\frac{\epsilon^R}{\epsilon^R_L})\ G(S_p)\ (\epsilon^R)^{1.386} \tag{24}$$

where

$$I = \frac{\sigma}{\epsilon_R} \tag{25}$$

$$F = 0.47 + 0.6553\ [\frac{\epsilon^R}{\epsilon^R_L}]^{-1.024} \tag{26}$$

when $\epsilon_R/\epsilon^{RL} < 0.9$

$$F = 1.2, \quad \text{when } \epsilon^R/\epsilon^R_L \geq 0.9 \tag{27}$$

$$G = 11.073 - 1019.782(S_p) - 180623.458(S_p)^2 + 40615298.665(S_p)^3 \tag{28}$$

when $S_p < 0.0033$ and

$$G = (S_p)^{-0.345} \quad \text{when } S_p \geq 0.0033. \tag{29}$$

Extensive verification testing was performed using three types of uniaxial testing: constant strain rate simple loading with various lengths of rest periods, multi-level loading with 30-second rest periods and multi-level loading with various lengths of rest periods. Figures 38 illustrates the strain histories of multi-level loading used for verification testing.

The strain histories of multi-level loading tests with 30-second rest periods and with random durations of rest period were designed to investigate the effect of the healing mechanism on constitutive modeling. More cycles will, of course, induce more damage, and, if healing is a

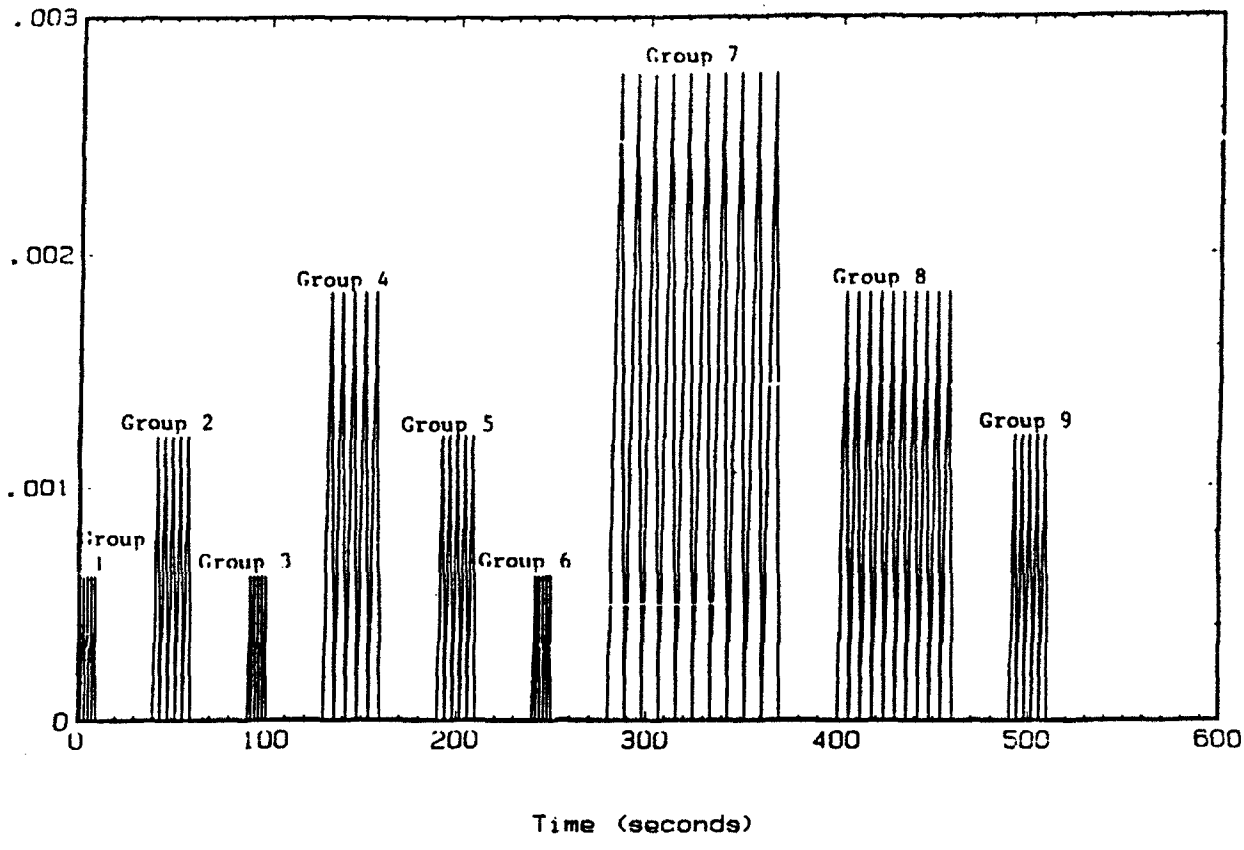

Figure 38. Strain history of a multi-level loading verification test with 30-second rest periods (After Kim, 1988).

"real" phenomenon as previously determined, longer rest periods after greater damage will produce greater effects of healing. This was verified in the testing.

The verification testing proved the excellent capability of the constitutive model to predict the effect of loading history on stress. However, the verification testing proved that a ISV which addresses the beneficial effects of healing is necessary to improve the constitutive model. The authors state:

> "Especially, when the effect of healing becomes significant, that is, at an elevated temperature or through the modification of asphalt cement, an appropriate constitutive model should be able to predict the beneficial effect of healing as well as relaxation and detrimental damage accumulation."

APPLICATION OF CORRESPONDENCE PRINCIPLE TO DENSELY GRADED MIXTURES AS WELL AS SAND ASPHALT MIXTURES AND TO THE COMPRESSIVE MODEL OF TESTING AS WELL AS THE UNIAXIAL TENSILE MODEL OF TESTING

In this study uniaxial compressive testing was performed on 4-inch by 8-inch cylinders. The testing was performed over a range of temperatures. The purpose of this task was to verify that the correspondence principle applies to densely graded asphalt mixtures as well as to sand asphalt mixtures tested by Kim (1988). The cylinders were made of densely graded Watsonville granite and SHRP asphalt AAG-1. Samples were fabricated using the Corps of Engineers Gyratory compactor to a target air voids content of 4 percent.

The major findings of this study investigating the applicability of the correspondence principle to density graded mixtures are:

a. The samples responded to testing in a "thermorheologically simple" manner, and the definition of pseudo strain with this thermorheologically simple behavior can be used to predict the linear viscoelastic stress-strain behavior at various temperatures form the stress-strain relationship at a reference temperature.

b. In monotonic loading (without damage) the concept of the correspondence principle can be successfully applied to uniaxial compressive constant-strain rate test data to eliminate rate dependency, therefore validating the applicability of the correspondence principle to the analysis or densely-graded asphalt concrete.

c. The pseudo strain can be adequately determined from a predicted relaxation modulus from creep compliance instead of from measured relaxation modulus.

d. The pseudo strain concept was successful in accounting for the change is strain due to relaxation during rest periods in cyclic uniaxial controlled-stress testing with negligible damage.

e. Uniaxial compressive controlled-stress repetitive testing with significant damage growth demonstrated that the beneficial effect of the time-dependent relaxation is accounted for by the use of pseudo strain and that a significant increase in pseudo strain energy occurs after rest periods, which must be due to the fracture healing in microcracks.

This study is completely documented in Appendix A.

SENSITIVITY OF HEALING INDEX TO MIXTURE PROPERTIES

The approach developed by Kim (1986) and Kim and Little (1988) was used to evaluate the damage healing potential of a number of mixtures. The effects of the following factors were considered on microdamage healing:

(1) binder type, (2) aggregate type, (3) length of rest period, (4) strain amplitude and (5) temperature.

Binder Type

Eleven different binder types were considered in this study: six of the core SHRP asphalt cements, two additional asphalt cements (Santa Maria, California, asphalt and a Texaco asphalt), the Santa Maria asphalt modified with 5 percent low density polyethylene (LDPE) and the Texaco asphalt modified with polymer APAO-3 and with polymer APAO-4.

Aggregate Type

Two fine grained aggregates were used in the study: syenitic granite fines and limestone fines. Both carrier aggregates were sand-sized aggregates with 100 percent passing the number 10 sieve. However, the limestone aggregate was slightly coarser than the granite aggregate.

Length of Rest Periods

The duration of the rest periods varied from 2.5 minutes to 40 minutes. The majority of testing was performed at rest periods of 5, 10, 20 and 40 minutes with limited testing at the shorter rest period of 2.5 minutes.

Strain Amplitude

Three strain amplitudes were considered in the healing portion of testing: ranging from 1.84 x 10^{-3} mm/mm to 9.231 x 10^{-3} mm/mm. The three strain amplitudes actually used in testing were selected depending on the stiffness of the mixtures tested and were selected in order to provide an appropriate rate of fracture propagation.

Temperature

Two test temperatures were used: 25°C and 31°C.

Testing Protocol

The testing protocol employed the three types of tests discussed in the previous section: relaxation tests, verification tests and healing tests. The protocol used was that established by Kim and Little (1988) and discussed in the section entitled "Use of Non-Linear Viscoelastic Correspondence Principle to Analyze Fracture Healing Data".

The relaxation test data are summarized in equation form in Table 8 for the eleven different binders used in this study. Plots of the relaxation test data are presented in a Master of Science Thesis prepared as part of this research project (Telikicherla, 1992).

Verification tests used to determine whether or not the pseudo strain approach could successfully be used to account for time dependency and thus eliminate the hereditary (hystersis) effects of cyclic loading proved successful for each binder system evaluated.

Beams with 25.4-mm starter cracks were used in the healing test. Pseudo strain energy, which is essentially the area under the tensile portion of the stress-strain plot, was used to calculate the pseudo

Table 8. Summary of relaxation data of the asphalt mixtures studied.

Asphalt Mixture Type	Relaxation Eqn. I $E_1(t)$ =	Break Point (sec)	Relaxation Eqn. II $E_2(t)$ =
AAA	$267.68 + 636.22t^{-0.601}$	71.5	$253.3 + 1260.6t^{-0.698}$
AAB	$-265.53 + 7040.4t^{-0.473}$	68	$83.9 + 3282.2t^{-0.401}$
AAD	$-23.89 + 1647.4t^{-0.338}$	53	$-39.6 + 967.8t^{-0.195}$
AAK	$-336.2 + 6190.7t^{-0385}$	25.3	$233.8 + 11655.7t^{-C.701}$
AAG	$268.53 + 2554.4t^{-0.669}$	58	$305.6 + 771.1t^{-0.435}$
AAM	$-4007.8 + 20878.4t^{-0.258}$	50	$-71.3 + 21382.9t^{-0.45}$
LLM[1]	$-68540.3 + 96475.2t^{-0.07}$	20	$804.65 + 28726.0t^{-0.35}$
LLG[1]	$-88887.1 + 114101t^{-0.095}$	3.4	$384.7 + 26022.2t^{-0.61}$
LLK[1]	$-228.6 + 3830.5t^{-0.395}$	42	$179.45 + 4661.7t^{0.612}$
AAMH[2]	$4917.8 + 11718.8t^{-0.186}$	26.6	$-182.8 + 4293.3t^{-0.295}$
California AC-10	$-1051.4 + 6026.5t^{-0.505}$	6.6	$656.7 + 4204.7t^{-0.925}$
California AC-10 with Novophalt	$-281.5 + 5727.7t^{-0.52}$	4.6	$1049.4 + 4103.7t^{-0.74}$
Texaco AC-10	$-6137.1 + 13280.3t^{-0.125}$	40.9	$329.6 + 10255.6t^{-0.45}$
Texaco AC-10 with APAO-3	$302.8 + 7444.9t^{-0.375}$	253	$627.1 + 6570.9t^{-0.41}$
Texaco Ac-10 with APAO-4	$-1553.3 + 7754t^{-0.268}$	23.7	$-217.9 + 4713.7t^{-0.272}$

Note: Granite aggregate was used for all asphalt mixes and all tests were performed at 77°F, unless otherwise noted.

[1] Limestone aggregate was used for these asphalt mixes.

[2] Testing was performed at a higher temperature of 88°F.

energy density of the specimen before and following rest periods. The healing index was calculated for each specimen after various rest periods using equation 17.

Figures 39, 40, 41 and 42 present the representative plots illustrative of the data from verification tests, damage tests without rest periods and damage tests with rest periods (healing tests), respectively, for asphalt AAK-1.

Results and Discussion of Healing Tests

The influence of binder type on the healing index is substantial. This healing index factor is evident in Figure 43 which compares the healing index for five of the six SHRP asphalt studied at a constant strain amplitude. The results are tabulated in Table 9. Note that the healing index is affected by the length of the rest period, the number of strain cycles at a specific level of strain and the strain amplitude of testing as defined in Table 9.

Due to the very different stiffnesses of the six mixtures, it was necessary to test the mixtures at different strain amplitudes, in order to insure crack growth throughout the test, during the healing test. However, for comparison purposes, Figure 43, a strain amplitude of 0.00923 mm/mm was selected as most of the asphalts were tested at this level of strain. Asphalt AAM-1 was not tested at this high a strain level. Hence, the healing index of this asphalt were extrapolated from the data collected to the 0.00923 mm/mm strain level. Since the healing index of asphalt AAK-1 is independent of stress level, it is not plotted in Figure 43.

From Figure 43 it is apparent that, for a set strain amplitude, asphalt AAM-1 has the best healing potential and AAB-1 is the worst. The

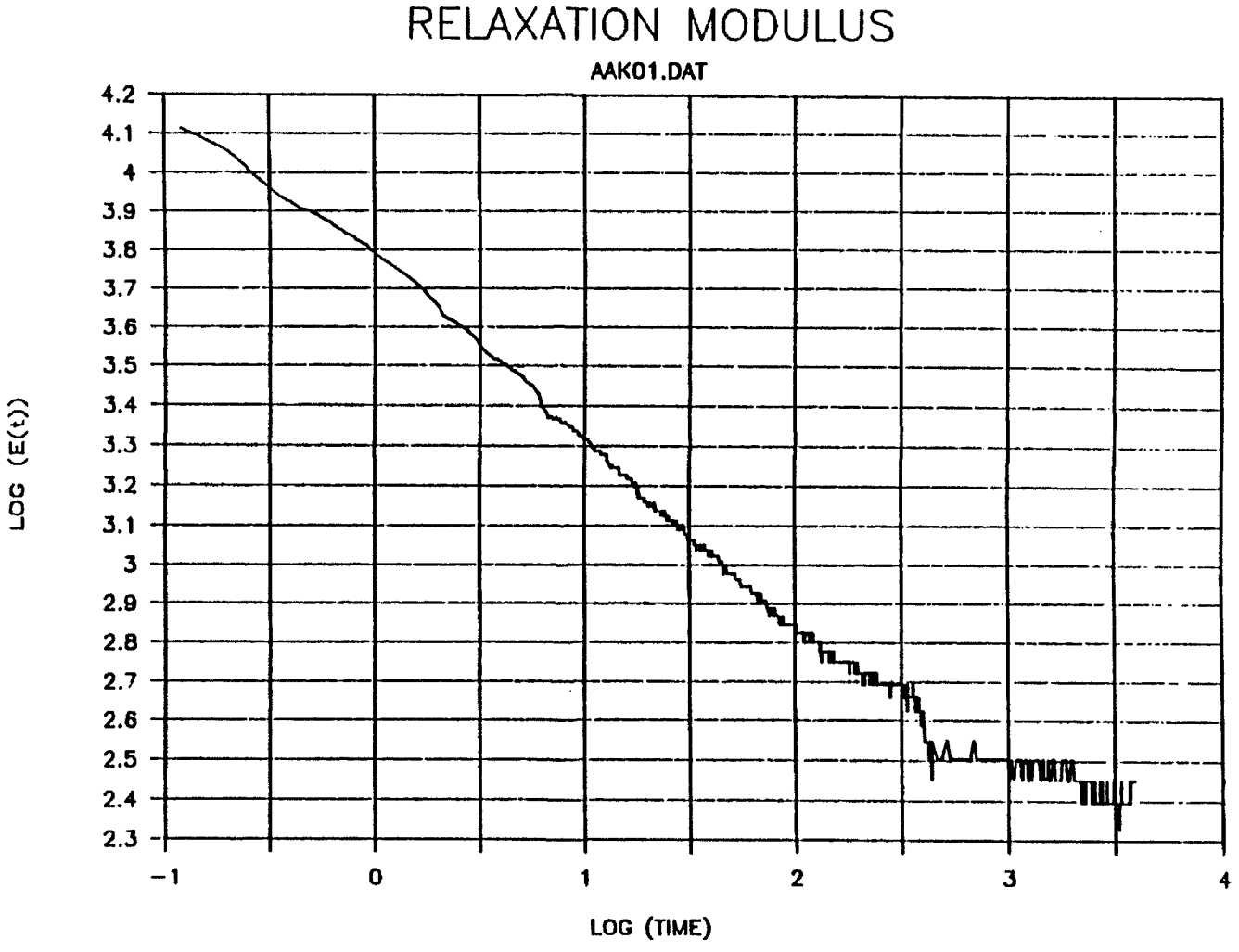

Figure 39. Relaxation modulus for asphalt AAK-1 with granite fines.

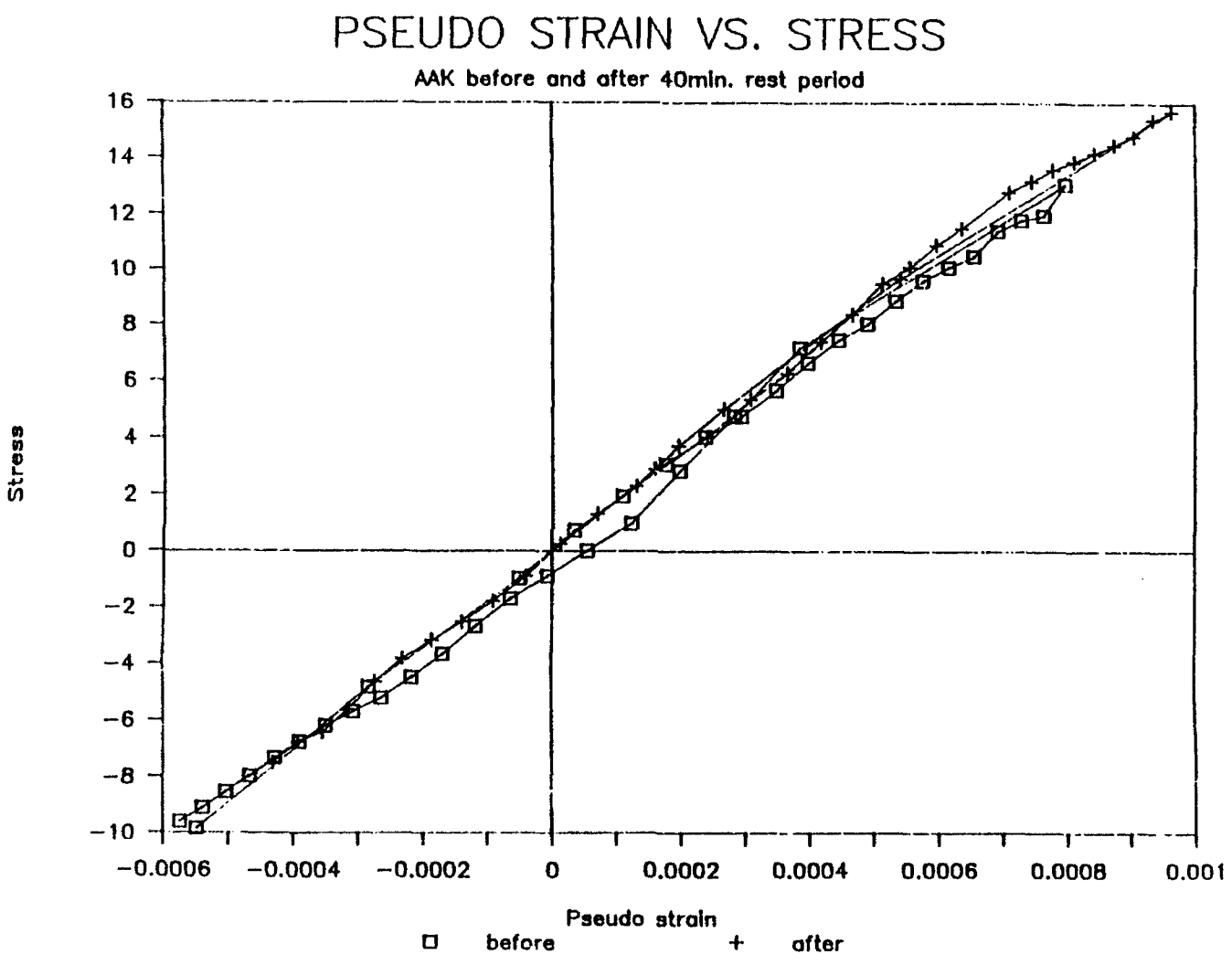

Figure 40. Verification testing before and following 40-min. rest period for asphalt AAK-1. Induced strain is too low to cause crack growth.

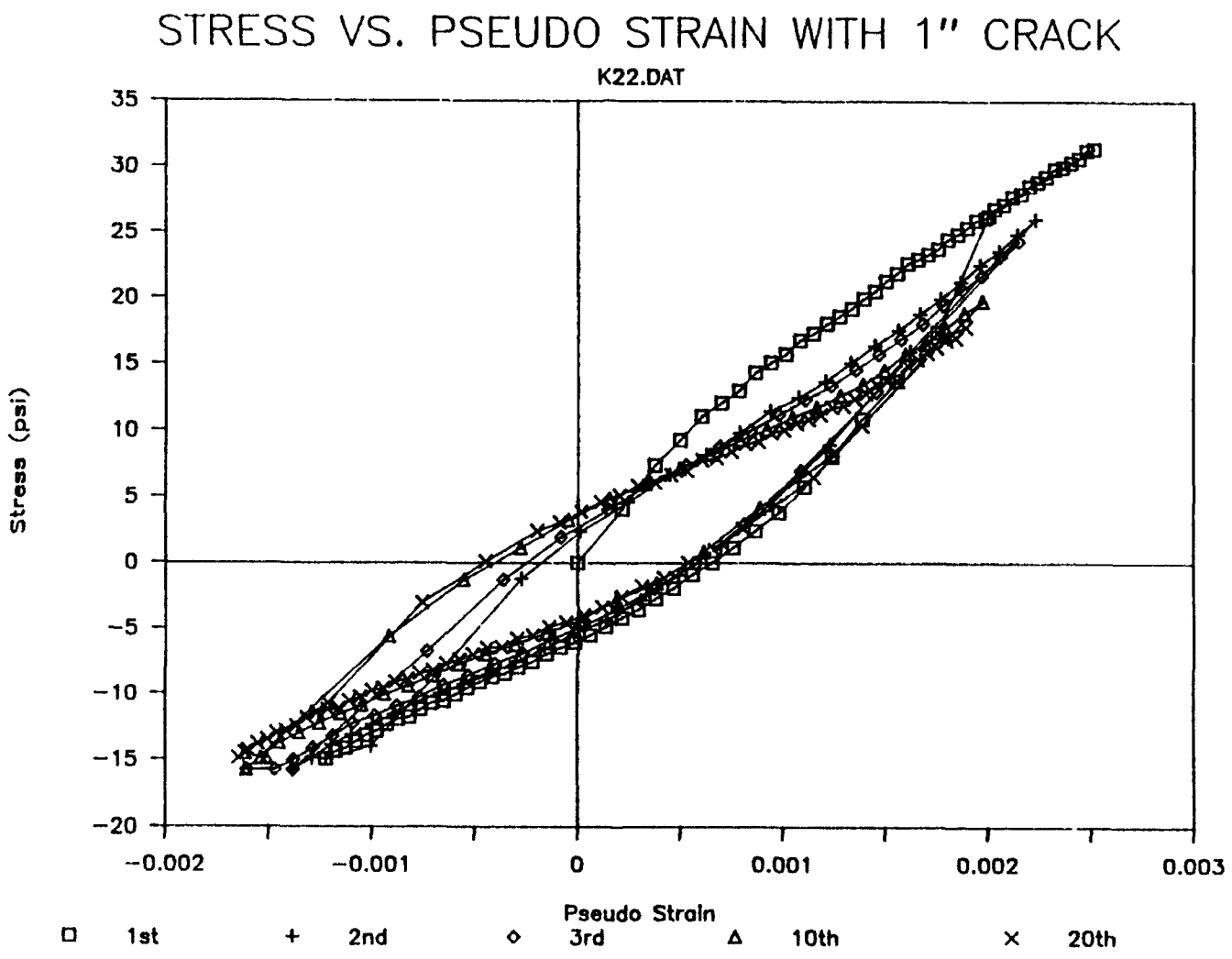

Figure 41. Stress versus pseudo strain plot for asphalt AAK-1. Induced strain is large enough to cause damage (crack growth).

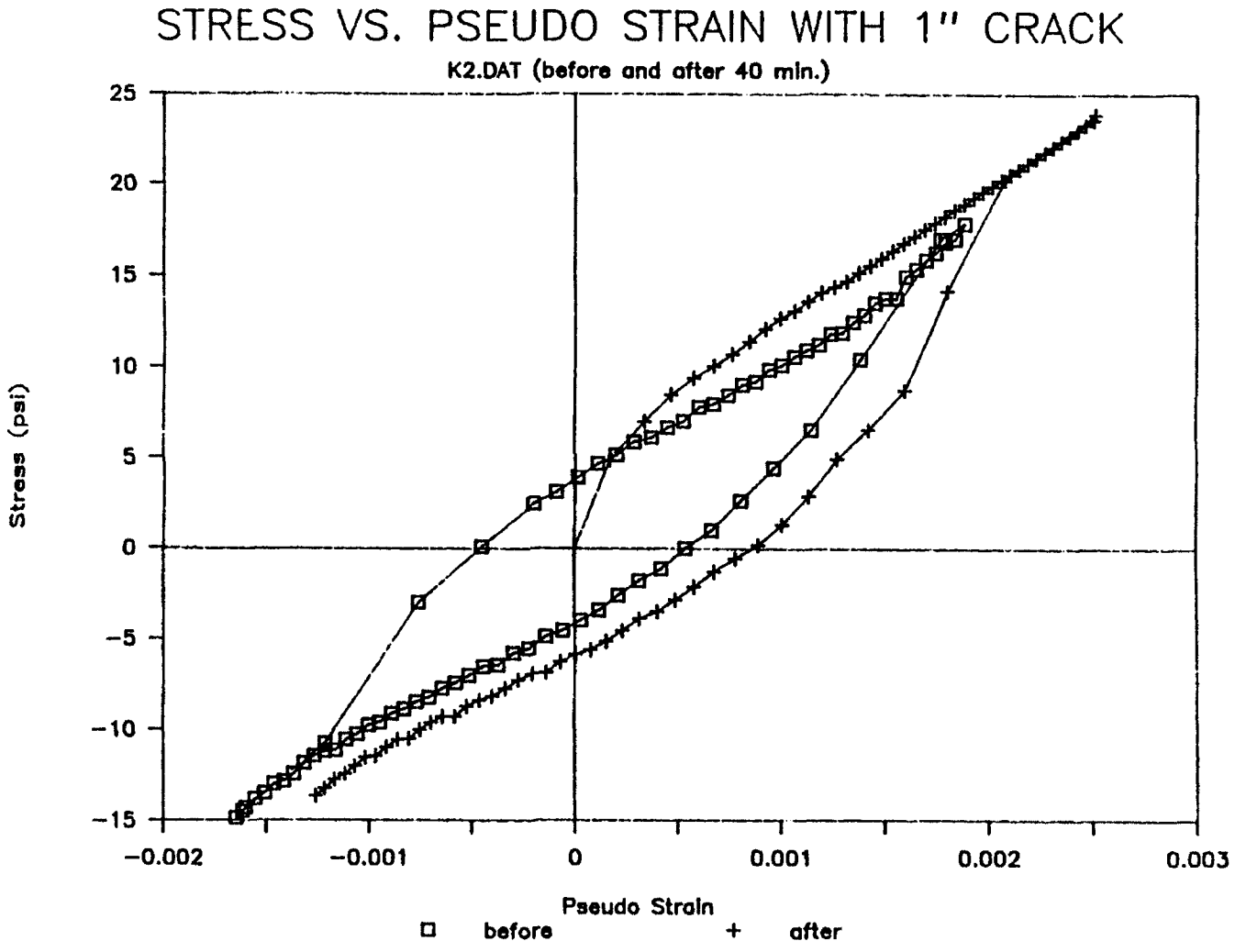

Figure 42. Stress versus pseudo strain plots before and following 40 min. rest period. Strains are large enough to cause crack growth.

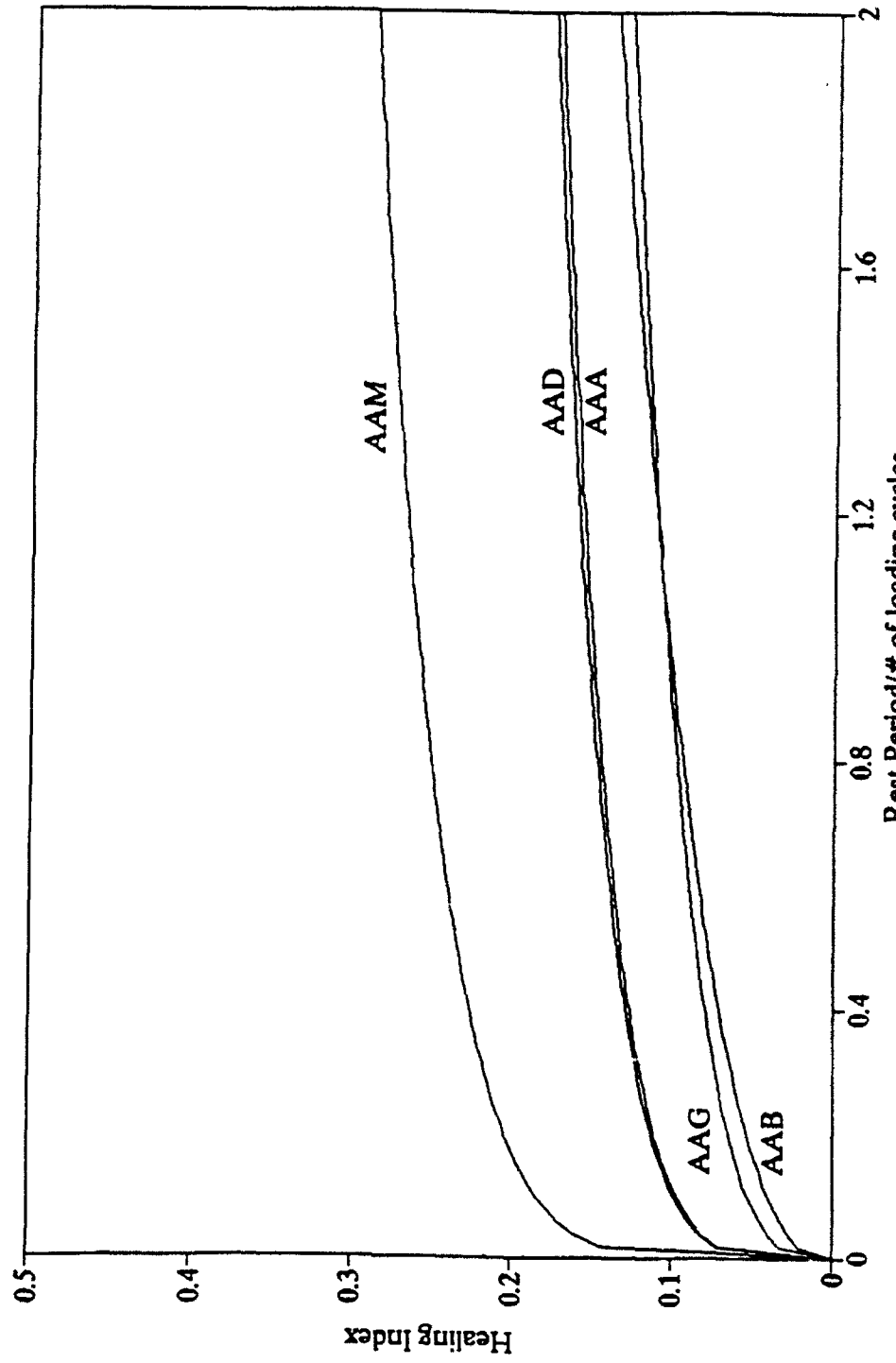

Figure 43. Comparison of healing indices as a function of RP/# and SA for five S asphalts, at a strain amplitude (SA) of 0.009231 units.

Table 9. Healing index equations for the asphalt mixtures studied.

Asphalt Mixture Type	log (HI) =
AAA	-4.51066 + 0.193534 log (RP/#) - 1.814 log (SA)
AAB	-4.49482 + 0.414195 log (RP/#) - 1.725 log (SA)
AAD	-2.90893 + 0.195005 log (RP/#) - 1.031 log (SA)
AAG	-2.63387 + 0.299535 log (RP/#) - 0.813 log (SA)
AAK	-0.541829 + 0.130143 log (RP/#)
AAM	-1.03093 0 149133 log (RP/#) - 0.219 log (SA)
LLG[1]	-5.94730 _ 0.192729 log (RP/#) - 2.139 log (SA)
LLK[1]	-0.515454 + 0.159183 log (RP/#)
LLM[1]	-3.30941 + 0.241860 log (RP/#) - 1.096 log (SA)
California AC-10	-4.68432 + 0.321480 log (RP/#) - 1.896 log (SA)
California AC-10 with Novophalt	-2.91298 + 0.324562 log (RP/#) - 1.102 log (SA)
Texaco AC-10	-4.09826 + 0.233788 log (RP/#) - 1.541 log (SA)
Texaco AC-10 with APAO-3	-2.63188 + 0.184796 log (RP/#) - 0.843 log (SA)
Texaco AC-10 with APAO-4	-2.83709 + 0.179982 log (RP/#) - 0.836 log (SA)
AAMH[2]	-2.28299 + 0.266075 log (RP/#) - 0.753 log (SA)

Note: Granite aggregate was used for all asphalt mixes and all tests were performed at 77°F, unless otherwise noted.

[1] Limestone aggregate was used for these asphalt mixes.

[2] Testing was performed at a higher temperature of 88°F

rank order of the five asphalts with decreasing magnitude of healing potential is: AAM-1, AAD-1, AAA-1 and AAB-1.

Work by Kim, Little and Benson (1990) which is discussed is this chapter substantiates these results. In this work, the Fina and Shamrock asphalts were substantially better healers than the Witco asphalt.

Effect of Rest Period

Healing tests were conducted for all asphalts at rest periods of 5, 10, 20 and 40 minutes. All asphalts demonstrated an increase in healing index with increase in the duration of the rest period. However, as can be clearly seen from Figure 44, which is a plot of healing index versus rest period for (representation) asphalt AAK-1, the great majority of the healing apparently occurs during the first minute or so of the rest period.

In order to verify this, healing indices were calculated at a rest period of 2.5 minutes for asphalts AAB-1, AAK-1 and AAM-1. These tests results, summarized in Tables 10, 11 and 12, verify the results anticipated from Figure 44. Additionally, it should be noted that the rank of healing potential is the same in the short term healing tests as in the extended healing testing with asphalts AAM-1 and AAK-1 demonstrating substantially superior healing potential than asphalt AAB-1. This is significant since the short term healing tests were performed at a different time and on different replicate samples than the experiments for long-term healing.

An additional set of tests were performed at rest periods of only 1 minute further verifying that the vast majority of healing, approximately 70 percent, occurs within the first minute of the rest period.

Table 10. Healing data of asphalt AAB-1 with granite fines at a short rest period of 2.5 minutes.

Number of Loading Cycles	Healing Index at SA of 0.004923 in/in.	Healing Index at SA of 0.006154 in/in.	Healing Index at SA of 0.0054 in/in.
20	0.093583	0.089369	0.108078
25	0.091558	0.075101	0.094280
30	0.085928	0.006196	0.098053
35	0.082937	-	0.082797
40	0.079149	-	0.083079
45	0.074388	-	0.083927
50	0.069330	-	0.069700
55	0.073590	-	0.063861
60	0.064312	-	0.058457
65	0.057800	-	0.058085
70	0.051653	-	0.048420
75	0.049296	-	0.036209
80	0.044955	-	0.033965
85	0.041663	-	0.031436

Table 11. Healing data of asphalt AAK-1 with granite fines at a short rest period of 2.5 minutes.

Number of Loading Cycles	Healing Index at SA of 0.00246 in/in.	Healing Index at SA of 0.00277 in/in.	Healing Index at SA of 0.003077 in/in.
20	0.188962	0.245011	0.266740
25	0.209866	0.243181	0.266792
30	0.207111	0.267142	0.240322
35	0.173984	0.249905	0.214854
40	0.209050	0.250505	0.231191
45	0.141226	0.256411	0.215555
50	0.144737	0.243112	0.200511
55	0.132975	0.207095	0.207493
60	0.142518	0.151271	0.210411
65	0.128460	0.229213	0.195172
70	0.095884	0.236513	0.194694
75	0.116560	0.212828	0.182438
80	-	0.221823	0.193380
85	-	0.188916	0.192746

Table 12. Healing data of asphalt AAM-1 with granite fines at a short rest period of 2.5 minutes.

Number of Loading Cycles	Healing Index at SA of 0.00246 in/in.	Healing Index at SA of 0.003077 in/in.	Healing Index at SA of 0.0037 in/in.
20	0.297043	0.242160	0.227733
25	0.272024	0.235139	0.199853
30	0.232745	0.233469	0.193301
35	0.230706	0.235975	0.205849
40	0.225485	0.172264	0.174910
45	0.214676	0.214746	0.168940
50	0.213487	0.214102	0.188112
55	0.192749	0.186657	0.139503
60	0.203139	0.183116	0.124911
65	0.196312	0.155679	0.125902
70	0.182753	0.122247	0.112810
75	0.160977	0.113857	0.103356
80	0.165671	-	-
85	-	-	-

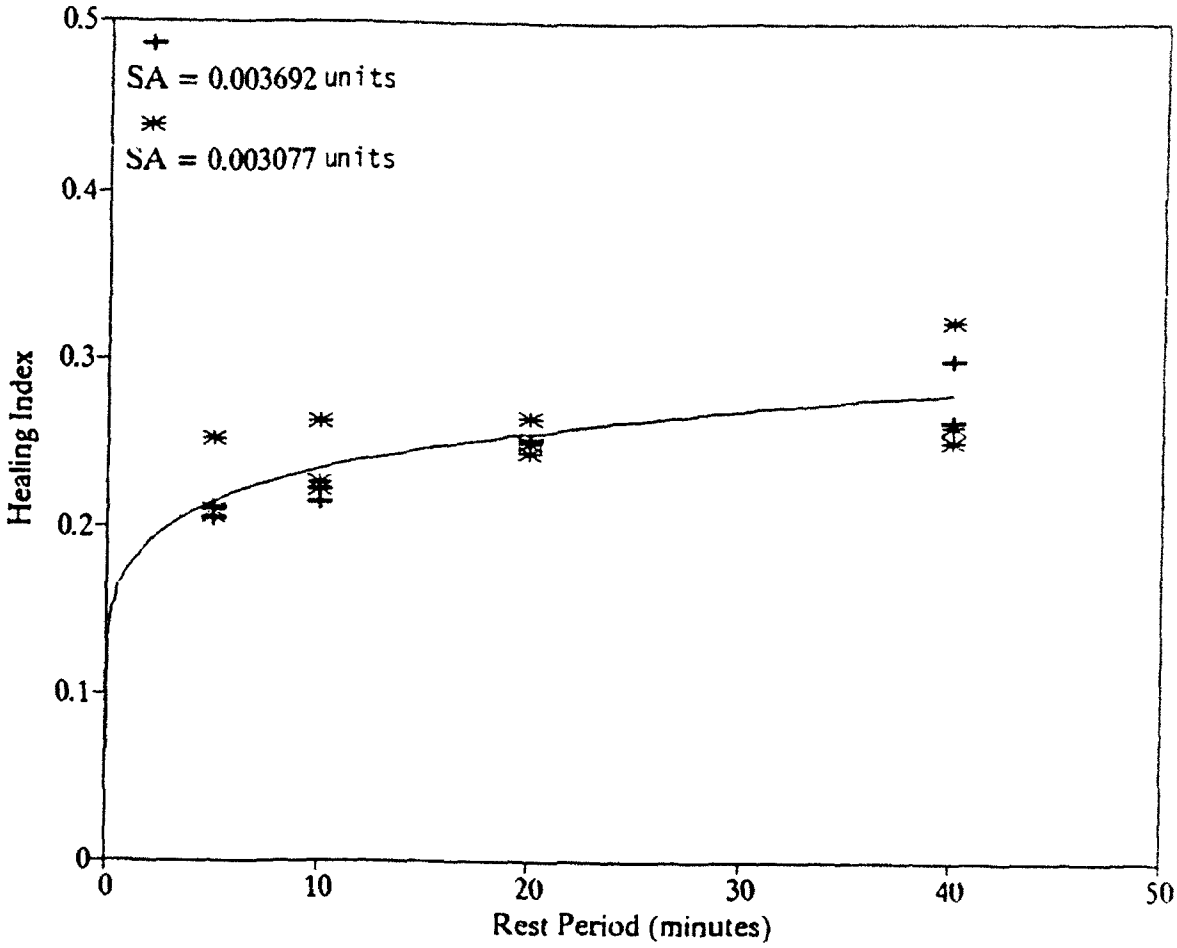

Figure 44. Healing index as a function of rest period for asphalt AAK-1 with granite fines.

Effect of Aggregate Type

Healing tests were performed for asphalt types AAG-1, AAK-1 and AAM-1 with both granite and limestone fine aggregates. For purposes of simplification, mixtures of asphalts with granite fines are represented simply by the designation of the binder while mixtures of the asphalts with limestone fines are designated as LLG, LLK and LLM, with the last letter in the designation representing the respective asphalt.

From the relationship between healing index versus the ratio of rest period and number of loading cycles, Figure 45, the following conclusions may be drawn:

1. The relative healing potential among the three asphalts is not affected by the carrier aggregate. In other words, the order of healing potential from best to worst remains aspnalt AAM-1, AAK-1 and AAG-1 regardless of the carrier aggregate used. In this analysis each mixture for the three asphalts was evaluated at a strain of 0.00308 mm/mm.

2. The order of healing within an asphalt type is different among the asphalts evaluated. For example, asphalt M heals better when combined with the granite carrier aggregate, while asphalts K and G heal better with the limestone carrier aggregates.

Effect of Polymer Additives

A Santa Maria, California, asphalt was evaluated for healing potential in its virgin state and after modification with 5 percent low density polyethylene (LDPE). Figures 46 and 47 demonstrate the healing indices of these two binders with the granite carrier aggregate at three strain levels. Figure 48 demonstrates the relative position of the healing index versus the ratio of rest period to number of loading cycles

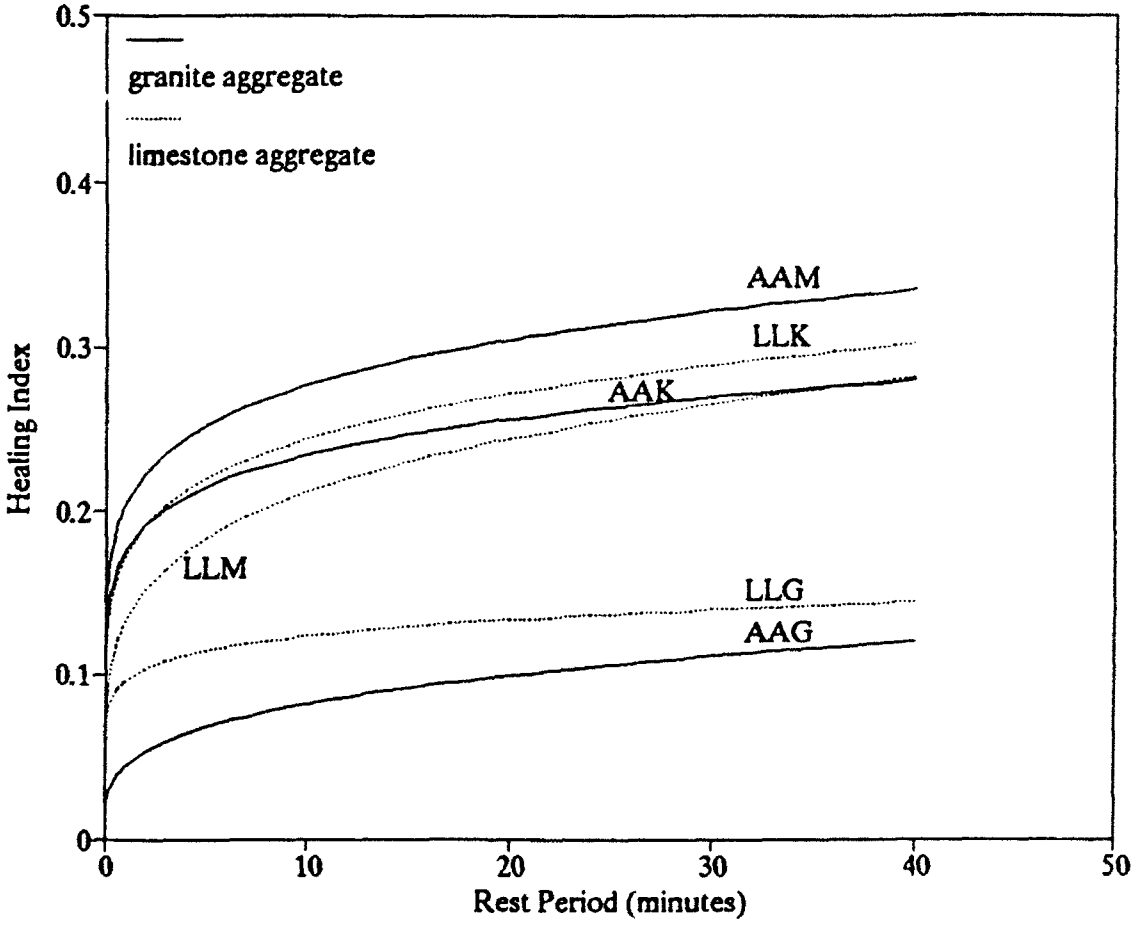

Figure 45. Healing index as function of rest period for asphalts AAG-1, AAK-1, and AAM-1 with granite and limestone aggregates.

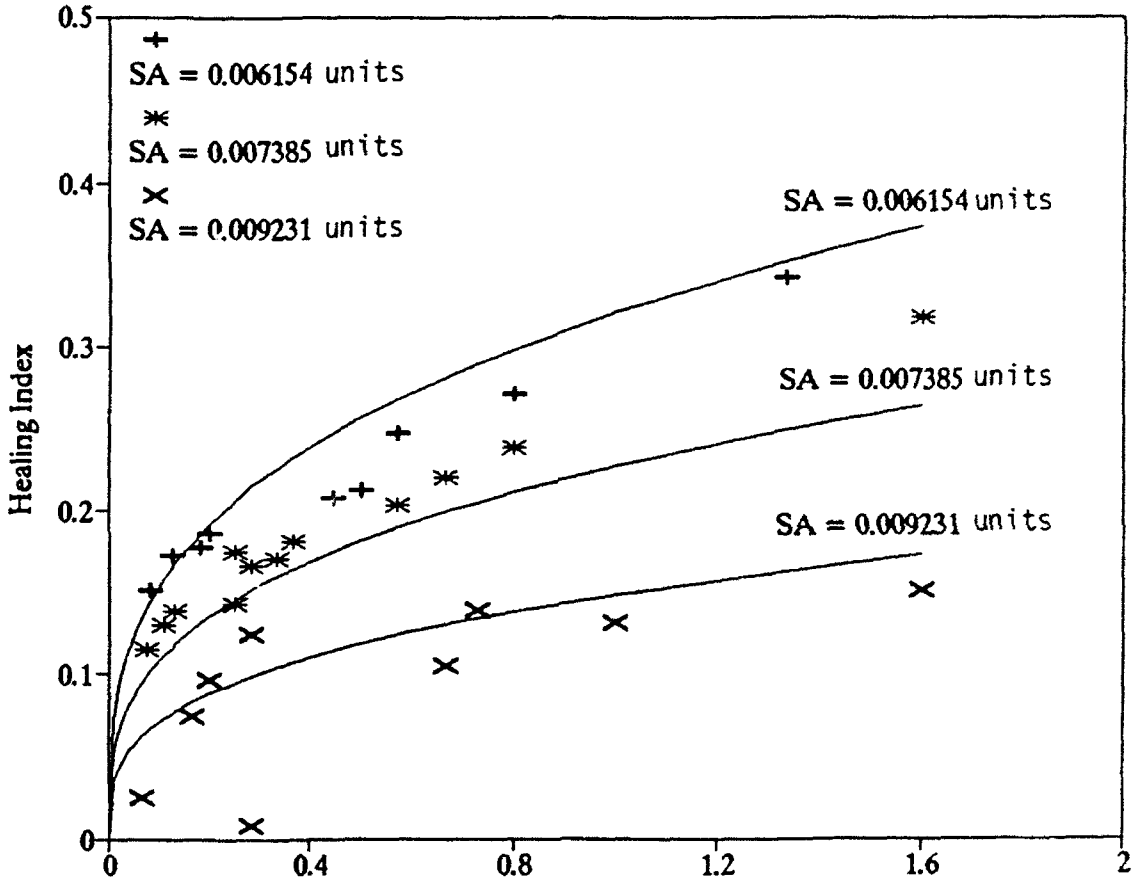

Figure 46. Healing index as a function of RP/# and SA for California Valley (virgin) asphalt.

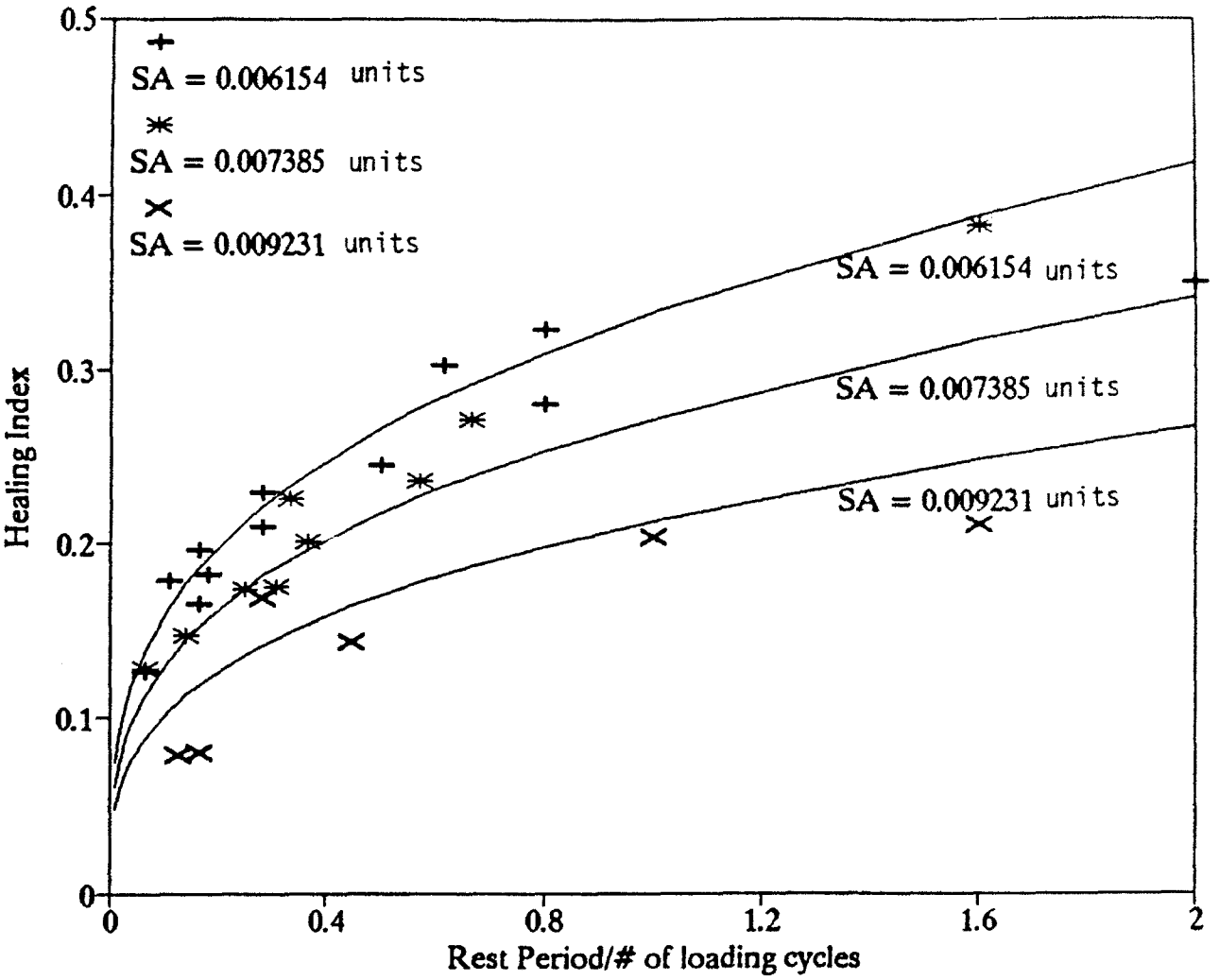

Figure 47. Healing index as a function of RP/# and SA for virgin asphalt modified with 5 percent LDPE.

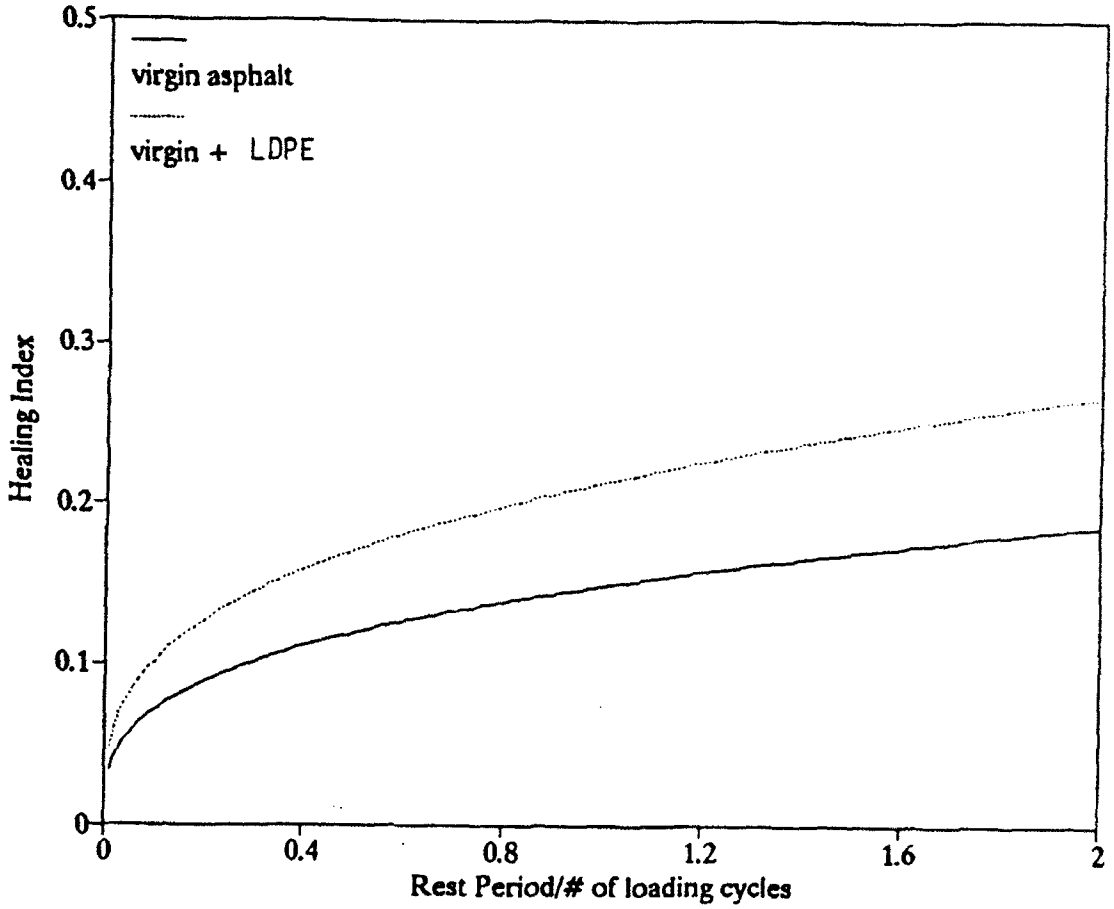

Figure 48. Comparison of healing indices as a function of RP/# and SA for the virgin and LDPE modified asphalts at a strain amplitude (SA) of 0.009231 units.

for the two binders for the strain amplitude of 0.00923 mm/mm. As can be seen the LDPE modification significantly increases the healing potential of the Santa Maria asphalt.

A second evaluation of the effect of modification was performed with a Texaco AC-10 base asphalt modified with 8 percent of two different polymeric additives identified as APAO-3 and APAO-4. When comparing the healing potential of these three binders mixed with the granite carrier aggregate at a common strain amplitude of 0.0049 mm/mm in Figure 49, it is apparent that the healing index of the mixtures is highest for the control or unmodified binder.

Effect of Temperature and Strain Amplitude

The effect of temperature was evaluated by performing the healing test at 25°C and 31°C on mixtures of AAM-1 and granite fines. The experiments were performed at three strain amplitudes for the mixtures at each temperature. Consistently, the mixtures tested at the lower temperatures, 25°C, resulted in the better healing potential.

The level of strain amplitude employed during testing has a significant effect on the healing response of the mixtures evaluated. The healing index is lower as the strain amplitude is increased. This effect was consistently noted for each binder tested with the exception of asphalt AAK-1. It should also be noted that the healing properties of the asphalts evaluated by Kim (1988) were not sensitive to the strain amplitude.

Of the five unmodified asphalts evaluated in this study that are apparently sensitive to strain amplitude, the healing properties of asphalt AAM-1 are least affected by strain amplitude. Strain amplitude has the most influence on the healing properties of asphalt AAA-1. The

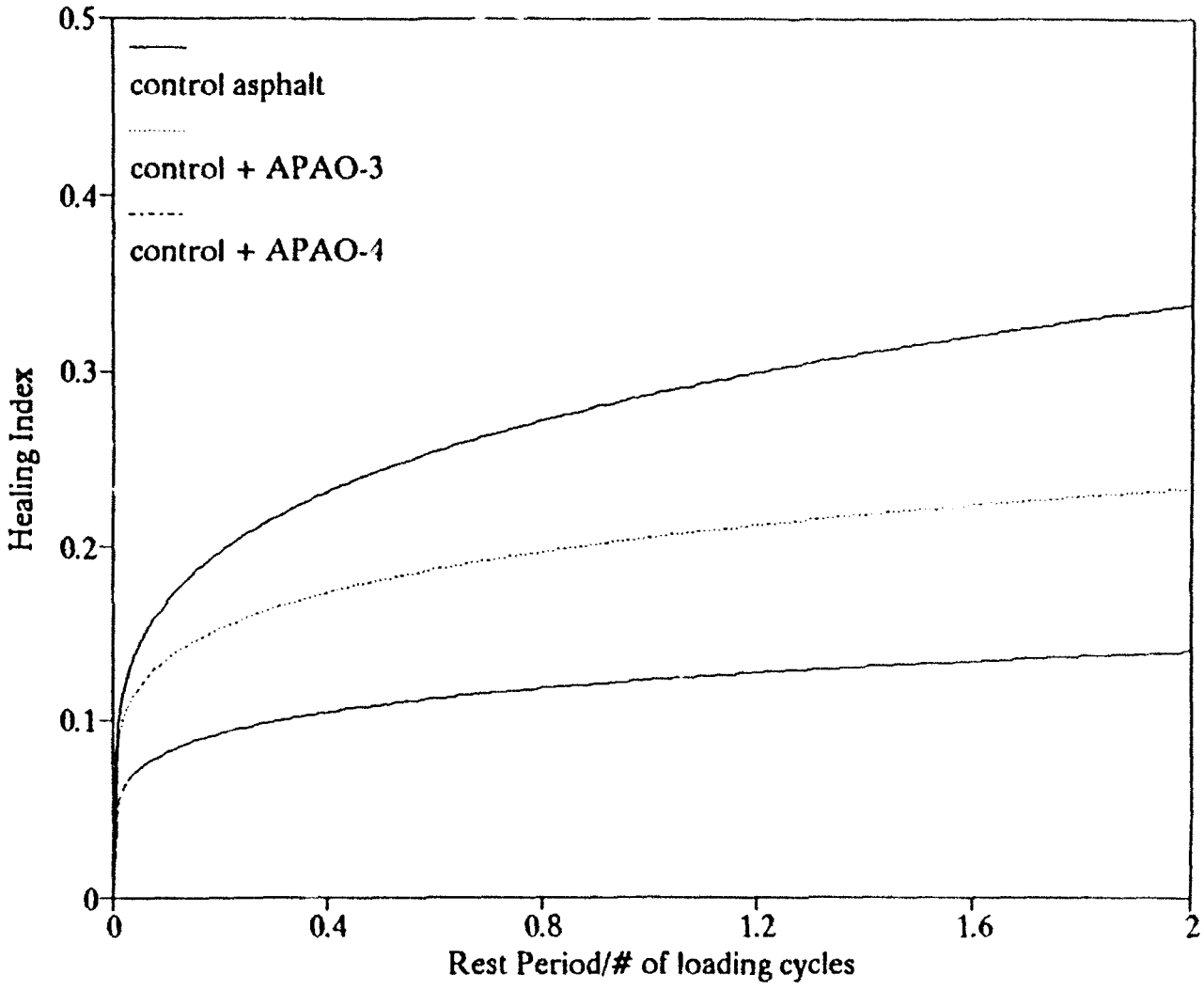

Figure 49. Comparison of healing indices as a function of RP/# and SA for the control, control modified with 8 percent APAO-3, and control modified with 8 percent APAO-4 asphalts, at a strain amplitude of 0.004923 units.

rank order of the six SHRP asphalts with increasing order of impact of strain amplitude on the magnitude of healing are: AAK-1, AAM-1, AAG-1, AAD-1 and AAA-1. Note that the best healers i.e., asphalts AAK and AAM, are those that are least affected by changes in strain amplitudes.

It should be noted that although the strain amplitude varied in the experiments performed, the strain rate among the tests was maintained constant at 0.0006154 mm/minute. From the test results, it was determined that the healing indices decreased with the number of loading cycles for each mixture. This trend is expected because the damage level tends to increase with increase in the number of loading cycles. For this reason the healing index is plotted versus the ratio of rest period to number of loading cycles instead of simply against length of the rest period.

STATISTICAL EVALUATION OF FACTORS INFLUENCING THE HEALING INDEX

Kim and Little (1988) have shown that the basic form of the relationship between healing index and rest periods is of the form:

$$HI = A(RP)^B \tag{30}$$

where HI is the healing index value, RP is the length of the rest period and A and B are regression constants. Rewriting the equation in logarithmic form produces:

$$\log(HI) = A_1 + B_1 \log(RP) \tag{31}$$

However, this research indicated that the simple equation 31 does not adequately explain the relationship between healing and rest periods and that other parameters must be considered, such as the number of rest periods induced and the strain amplitude induced during the damage loading process or the process of inducing damage through crack growth.

As a result three other forms of the regression equation were considered:

$$\log(HI) = A_2 + B_2\log(RP/NUM) \quad (32)$$

$$\log(HI) = A_3 + B_3\log(RP) + C_3\log(NUM) \quad (33)$$

$$\log(HI) = A_4 + B_4\log(RP/NUM) + C_4\log(SA) \quad (34)$$

where NUM is the number of loading cycles, SA is the strain amplitude induced during cyclic loading and A, B and C are regression constants.

These four forms of regression equations were evaluated to see which one if any produced a realistic model of healing as influenced by the variables presented.

During the process of regression analysis two factors were considered: whether or not the parameters in each regression model (equations 32 through 34) are significant and which model among the proposed models best explains the variability in the data and would be the most appropriate model to represent the healing process in each asphalt concrete mixture. In order to evaluate these two factors, two statistical tests were conducted: the t-test and the F-test.

The results of this detailed statistical analysis are discussed by Telikicherla, 1992. From this detailed analysis the following conclusions were drawn:

1. In equation 31, the length of the rest period is significant in describing the healing index of most of the 15 asphalt mixtures evaluated. The length of the rest period was determined to be significant for 12 of the 15 mixtures.

2. In equation 32, the parameter representing the ratio of length of rest period to number of loading cycles (RP/NUM) was determined to be significant for all 15 mixtures evaluated.
3. Equation 33 was determined not to be an appropriate model for explaining the healing index of the 15 mixtures evaluated.
4. In equation 34, the parameters (RP/NUM) and SA are statistically significant for all the mixtures tested and were the best statistical models for all mixtures except for mixtures produced with granite fine carrier aggregate and asphalt cements AAB and AAK.

Further statistical evaluation was performed using the F-statistic, p-value and R^2 analysis for equations 31 through 34. The detailed results of this statistical evaluation are presented by Telikicherla, (1992). As a result of the investigation, it was determined that equation 34 is the most appropriate model for describing the healing index of mixtures AAA (AAA-1 asphalt with granite fines), AAB (AAB-1 asphalt with granite fines), AAD (AAD-1 asphalt with granite fines), AAG (AAG-1 asphalt with granite fines), AAM (AAM-1 asphalt with granite fines), LLG (AAG-I asphalt with limestone fines), LLM (AAM-1 asphalt with limestone fines), Santa Maria (Santa Maria asphalt with limestone fines), SM + LDPE (Santa Maria asphalt with 5 percent low density polyethylene modification), Texaco AC-10 (Texaco AC-10 asphalt with granite fines), TX - APAO-3 (Texaco asphalt modified with APAO-3 polymer), TX - APAO-4 (Texaco asphalt modified with APAO-4 polymer) and AAMH (AAM-1 asphalt with granite fines tested at 31°C instead of 25°C). On the other hand

equation 32 is most appropriate model for mixtures AAK (asphalt AAK-1 with granite fines) and LLK (asphalt AAK-1 with limestone fines).

Table 9 summarizes the most appropriate models for each mixture.

In order to perform multiple comparisons of the various mixtures presented in Table 9 a least squares analysis was used as explained by Telikicherla (1992). This approach calculates the least square means of healing index of the unbalanced data after accounting for the effects of the two independent variables of RP/NUM and SA.

Using this approach, the six SHRP asphalt mixed with granite fines and tested at 25°C were grouped together to evaluated the influence of binder type on the healing index. From this analysis the following conclusions are drawn:

1. Healing potential of asphalt AAA-1 is significantly higher than that of asphalts AAB-1 and AAG-1. The p-values indicate that the healing potential of asphalt AAA-1 is not statistically different from that of asphalt AAD-1 and is significantly lower than AAM-1 and AAK-1.
2. Healing potential of asphalt AAB-1 is significantly different from that of the rest of the asphalts evaluated. Asphalt AAB-1 demonstrates the worst healing potential among the asphalts.
3. The healing potential of asphalt AAD-1 is higher than that of asphalts AAB-1 and AAG-1 and lower than that of asphalts AAM-1 and AAK-1. However, the healing potential of asphalt AAD-1 is not significantly different from that of asphalt AAA-1.
4. Healing potential of asphalt AAG-1 is significantly different from that of the rest of the asphalts evaluated. Healing potential of asphalt AAG-1 is better than that of AAB-1 and

worse than the rest of the asphalts evaluated.

5. Healing potential of asphalt AAK-1 is significantly higher than that of asphalts AAA-1, AAD-1, AAB-1 and AAG-1, but not statistically different from asphalt AAM-1.
6. Healing potential of asphalt AAM-1 is significantly higher than that of all asphalts except AAK-1.
7. The rank order of the six SHRP asphalts with increasing order of magnitude of healing index is: AAB-1, AAG-1, AAD-1, AAK-1 and AAM-1.

The supplementary testing to evaluate influence of aggregate type, polymer modification and temperature on healing index demonstrated that each of these factors does have a statistically significant influence on the healing index in the manner previously discussed.

DISCUSSION OF FACTORS INFLUENCING THE HEALING INDEX

The mechanisms that control microdamage healing are very complex and interactive. It is quite clear that this study has not uncovered the full mechanism of microdamage healing. However, the study has revealed certain aspects of the microdamage healing mechanism which provides the impetus for future work and a working hypothesis.

The research reported by Kim et al. (1990) evaluated the healing properties of three asphalts: an asphalt produced by the Witco refinery, an asphalt produce by the Fina refinery and a Shamrock asphalt. As discussed previously, the Fina and Shamrock asphalts demonstrated very good healing potential. However, the Witco asphalt was a very poor healer. Also as discussed previously, the healing index was determined to

be strongly related to the aliphatic chain length attached to the various generic fractions.

In this study, as discussed in Chapter 2, the relaxation properties of the asphalts studied are keenly related to the nature and length of the aliphatic chain fraction. Three of the asphalts studied to determine the mechanism of relaxation were SHRP asphalts AAM-1, AAG-1 and AAA-1. The AAM-1 SHRP asphalt is a West Texas intermediate crude processed by solvent deasphalting. This asphalt should be similar in nature to the Shamrock asphalt cement studied by Kim et al. (1990). The AAG-1 SHRP asphalt is a California Valley asphalt and is similar to the asphalt studied by Kim et al. (1990) produced by the Witco refinery.

It is important to note that the Witco and AAG-1 asphalts and the Shamrock and AAM-1 asphalts demonstrate the same relative healing potential as demonstrated by the two different studies, i.e., this research study and the Kim and Little study (1990). It is further important to note that both studies have noted the importance of the aliphatic chain structure on the healing potential through separate testing and different type testing. Furthermore, this study has demonstrated the importance of the aliphatic chain structure on rheological properties and relaxation properties.

HYPOTHESIZED MICROSTRUCTURAL MODEL

The extensive work performed by Western Research Institute under the SHRP research project A-002a has provided considerable insight into the microstructure of asphalt cement. As opposed to the old micellar model in which the asphalt cement was viewed as large assembledges of molecules concentrated into a micellar mass, the dispersed polar fluids model views the structure of asphalt as one without any large assembledges. Neither

the nuclear magnetic resonance used in the SHRP study nor the x-ray analysis used in this study was able to identify large assembledges.

Thus the asphalt cement must be comprised of small species which interact through strong yet momentary polar bonding. Petersen (1984) has shown how the oxidation of certain functionalities such as benzylic carbon can produce even more polar interactions among the molecules through the development of carbonyl groups. Other oxidation products can include carboxylic acids, sulfoxides and anhydrides.

Through means of increased polarity and steric interactions these relatively small particles (probably much smaller than 1 mm) can develop more interactivity leading to a dispersed polar fluid that is more resistant to flow, stiffer and more likely to fracture when overstressed. If aliphatic appendages are attached to the particles which comprise the polar fluid, these appendages may provide a geometric restraint to interaction. Thus when the interactivity increases due to an increase in polarity or through steric interactivity, the appendages may react as tiny "springs" which geometrically resist close interaction and agglomeration. The net result may be improved flow, under conditions of the highest interactivity, and thus greater resistance to fracture.

One can visualize that the geometric restraint to close interactivity provided by the aliphatic appendages may improve dispersion of the polar assembledges and thus improve compatibility and reduce the potential for aggoleration. A better dispersed fluid with less potential to develop strong steric interactivity should be a fluid which is a better healer as the material has an improved potential to flow across fracture faces and heal. Once this flow is accomplished, the interaction among aliphatic chains may further enhance microfracture healing.

CONSIDERATION OF HEALING INDEX IN ASPHALT PAVEMENT PERFORMANCE PREDICTIVE MODELING

In SHRP research contract A-005, Lytton (1992) has used the following relationship to compute the lab-to-field fatigue shift factor:

$$SF = 1 + \frac{n_{ri}}{N_0} \cdot m \cdot \left(\frac{t_i}{t_0}\right)^h \tag{35}$$

where n_{ri} is the number of rest period in the field, N_0 is the number of loads to failure in the lab test, t_i is the traffic rest period, t_0 is the time between loading applications with no rest period corresponding to the lab test, m is the healing coefficient and h is directly related to the healing index. Thus two parameters in this relationship, m and h, are directly related to the concept of fracture healing.

The healing index is a number that rises from 0 to 1 as the rest period increases. Mixtures which heal well rise faster than poorly healing mixes. The form of the equation for the healing index, HI, is:

$$HI = \frac{\phi_{after} - \phi_{Before}}{\phi_{After}} = 1 - \frac{\phi_B}{\phi_A} = \frac{a t_r^h}{1 + a t_r^h} \tag{36}$$

where

ϕ_A = the dissipated energy after a rest period of t_r and

ϕ_B = the dissipated energy before the rest period

The ratio of the two dissipated energy terms is:

$$\left[\frac{\phi_B}{\phi_A}\right] = \frac{1}{1 + a t_r^h}$$

The term in the denominator is of the same form as in the shift factor noted above and, in fact, is the shift factor between ϕ_B and ϕ_A. As seen in the shift factor equation, the a term depends upon the exponent, h, and the ratio of the rest periods associated with ϕ_B and ϕ_A . The exponent h, however, is a material property that is independent of the length of the rest periods. The exponent can be measured in the lab or can be inferred by backcalculation from fatigue cracking data observed in the field. Table 13 shows values of a and h determined in the calibration runs with the SHRP A005 pavement performance prediction model. In this case, the coefficient, a depends upon the actual traffic rate on each of the pavement test sections.

The values in Table 13 were determined by Liu (1993) from eight SHRP field pavement sections located in the four climatic regions listed in Table 13. The methodology for determining the values of a and h are based on a crack initiation and crack propagation model. Material properties related to crack initiation and crack propagation were backcalculated from field deflection tests. The actual field fatigue cracking was then determined by a systems identification methodology. This methodology is based on the application of a "healing shift factor" to the number of traffic load application, N_f, necessary to produce fatigue based on in situ derived material properties, to calculate the actual number of traffic load applications required to cause fatigue cracking of a specified level in situ, N_f':

$$N_f' = N_f \cdot (1 + a t^h) \qquad (37)$$

Table 13. Healing coefficients inferred from field fatigue data.

Climatic Zone	Healing Coefficients	
	a	h
Wet-No Freeze	0.09	0.843
Wet-Freeze	0.059	0.465
Dry-No Freeze	0.05	0.465
Dry-Freeze	0.07	0.479

The healing shift factor in equation 37 produces shift factors which are consistent with the range verified empirically and discussed in Chapter 1 (i.e., 1 to 10). If one estimates the rest period as a function of traffic, then the rest period may be approximated as follows:

$$t(seconds) = \frac{86{,}400 \ \ sec/day}{ADT \ \frac{vehicle}{day}} \tag{38}$$

Based on this approximation, Table 14 defines a typical range of shift factors due to microdamage healing. Note that the equivalent single axle load factors, (ESAL's) are predicted from average daily traffic (ADT) data. It may be that the time used (rest period) should be the time between vehicles with particular load level that will cause the formation and growth of microcracks for a certain pavement structure. This will mean a change in the actual coefficients and calculated shift factors in Table 14. One should not try to make too much of the coefficients and exponent in Table 14 nor the shift factor in Table 14 except to note that they are in the right range.

Table 14. Calculated healing shift factors based on a range of approximate traffic levels.

ADT with 20% Track Traffic	Approximate ESAL's	t, sec.	Healing Shift Factor ($SF=1+at^h$)
200,000	28,800	3	1.2
100,000	14,400	6	1.4
50,000	7,200	12	1.7
25,000	3,456	25	2.5
5,000	720	120	6.4
2,000	288	300	12

STATUS OF MICROSTRUCTURAL DAMAGE HEALING RESEARCH

An excellent data base exists which establishes the influence of binder source on healing properties. However, the effect of asphalt-aggregate interaction, polymer modification of asphalt mixtures, moisture conditioning and aging and temperature have not satisfactorily been determined. In addition, although some work has been done relating chemical, microstructural and rheological properties of the asphalt binder to healing, much work in this area is required to provide answers to imposing questions.

Recent work by Jacobs of the Delft University (1991) has substantiated calculations at TTI concerning the energy released during asphalt-aggregate fracture. These TTI calculations were, in turn, based on the bonding energy measurements supplied by WRI (enthalpy) and the Gibbs free energy measurements supplied by Auburn (toluene asphalt adsorptivity). It is felt that these recent developments point strongly to the need to completely understand the role of asphalt aggregate interaction and fracture on healing. Perhaps the fracture healing at the asphalt-aggregate bond controls the fatigue process.

The general consensus is that fracture healing is dominant in the initiation phase and occurs to a lesser level in the propagation phase. The majority of work in calculation of the healing index as defined by Kim and Little (1988) has been based on healing in crack propagation. A pressing need exists and in this study more closely study the healing effects on the initiation phase and in samples with a random dispersion of microcracks. The methodologies developed by Lytton (1992) in SHRP study A-005 offer the opportunity to do this.

Influence of Aggregates on Rate of Fracture within a Mixture

Jacobs (1992) used rate theory and deformation kinetics to develop a relation which describes the crack growth process in asphalt concrete specimens. The rate equation used by Jacobs employs three approaches for defining the crack growth process: bond-slipping, bond rupture and bond rupture and bond slipping. The bond rupture approximation is divided into two processes by Tobolsky and Eyring (1943): bond-repair or bond forming and bond breaking. The bond-repair process is essentially healing and is defined in the approach to be proportional to the number of broken bonds.

Knauss (1970) assumed that in a viscoelastic material the elastic energy is responsible for the forward process which means that the elastic energy determines the bond breaking process. Jacobs (1991) also assumed that the dissipated energy under the application of an external load is not only responsible for the temperature rise in the specimen but also for the backward process, which in fact is the bond-forming or the healing process. This assumption was made by Jacobs (1991) because of the fact that the healing process in asphalt concrete mixes depends largely upon the temperature of the mix: at low temperature the healing

process is negligible, and at high temperatures the healing process is of major importance in the determination of the life span of the asphalt concrete mixtures.

The final form of Jacob's crack growth equation is divided into two components as follows:

$$-\frac{dN}{dt} = NC_f - (N_0 - N)C_b \tag{39}$$

where dN/dt is the rate of crack growth, N is the number of bonds at t=t, N_0 is the number of bonds at t=0, C_f is the forward or bond-breaking process and C_b is the backwards or bond-forming process.

The term C_f accounts for the elastic and the viscoelastic components of applied mechanical energy per particle. In this parameter, a larger component of viscoelastic applied energy relative to elastic applied energy results in greater healing potential.

Using his crack growth rate equation, Jacobs calculated the mean value of the energy which is needed to break a bond. This value was calculated from crack growth measurements. The value calculated by Jacobs was 1.5×10^{-19} J/bond. This average value considers the (1) asphalt-asphalt bond, (2) asphalt-aggregate bond and (3) the healing process.

The mean value of energy required to break a bond was also calculated by Curtis, Lytton and Brannon (1992). Their approach was directed specifically at the asphalt-aggregate interfacial bond and was calculated through the use of the Gibbs free energy relationship. In this procedure, the product of temperature and change of entropy was defined as the total energy which bonds the asphalt to the aggregate

surface. This value ($T\Delta S$) was calculated from the definition of Gibb's free energy (ΔG) as:

$$T\Delta S = \Delta H - \Delta G \tag{40}$$

where ΔH is the enthalpy. This value was determined by Curtis et al. (1992) to be 41.52 KJ/mole. Since there are 6.0223×10^{23} bonds per mole, this means that the total energy which bonds the asphalt to the aggregate surface is 6.0×10^{-20} J/bond. This is in very close agreement with the value calculated by Jacobs. The difference between the two values could be due, in part, to the effect of healing which was considered by Jacobs but not by Curtis et al. The chemical process used by Curtis et al. and the rate equation used by Jacobs offers an intriguing approach by which to evaluate the fracture bonding at asphalt aggregate interfaces and in the mixture in general. The approach also offers the potential to separate and identify the relative bonding energy associated with various mixture interfaces and hence evaluate their contribution to fracture fatigue damage and microfracture healing.

As previously discussed, Lytton (1992) has incorporated this shift factor which strongly accounts for the fracture healing phenomenon in his A-005 pavement performance prediction model, FLEXPASS. In detailed analysis of pavement performance prediction, six variables were found to dominate the predicted life of the pavement: (1) healing coefficient, m; (2) healing exponent, h; (3) tensile strength; (4) stiffness of the asphalt-aggregate mix; (5) rutting coefficient and (5) slope of the creep compliance curve of the asphalt concrete mixture.

Evidence of Microfracture through Vibration Analysis

ASTM C215 describes a procedure in which an impact lead can be applied to induce a stress wave defined as a traveling dynamic transient disturbing particles away from their previous positions. This disturbance involves motion and changes in relative positions of particles. Therefore, the concepts of strain, stress, kinetic energy, potential energy and motion can be applied. This approach was evaluated in asphalt concrete samples by Kim (1992).

Kim tested asphalt concrete samples at 1, 2, 6, 7, 10, 16, 21 and 27°C. All samples tested were prepared by gyratory compaction and samples were then saw cut to the appropriate size. The testing performed at 10 and 16°C was after a conditioning period at 43°C for one day. Figure 50 shows the elastic modulus as a function of temperature for the three specimens tested. Notice that the best fit polynomial curve for the test data at 1, 2, 6, 7, 21 and 27°C does not fit the data at 10 and 16°C data. This vertical shift in the modulus-temperature curve suggests that the specimens have undergone some beneficial structural change while exposed to the 43°C temperature and thus developed an increase in stiffness. This structural change may well be due to the healing of intrinsic microcracks (produced during fabrication) at the elevated temperature.

Figure 51 shows similar data for the relationship between shear moduli and temperature for the three specimens. This vertical shift between the best fit polynomial curve and the specimens which underwent the high temperature conditioning (10 and 16°C) reinforces the possibility that the specimens have undergone fracture healing while exposed to high temperature.

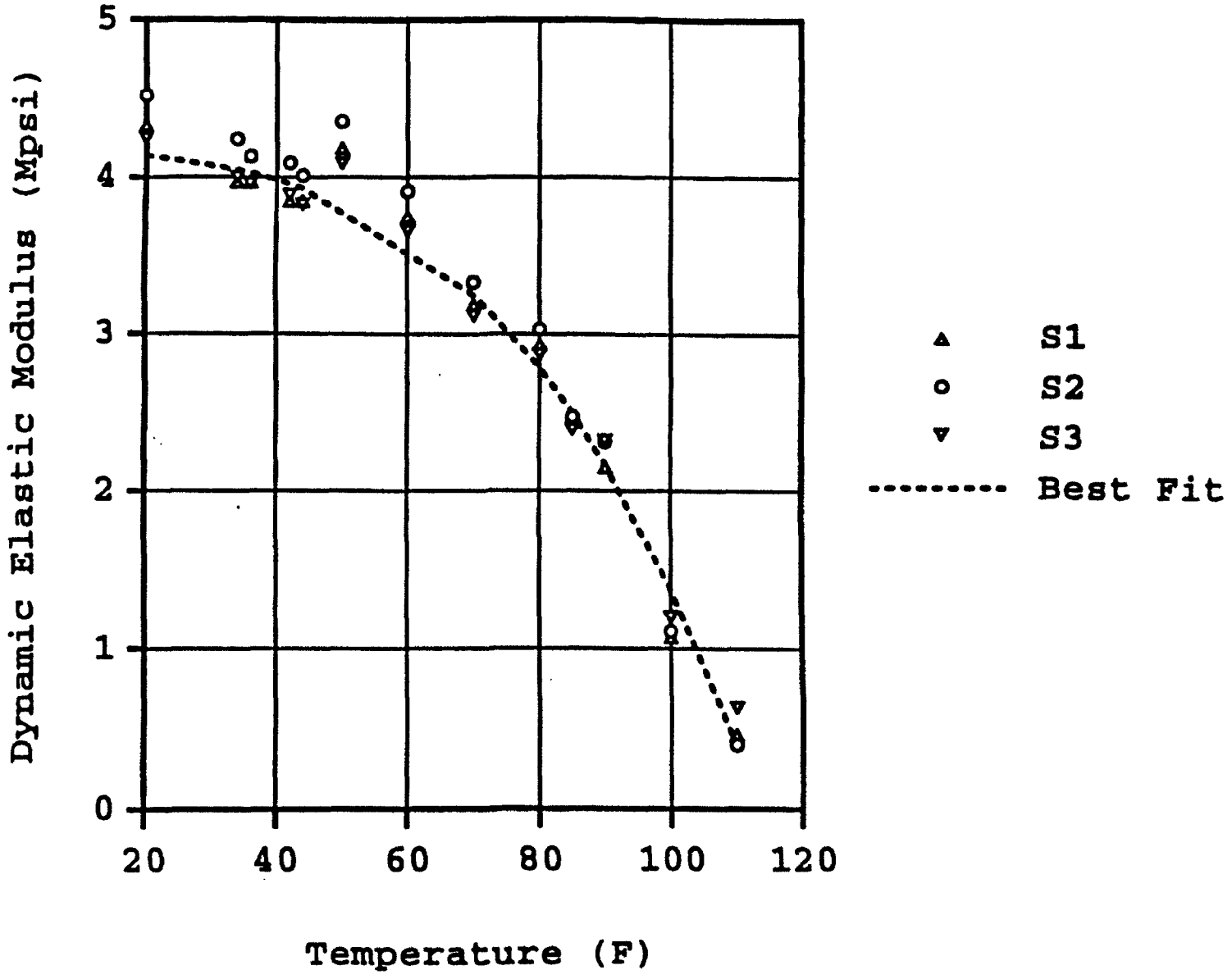

Figure 50. Elastic modulus as a function of temperature from vibrational analysis (After Kim, 1992).

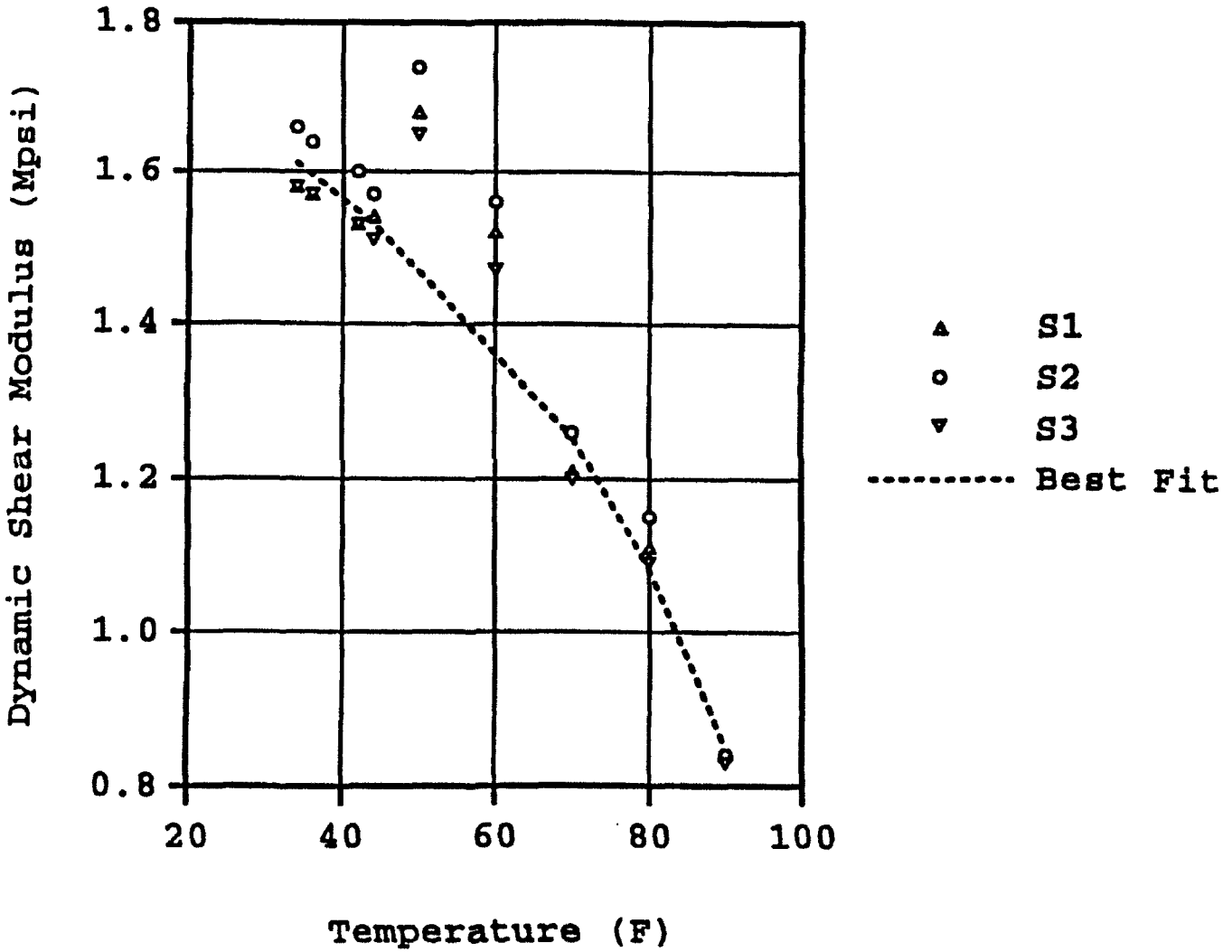

Figure 51. Shear modulus as a function of temperature from vibrational analysis (After Kim, 1992).

In general the vibrational analysis demonstrated by Kim yielded extremely consistent values in terms of elastic and shear modulus determination. Since the determination of elastic and shear modulus is a key factor in the evaluation of the effect of rest periods on damage healing, this concept is of great significance to this study both in terms on the findings of Kim (positive healing effects) and in terms of the applicability of the concept to further research in healing both in the lab and in the field.

APPROACH FOR FUTURE RESEARCH

Two methods have been used to determine or measure the healing index. The method used in this study uses a direct method to determine the healing index. This method uses controlled displacement testing or a pre-notched beam and computes the energy needed to drive the crack before and following rest periods of varying length. A non-linear viscoelastic correspondence principle is used to account for time of loading effects in the form of pseudo-strain.

This approach offers the ability to determine healing potential in a notched beam where the process or microfracture zone preceding the macrocrack is rather well defined. This testing protocol has been very effectively analyzed at TTI using the concept of pseudo-strain to determine the healing index based on pseudo-strain - stress relationships before and after healing. The non-linear correspondence principle has been effectively used to account for time-dependency effects during testing and to allow researchers to separate the re-bonding or "healing" effects from time dependent loading and unloading effects. The approach using pseudo-strain has worked very well with SHRP core asphalts and with modified asphalts. The process works better with densely-graded

aggregates than with the sand-aggregate originally used as a "carrier aggregate." Thus shifting from a sand asphalts system as used to minimize aggregate effects in early testing to a more traditional dense-graded mix is not a limitation. It is actually easier to test actual mixtures and the pseudo-strain approach works better.

A second approach is advocated by Lytton (1992). It does not use a notched beam, but instead allows distributed microcracks to grow into visible cracks, and is based upon the same theory of crack growth, was used by Lytton, et al. in the SHRP A005 Study. In this approach the first step in characterizing the asphalt-aggregate mixture is to run a frequency sweep test on the mixture and derive the relaxation modulus coefficients from the data. The relaxation modulus obeys the power law equation:

$$E(t) = E_0 + E_1 t^{-m} \tag{41}$$

The three coefficients are found from the frequency sweep data by measuring the real and imaginary parts of the complex modulus E*(w) as it varies with frequency. The real part is

$$E^1(w) = E_0 + E_1 \Gamma(1 - m) w^M \cos(\frac{\pi m}{2}) \tag{42}$$

and the imaginary part is

$$E^{11}(w) = E\Gamma(1 - m)\, w^m \sin(\frac{\pi m}{2}) \tag{43}$$

where

Γ = the Gamma function

and w = the frequency of loading in radians per second

By using a non-linear regression technique, the relaxation properties E_0, E_1, and m are found.

The next step is to run uniaxial constant strain rate tension tests at different rates of strain and temperature. The values of pseudo-strain, E^R, as defined in equation 20, correspond to different times of loading for each constant strain rate test. The reason for using equation 20 is that it allows a material to be non-linearly viscoelastic, while the pseudo-strain calculated with that equation, E^R, no longer depends upon the strain rate. The stress-strain-strain rate-temperature data are analyzed to produce the coefficients in the following constitutive relation:

$$\sigma = I \epsilon^R F(\epsilon^R)\, Sp\, G(Sp)\, a_t(T) \tag{44}$$

where

σ = the uniaxial tensile stress,

I = a coefficient which has the dimensions of modulus,

ϵ^R = the pseudo-strain corresponding to the stress at loading time, t,

Sp = the damage parameter as defined in equation 22,

$a_T(T)$ = the time-temperature shift function which is a function of temperature alone,

$F(\epsilon^R)$ = a hyperelastic pseudo-strain function to include a non-linear relation between stress and pseudo-strain and

G(Sp) = a damage function with a value of 1.0 when no damage exists and decreasing as damage increases.

The forms of the function a_t, G, and F are as follows:

$$a_T(T) = \left(\frac{T - T_a}{T_o - T_a}\right)^{\beta} \tag{45}$$

where

T_0 = the temperature of the master stress-pseudo-strain curve

and T_a, ß = material coefficients

$$F(\epsilon^R) = 1 + a_0\epsilon^R + a_1(\epsilon^R)^2 \tag{46}$$

$$G(Sp) = 1 + b_0 Sp + b_1(Sp)^2 \tag{47}$$

where

a_0, a_1, b_0, b_1 = pseudo-strain and damage parameters, respectively.

This constitutive equation gives the complete response of this material to tensile stress applied at different strain rates and temperatures. One of the material properties that is found in defining the damage parameter, Sp, is the exponent, p, which figures prominently in determining the size of the damage process zone, α, which precedes a visible crack in the material

$$\alpha = \left|\frac{\sigma_0}{\sigma_m}\right|^{\frac{1}{p}} \frac{J_v}{|\sigma_m| I_1} \tag{48}$$

where

σ_0 = the maximum tensile stress that is applied to the material,

σ_m = the tensile strength of the material,

p = the parameter in equation 22 that makes equation 22 fit the test data with the least sum of square error,

J_v = the J-integral for a viscoelastic material and

I_1 = the integral of the dimensionless stress-pseudo-strain curve of the material over the length of the damage zone, α. It has a value that is bounded between 1 and 2.

This size of the damage process zone, α, depends upon p which is found by analyzing the constant strain rate tension tests. The size of the damage process zone, in turn, governs the size of A, the Paris' law coefficient of crack growth. Paris' law is given by

$$\frac{dc}{dN} = A(J_v)^n \tag{49}$$

where

c = the crack (or microcrack) length,

N = the number of load applications,

$\frac{dc}{dN}$ = the rate of crack growth per load cycle,

A, n = the fracture coefficient and exponent in Paris' law and

J_v = the viscoelastic J-integral

The expression for A is complicated and will not be repeated here but it is of the form

$$A = k\,\alpha\, f(\sigma_m,\ m,\ E_0,\ E_1,\ \textit{and others variables}) \tag{50}$$

The equation shows that the Paris' law coefficient A is directly proportional to the length of the damage process zone, α. The fact that α depends on the exponent, 1/p, shows the importance of determining the value of p.

MICROFRACTURE FATIGUE RELATIONSHIPS

Lytton (1992) has developed a finite element model which can be used to analyze fatigue test data in which the loads are applied repeatedly. The program is capable of analyzing and bind of loading whether it is tensile, compressive, shear or bending.

In this model, an energy balance approach is used to predict stiffness reduction due to microcrack growth as a function of A and n, of Paris' law, the surface energy density, Γ, for the formation of crack faces, the distribution of microcrack lengths and dissipated energy.

Lytton (1992) demonstrates that damage, and thus healing, due to microcrack growth can be modeled through a stiffness reduction based on an energy balance. The energy balance relationship leads to a calculation of stiffness reduction caused by dissipated energy and crack growth of the form:

$$\frac{E'}{E} = \frac{(F_1+F_2)}{F_4\left\{1+2\pi\left(\frac{m}{bl}\right)\left[\frac{4\Gamma}{\pi}\,\frac{A\,t\,\pi\,\overline{c}^{(2+\frac{n}{2})}\,(\sigma^2+\tau^2)^{n/2}}{\frac{dW}{dN}} - \overline{c^2}\right]\right\} - F_3} \quad (51)$$

where

F_1, F_2, and F_4 are factors related to shear stress intensity and microcrack orientation,

m/bl is microcrack density,

C^2 is the square of microcrack length which is determined by a Weiball distribution function,

dw/dN is dissipated energy,

Γ is the gamma fraction and

A and n are Paris fracture parameters.

Lytton's approach should be pursued as a methodology to further evaluate the microdamage healing phenomenon. The approach is particularly relevant to confirming that the same fracture parameters control the propagation of both microcracks and visible cracks and that healing properties are the same for both scales of cracking. Application

of these "second" approach to study healing can be applied to tests which develop a tensile stress state within the specimen as well as a shear stress state.

A test that can duplicate shear and evaluate its effect on microcrack growth as well as visible crack growth is vitally important to the study of healing under realistic pavement stress states as recent studies (i.e., Lytton (1992)) have demonstrated that crack propagation is more often associated with the shear mode than the tensile mode.

The second approach remains vitally important as a process by which the healing factor can clearly be evaluated for various mixtures (with different asphalt binders) in terms of crack initiation (microcrack initiation and propagation).

REFERENCES

1. Aklonis, J. J., and MacKnight, W. J. (1983). "Introduction to Polymer Viscoelasticity," 2nd Ed., John Wiley and Sons, New York.
2. Alexander, L. E. (1985), "X-ray Diffraction Methods in Polymer Science," R. E. Publishing Company, Malabar, Florida.
3. Bale, H. D. and Schmidt, P. W. (1984). Phys. Rev. Lett., 53,596.
4. A. H. Al-Balbissi (1983), "A Comparative Analysis of the Fracture and Fatigue Properties of Asphalt Concrete and Sulphlex," Ph.D. Dissertation, Texas A&M University, College Station, Texas.
5. Barnes, H. A., Hutton, J. F., and Walters, K. (1989). "An Introduction to Rheology. Elsevier Science Publishing Company," New York.
6. Baumgaertel M., and Winter H. H. (1989). "Determination of Discrete Relaxation and Retardation Time Spectra from Dynamic Mechanical Data," Rheologica Acta, 28(6), 511-519.
7. Baumgaertel M., Schausberger., A., and Winter H. H. (1990). "The Relaxation of Polymers with Linear Flexible Chains of Uniform Length," Rheologica Acta, 29(5), 400-408.
8. P. Bazin and J. B. Saunier (1967). "Deformability, Fatigue and healing Properties of Asphalt Mixes," Proc., Second International Conference on the Structural Design of Asphalt Pavements, Ann Arbor, Michigan, pp. 553-569.
9. Beitchman, B. D. (1959). "Infrared Spectra of Asphalts," Journal of Research of the National Bureau of Standards, 63A(2), 189-193.
10. Bellamy, L. J. (1958). The Infrared Spectra of Complex Molecules. 2nd Ed., Nethuen, London.
11. Bellamy, L. J. (1980). Advances in Infrared Group Frequencies. 2nd Ed., Chapman and Hall, London.

12. F. C. Benson (1988). "Correlation among Asphalt Concrete Mechanical Healing, Asphalt Cement Dispersion, FT-IR Chemical Functional Groups and NMR Chemical Structure," Ph.D. Dissertation, Texas A&M University, College Station, Texas.

13. Benson, F. C. and Little, D. N. (1988). "Correlation Among Asphalt Concrete Mechanical Healing, Asphalt Cement Dispersion, FTIR Chemical Functional Groups and ^{1}H NMR Chemical Structure," Final Report, Grant No. ECE-8511851, National Science Foundation.

14. "Binder Characterization and Evaluation," (1991). Quarterly Report, Technical Section, SHRP A-002A, Western Research Institute, University of Wyoming Research Corporation, Laramie, June 1991.

15. Boduszynski, M. M., McKay, J. F., and Latham, D. R. (1980). "Asphaltenes, where are you?," Proceedings of the Association of Asphalt Paving Technologists, 49, 123-143.

16. F. P. Bonnaure, A. H. J. J. Huibers, and A. Boonders (1982). "A Laboratory Investigation of the Influence of Rest Periods on the Fatigue Characteristics of Bitumious Mixes," Proc., Association of Asphalt Paving Technologists, Vol. 51, pp. 104-128.

17. B. J. Briscoe (1978). Some Aspects of the Autoadhesion of Elastomers. In: Polymer Surfaces, D. T. Clark, and W. J. Feast (eds.), Wiley Interscience Pub., New York, pp. 25-46.

18. C. B. Bucknall, I. C. Drinkwater, and G. R. Smith (1980). Hot Plate Welding of Plastics: Factors Affecting Weld Strength. Polymer Engineering and Science, Vol. 20, No. 6, pp. 432-440.

19. Corbett, L. W. (1969). "Composition of Asphalt Based on Generic Fractionation Using Solvent Deasphaltening, Elution-Adsorption Chromatography, and Densimetric Characterization," Analytical Chemistry, 41, 576-579.

20. Corbett, L. W. (1970). "Relationship Between Composition and Physical Properties of Asphalt," Proceedings of the Association of Asphalt Paving Technologists, 39, 481-489.

21. Curtis, C. W., Lytton, R. L. and Brannan, C. J. (1992), "Influence of Aggregate Chemistry on the Adsorption and Desorption of Asphalt," Transportation Research Board 1362, Washington, D. C.

22. De Gennes, P. G. (1990). Introduction to Polymer Dynamics. Cambridge University Press, New York.

23. Dealy, J. M. (1979). "Rheological Properties of Oil Sand Bitumens," The Canadian Journal of Chemical Engineering, 57, 677-683.

24. K. DeZeeuw and H. Potente (1977). "The Determination of Welding Parameters in the Hot Plate Welding of Large-Diameter Pipes of rigid Polyethylene," Society of Plastics Engineers, Technical Paper, Vol. 2, pp. 55-80.

25. Doi, M., and Edwards, S. F. (1986). The Theory of Polymer Dynamics. Clarendon Press, Oxford, New York.

26. F. Finn, C. Saraf, R. Kulkarni, K. Nair, W. Smith, and A. Abdullah (1977). "The Use of Prediction Subsystems for the Design of Pavement Structures," Proc., Fourth International Conference on Structural Design of Asphalt Pavements, pp. 3-38.

27. Girdler, R. B. (1965). "Constitution of Asphaltenes and Related Studies," Proceedings of the Association of Asphalt Paving Technologists, 34, 45-79.

28. Halstead, W. J. (1985). "Relation of Asphalt Chemistry to Physical Properties and Specifications," Proceedings of the Association of Asphalt Paving Technologists, 54, 91-117.

29. Jacobs. M. M. J. (1992). "The Use of the Rate Theory to Describe the Crack Process in Asphalt Concrete Mixes," Report 7-91-116-7, the Delft University, The Netherlands.

30. Kim, Y. R. and Little, D. N. (1989), "One-Dimensional Constitutive Modeling of Asphalt Concrete," ASCE Journal of Engineering Mechanics, Vol. 59, pp. 240-275.

31. Y. Kim and R. P. Wool (1983). "A Theory of Healing at a Polymer-Polymer Interface. Macromolecules," Vol. 16, pp. 1115-1120.

32. Kim, Y. R. (1992). Personal Communications on Research on Vibrational Analysis.

33. Koeinig, J. L. (1991). Spectroscopy of Polymers, American Chemical Society, Washington, D.C.

34. Krausz A. S. and Eyring H. (1975). "Deformation Kinetics," A Wiley Interscience Publication, U.S.A..

35. Lambert, J. B., Shurvell, H. F., Lightner, D. A., and Cooks, R. G. (1987). Introduction to Organic Spectroscopy. Macmillan Publishing Company, New York, Collier Macmillan Publishers, London.

36.

37.

38. Mandelbrot, B. B. (1982). The Fractal Geometry of Nature, Freeman, San Francisco.

39. Martin, J. E., Hurd, A. J. (1987) J. Appl. Cryst., 20, 61.

40. Monismith, C. L. (1961). "Asphalt paving mixtures properties, Design, and Performance," Course Notes, Prepared for the Short Course in Asphalt Paving Technology, The Institute of Transportation and Traffic Engineering, University of California.

41. Murthy, N. S. and Minor, H. (1990). Polymer, 31, 996.

42. Murthy, N. S., Correale, S. T., Minor, H. (1991). Macromolecules, 24, 1185.

43. Petersen, J. C. (1967). "An Infrared Study of Hydrogen Bonding in Asphalt." Fuel, 46, 295-305.

44. Petersen, J. C. (1984). "Chemical Composition of Asphalt as Related to Asphalt Durability - State of the Art," Presented at the 63rd Meeting of the Transportation Research Board, Washington, D. C., Jan. 1984.

45. Petersen, J. C. (1986). "Quantitative Functional Group Analysis of Asphalts Using Differential Infrared Spectrometry and Selective Chemical Reactions - Theory and Application," Presented at the 65th Annual Meeting of the Transportation Research Board, Washington, D. C., Jan. 1986.

46. S. Prager and M. Tirrell (1981). The Healing Process at Polymer-Polymer Interfaces. Journal of Chemical Physics, Vol. 75, No. 10, November, pp. 5194-5198.

47. Prapnnachari, S. (1992). Investigation of Microstructural Mechanism of Relaxation in Asphalt. Ph. D. Dissertation, May 1992, Texas A & M University, College Station, Texas.

48. K. D. Raithby and A. B. Sterling (1970). The Effect of Rest Periods on the Fatigue Performance of a Hot-Rolled Asphalt under Reversed Axial Loading. Proc., Association of Asphalt Paving Technologists, Vol. 39, pp. 134-147.

49. Ruland, W. (1977). Pure Appl. Chem., 49, 505.

50. Schaefer, D. W. (1989). Science, 243, 1023.

51. R. A. Schapery (1982). Models for Damage Growth and Fracture in Nonlinear Viscoelastic Particulate Composites. Proc., Ninth U.S. National Congress of Applied Mechanics, ASME, pp. 237-245.

52. Silver stein, R. M., Bassler, G. C., and Morril T. C. (1981). Spectrometric Identification of Organic Compounds. 4th Ed., John Wiley and Sons, Inc., New York.

53. Stewart, J. E. (1957). "Infrared Spectra of Chromatographically Fractionated Asphalts," Journal of Research of the National Bureau of Standards, Washington D. C., 58(5), 265-269.

54. Telikicherla, R. (1991). "Statistical Evaluation of the Influence of Mixture Variables on Microcrack Healing on a Variety of Asphalt Concrete Mixtures," Master of Science Thesis, Texas A&M University.

55. Tobolsky A. and Eyrig H. (1943). "Mechanical Properties of Polymeric Materials," Journal of Chemical Physics. Vol. 11.

56. R. N. Traxler (1960). Relation Between Hardening and Composition of Asphalt. Preprints, Division of Petroleum Chemistry, American Chemistry Society, Vol. 5, No. 4, pp. A71-A77.

57. K. H. Tseng and R. L. Lytton (1988). Documentation of Flexible Pavement Performance Analysis Program. Final Report for Florida DOT, Texas Transportation Institute, College Station, Texas.

58. Walters, K. (1975). Rheometry. John Wiley and sons, New York.

59. R. P. Wool and K. M. O'Connor (1981). A Theory of Crack Healing in Polymers. Journal of Applied Physics, Vol. 52, No. 10, pp. 5953-5963.

APPENDIX A

CHARACTERIZATION OF DAMAGE GROWTH IN ASPHALT CONCRETE

INTRODUCTION

Understanding of the hysteretic stress-strain behavior of pavement materials under repetitive traffic loading is imperative to properly predict the pavement performance and ultimately remaining service life. Among the component materials of a flexible pavement, asphalt concrete mixture is considered as the most important material to be accurately characterized, not only because of its higher cost but also because of its contribution to pavement distresses. For example, it has been well known that the fatigue cracking is due to repetitive bending of asphaltic layers. A field study in Canada (Dawley et al. 1990) also suggested that rutting is due primarily to permanent lateral deformation of the asphalt concrete layer, not due to structural deficiencies in pavement thickness design.

When an asphalt concrete pavement is subjected to repetitive applications of multi-level vehicular loads with various durations of rest periods, three major mechanisms take place in the asphalt concrete: damage accumulation due to flow and/or micro- and macro-crack propagation; relaxation of stresses in the system due to viscoelastic nature of asphalt concrete; and chemical healing across micro- and macro-crack interfaces. Damage mechanisms degrade pavement performance, while relaxation and healing mechanisms lengthen the life of asphalt concrete pavement. The accuracy of predicting the response and performance of asphalt concrete under random traffic loading depends upon one's understanding of these mechanisms.

The difficulty of evaluating these mechanisms under

repetitive wheel loads arises from the fact that they occur simultaneously in an asphalt concrete pavement. For example, the degree of fatigue damage sustained under loading depends on how well the material relaxes, and healing as well as relaxation take place simultaneously in a damaged pavement. There is a need to develop a methodology of evaluating these mechanisms separately in order to accurately predict the pavement response under traffic loading.

BACKGROUND

A methodology of separately evaluating fracture healing, damage growth, and relaxation under repetitive loading has been already developed by Kim (Kim 1988; Kim and Little 1989; Kim and Little 1990; Kim et al. 1990). In Kim's earlier study, the nonlinear elastic-viscoelastic correspondence principle was applied to uniaxial cyclic stress-strain data of sand-asphalt as a means of reducing the viscoelastic analysis to an elastic case. The laboratory verification study revealed that the resulting constitutive model satisfactorily predicted the effects due to multilevel loading, due to sequence of multilevel loading, and due to various durations of rest periods.

Application of this concept to the pavement design and analysis requires the verification study in more realistic conditions. Therefore, the same analytical concept in Kim's earlier work (1988) has been applied in this study to more representative conditions of the in-service pavements. The major differences in cyclic testing conditions used in Kim's work and

in this study are as follows:

Conditions used in this study	Kim (1988)
Controlled-stress test	Controlled-strain test
Compressive loading	Tensile loading
Haversine wave form	Saw-tooth wave form
0.2 second/cycle	1 second/cycle
Short rest periods (1, 4, 8, 16 sec.)	Long rest periods (5, 10, 20, 40 min.)
Densely-graded AC	Sand-asphalt

MATERIALS AND TESTING METHODS

1. Sample Fabrication

All the specimens were fabricated using Watsonville granite aggregates and AR-4000 grade of California Valley asphalt cement. The aggregate gradation was selected in accordance with the specification limits by ASTM D3515 method which is a standard specification for hot-mixed, hot-laid bituminous paving mixtures (Fig. 1). The washed sieve analysis was used to select the gradation shown in Fig. 1. Aggregates were mixed with 4.9% asphalt (optimum asphalt content determined by the Marshall mix design method) by weight of dry aggregate at 140°C (284°F) for 4 minutes. The mixture was then cured at 60°C (140°F) for 15 hours and compacted at 116°C (240°F) into a 10.16 cm (4-inch) diameter and 20.32 cm (8-inch) height cylindrical specimen using the COE Gyratory Testing Machine.

The method used for measurement of the air voids was wet-

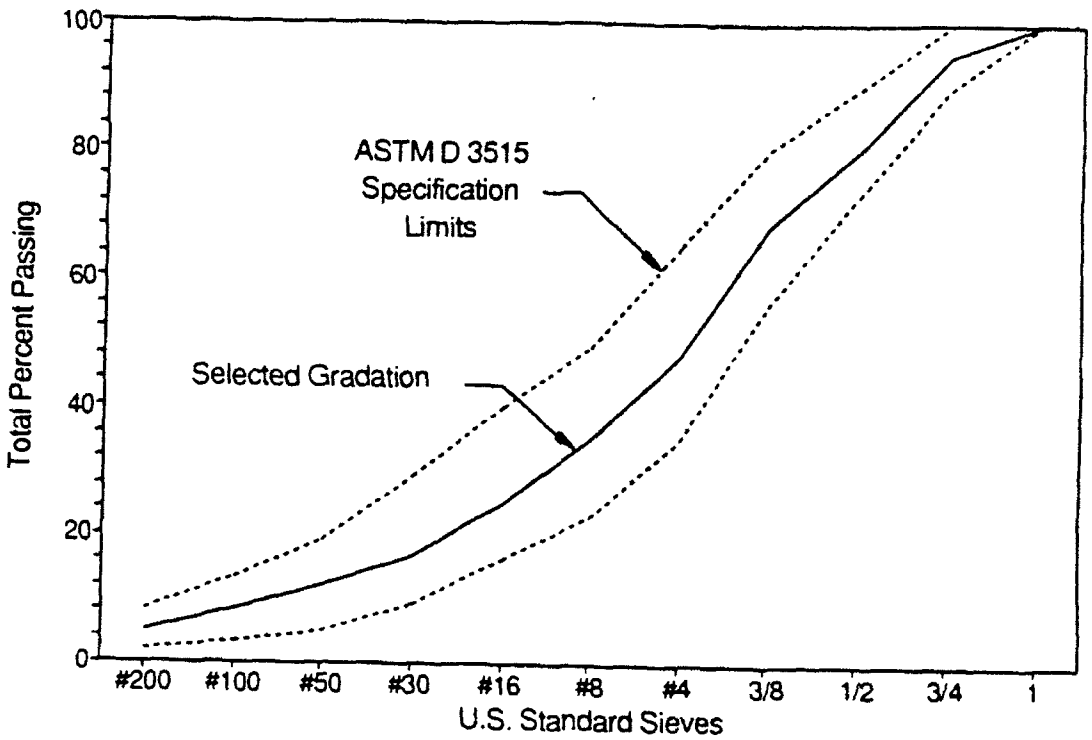

Fig. 1 Selected aggregate gradation.

with parafilm method. This method has been developed in course of the Strategic Highway Research Program A-003A project and employs elastic-wax paper, parafilm, as a substitute for paraffin wax. The use of parafilm during the air voids measurement prevents water from entering the specimen during submerged weighing which could result in underestimation of air voids (Harvey et al. 1992). Samples with air voids falling between 3 and 3.5% were only used in testing to minimize the variability in test results.

2. Testing Methods

All the tests were conducted at 25°C (77°F) in a uniaxial compression mode using a servo-hydraulic closed loop testing machine. Cylinder samples were capped with sulfur at both ends, and the interfaces between the caps and loading plates were lubricated in order to minimize any eccentric loading. Preconditioning was done by applying 133 N (30 lbs) of square load for 2 minutes followed by a 10-minute rest period.

Test data were collected by a data acquisition system with the multi-channel 12-bit board. Displacements were measured in two different ways; one using two extensometers in the middle portion of the sample with gage lengths of 10.16 cm (4 inches) and the other from the ram movement resulting 20.32 cm (8 inches) of sample height to be the gage length. Measurements using the 20.32 cm (8-inch) gage length include the effect of nonuniform stress distribution at the ends whereas the extensometers with the 10.16 cm (4-inch) gage length measure the displacement where

the stress distribution is relatively uniform. Stresses and strains used in the analysis were nominal (average) values calculated from the following equations:

$$\sigma = P / A \qquad \text{and} \qquad \epsilon = u / L$$

where P = load,

u = displacement,

A = cross-sectional area of the sample, and

L = initial gage length.

Types of the tests performed in this study are summarized in the following. Uniaxial compressive creep and relaxation tests were performed to determine the time-dependent properties of the mixture. These tests were repeated at changing temperatures to develop the time-temperature master curves. Uniaxial constant-strain-rate monotonic testing was conducted by controlling displacement measured from the 10.16 cm (4-inch) gage length. Finally controlled-stress cyclic testing with various rest periods was performed. Three levels of load amplitude, 0.556, 1.112, and 11.12 kN (125, 250, and 2500 lbs), were used in controlled-stress cyclic testing in an attempt to investigate the damage growth in asphalt concrete under cyclic loading. Low amplitude of 0.556 kN (125 lbs) was selected to ensure the negligible damage growth during the cylic loading, and 11.12 kN (2500 lbs) to induce a significant damage growth after each cycle.

ELASTIC-VISCOELASTIC CORRESPONDENCE PRINCIPLE

Theory of viscoelasticity allows one to take an appropriate

transformation of the governing field and boundary equations of viscoelastic problems with respect to time and reduce them so that they are mathematically equivalent to those for elasticity problems with the substitution of elastic moduli. This so-called elastic-viscoelastic correspondence principle thus eliminates the time-dependence of the material merely by working in a transformed domain with transformed elastic moduli. For linear viscoelastic media, the correspondence principle works in the Laplace-transformed domain.

The nonlinear viscoelastic correspondence principle was developed by Schapery (1984). He suggested that the constitutive equations for certain nonlinear viscoelastic media are identical to those for the nonlinear elastic case, but the stresses and displacements are not necessarily physical quantities in the viscoelastic body. Instead, they are "pseudo displacements" and "pseudo stresses" which are in the form of convolution integrals such that

$$u_i^R = \frac{1}{E_R} \int_0^t E(t-\tau) \frac{\partial u_i}{\partial \tau} d\tau$$

$$\sigma_{ij}^R = E_R \int_0^t D(t-\tau) \frac{\partial \sigma_{ij}}{\partial \tau} d\tau$$

where σ_{ij}, u_i = physical stresses and physical displacements, respectively,

σ^R_{ij}, u^R_i = pseudo stresses and pseudo displacements, respectively,

$E(t)$, $D(t)$ = relaxation modulus and creep compliance, respectively, and

E_R = the reference modulus which is an arbitrary constant.

For the case of growing traction boundary surface, such as crack growth problems, one can reduce the nonlinear viscoelastic problem to a nonlinear elastic case by using physical stresses and pseudo displacements. The explicit form of the constitutive equation is of course dependent upon material type, sample geometry, and loading geometry.

DEVELOPMENT OF COMPUTER PROGRAMS

Calculation of pseudo strain requires the following three operations: (1) the expression of relaxation modulus as a function of time, (2) the first derivative of the strain function (input for the controlled-strain tests and response for the controlled-stress tests), and (3) integration of the product of these two terms from the beginning of the initial load to the time of interest. Since the pseudo calculation is very sensitive to the accuracy of time, stress, and strain measurements, raw data have to be processed by the program "TRANSFER.BAS" in order to determine the time "zero" and eliminate the signals before the time "zero".

The relaxation modulus can be expressed by the pure power form, $E(t) = E_1 t^{-n}$, or by the generalized power form, $E(t) = E_0 + E_2 t^{-n}$. The coefficients in the pure power form can be determined by simply performing the linear regression in the logarithmic

scales of E(t) and time. Determination of the regression constants in the generalized power form is more involved and the trial-and-error method has to be used because of the number of regression constants. The method first assumes the value of n, and then a linear regression analysis is performed between E(t) and t^{-n}. This procedure is repeated for a series of n's, and the n that resulted in the smallest sum of squares of error is determined. Computer programs, "PWR_PU.BAS" for the pure power form and "PWR_GN.BAS" for the generalized power form, were written to find a set of regression coefficients that results in the best fit for the selected data points at an equal logarithmic time interval. Although the generalized power form fits the relaxation data a little better, the pure power form was used in the analysis for practical reasons.

One of the most difficult tasks with the pseudo calculation is to obtain the derivative of the strain function with respect to time because realistic test conditions generate random data instead of some assumed or predesignated mathematical functions. A program "DIDT.BAS" was developed for this specific purpose in which numerical analysis of the least-squares fitting of discrete points method was used. To calculate the derivative of the strain function at a given time, the program first takes a certain number of data points before and after that specific time (the number of data points selected depends on the number of data points in a loading cycle), determines the best fit equation through those points, and then differentiate this function at that specific time point.

After the relaxation modulus and the derivatives of strains for the entire testing period are calculated, pseudo strains are determined by a computer program "PSEUDO.BAS". The algorithm used in this program is described in the following.

Pseudo strain for the uniaxial loading can be determined from the following:

$$\varepsilon^R = \frac{1}{E_R} \int_0^t E(t-\tau) \frac{de}{d\tau} d\tau$$

For the relaxation modulus in a generalized power form, the above equation for pseudo strain can be reduced to:

$$\varepsilon^R = A \int_0^t \frac{de}{d\tau} d\tau + B \int_0^t (t-\tau)^{-n} \frac{de}{d\tau} d\tau$$

$$= R_1(t) + R_2(t)$$

where A and B are constants. The terms, $R_1(t)$ and $R_2(t)$, can be numerically integrated by dividing the total time, t, into q equal time segments of Δt:

$$R_1(t) = A(\Delta t) \sum_{m=1}^{q} C_m \quad \text{and}$$

$$R_2(t) = \frac{B}{1-n} (\Delta t)^{1-n} \sum_{m=1}^{q} C_m [(q-m+1)^{1-n} - (q-m)^{1-n}]$$

where C_m is the first derivative of strain at the time of (m x Δt). In case of using the pure power form, $R_1(t)$ is equal to zero. Pseudo stresses can be determined exactly the same way as

the above except that the creep compliance and stress function are used in the convolution integral.

Some other small utility programs were also developed for the specific purposes. The program "LESSDATA.BAS" reduces the amount of data points in a data file so that the data can be imported into a spreadsheet. The program "DIDTMONO.BAS" was written exclusively for calculating the monotonic test data. Benefits of using computer programs are not only saving computation time but also permitting the analysis of general strain or stress values that can not be presented in one explicit arithmetic function as a whole.

DISCUSSION OF RESULTS

1. Characterization of Time-Dependent Material Properties

(A) Creep and relaxation testing

Compressive creep tests were performed with load levels of 0.556 kN (125 lbs) and 1.112 kN (250 lbs). Creep compliance was calculated from the displacements with both the 10.16 cm (4-in.) and 20.32 cm (8-in.) gauge lengths and plotted against loading time in Figs. 2(a) and 2(b), respectively. As shown in Fig. 2(a), the creep curves with both the load levels were superimposed on each other when the creep compliance was determined from displacements of the 10.16 cm (4-in.) gauge length, indicating that the material is linearly viscoelastic within the load levels used. The pure power form of the best fit line was calculated as:

$$D(t) = 4.9486 \times 10^{-7} \times t^{0.481}$$

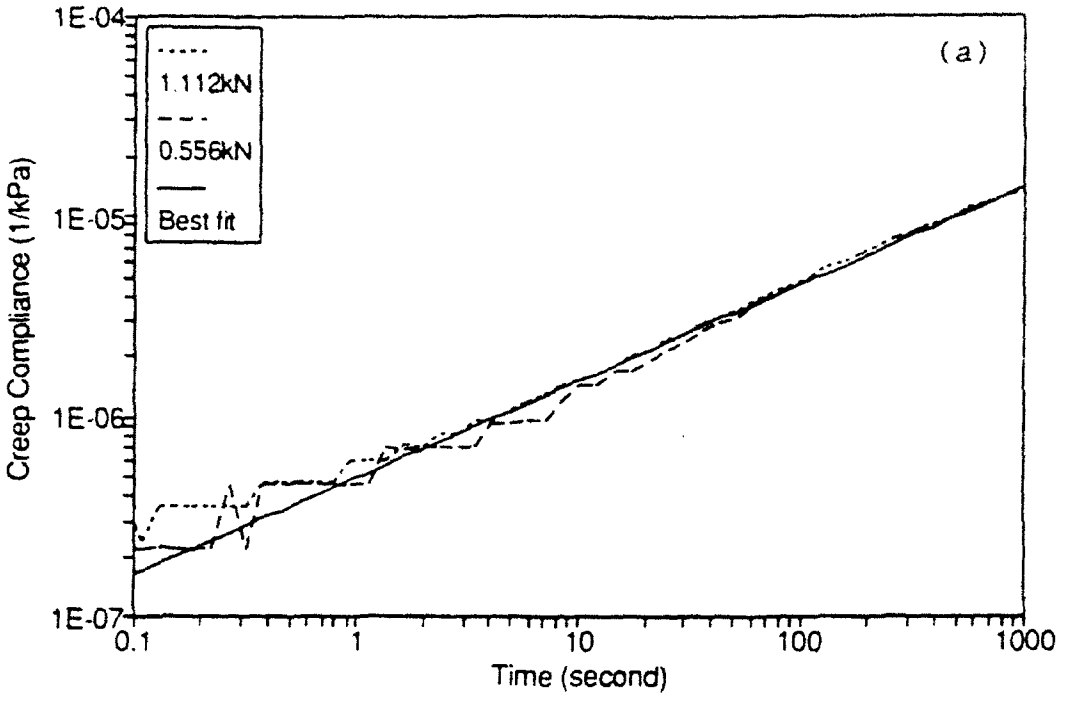

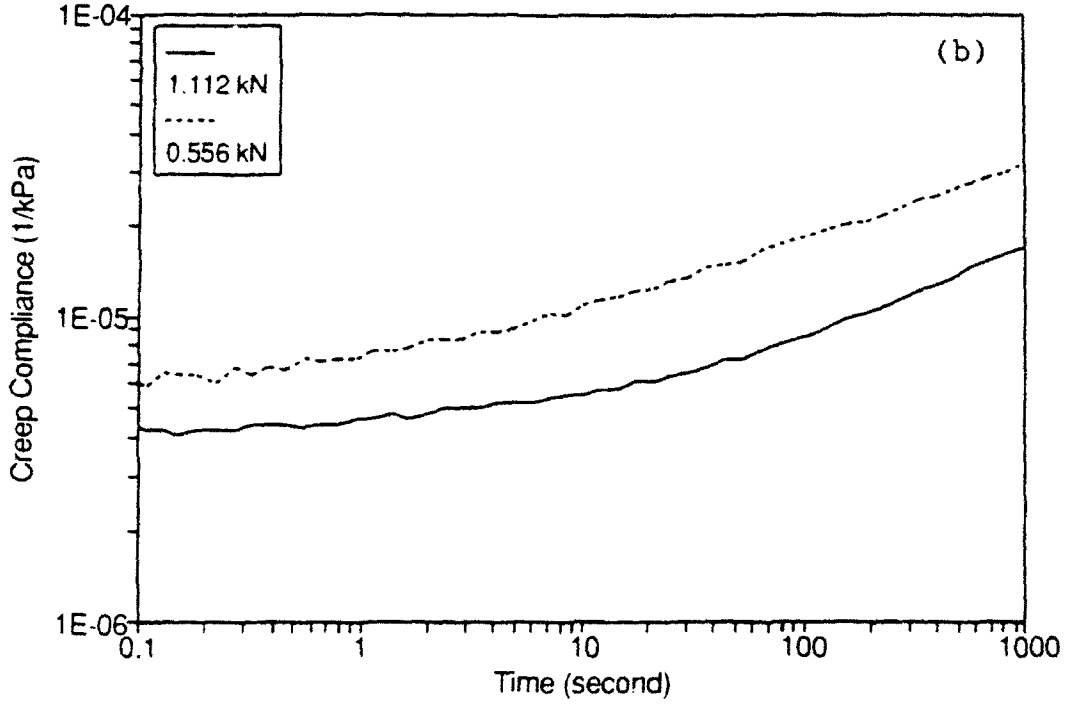

Fig. 2 Uniaxial compressive creep curves at 25°C:
(a) Displacement measured from 10.16 cm gage length and
(b) Displacement measured from 20.32 cm gage length.

where the unit of D(t) is the inverse of kPa.

On the contrary, the creep curves with the 20.32 cm (8-in.) gauge length in Fig. 2(b) showed a large discrepancy between the two load levels. This nonlinear behavior is due to the end effects causing nonuniform strain distribution near the ends of the specimen.

Compressive relaxation tests were performed by controlling the displacement measured from the 20.32 cm (8-in.) gauge length. Fig. 3 presents the relaxation modulus determined from the strain amplitude of 0.125%. The regression equation for the relaxation modulus is determined as:

$$E(t) = 135951\ t^{-0.460}$$

where the unit of E(t) is kPa.

(B) Backcalculation of relaxation modulus

The calculation of pseudo strain requires the expression of relaxation modulus as a function of time. The relaxation modulus testing is fairly difficult to perform because of large initial load response as a result of the immediate increase in strain input. For practical applications, it is desirable to predict the relaxation modulus from the creep test because it is much easier to perform.

The theory of linear viscoelasticity allows one to predict the relaxation modulus from the creep compliance as long as the load level in the creep testing is within the linear range. For the linear viscoelastic media, the uniaxial stress and strain are related through the following convolution integral:

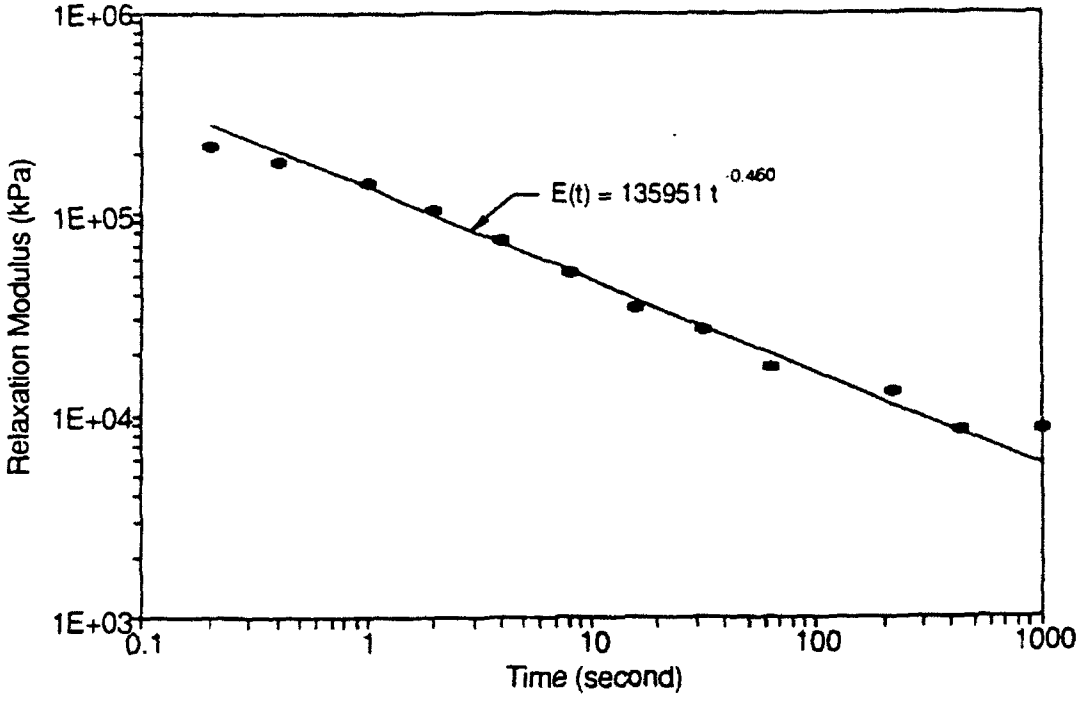

Fig. 3 Uniaxial compressive relaxation modulus at 25°C.

$$\sigma = \int_0^t E(t-\tau)\,\frac{d\varepsilon}{d\tau}\,d\tau$$

In case of creep testing, the stress input is a unity, and the strain response is represented as the creep compliance, D(t). Therefore, the above constitutive equation can be written as:

$$1 = \int_0^t E(t-\tau)\,\frac{dD(\tau)}{d\tau}\,d\tau$$

Taking the Laplace transform of both sides of the above equation yields:

$$S^2 \cdot L\{D(t)\} \cdot L\{E(t)\} = 1$$

where $L\{f(t)\}$ is the Laplace transformation of function f(t) and S is a real constant. Assuming the creep compliance is represented in a pure power form, $D(t) = D_1 \times t^n$, the equation can be reduced to:

$$D(t) \cdot E(t) = \frac{\sin(n\pi)}{n\,\pi}$$

As the value of n is approaching zero meaning a purely elastic case, the right side of the equation becomes unity. Also, this relationship suggests that, if the material is linearly viscoelastic, the time exponents in the measured creep compliance and relaxation modulus should be the same value with opposite signs. The time exponents of 0.481 and -0.460 respectively from the creep compliance and relaxation modulus testing indicate that one can predict the relaxation modulus of asphalt concrete from the creep test as long as the load level is within the linear

range.

Using the above relationship, the relaxation modulus was predicted from the creep compliance in the following equation:

$$E(t) = 1333929\ t^{-0.481}$$

where the unit of E(t) is kPa. Comparison of the above equation to the measured relaxation modulus shows that the coefficient in the predicted is about one order of magnitude larger than the one from the measured. This discrepancy will not affect the type of analysis performed in this study although the slopes of stress-pseudo strain curves will be different. For the remainder of this paper, the relaxation modulus predicted from the creep compliance was used for the analysis.

(c) Time-temperature correspondence principle

Another important aspect to be considered in the asphalt concrete testing and analysis is the temperature dependency. In this study, fundamental correspondence between time and temperature was evaluated by the creep and relaxation tests of asphalt concrete at varying temperatures. The creep compliance and the relaxation modulus at a range of temperatures were plotted against the loading time in Figs. 4(a) and 4(b), respectively.

Horizontal shift along the log time axis allowed the construction of the creep and relaxation master curves at the reference temperature of 25°C (77°F) shown in Figs. 5(a) and 5(b), respectively. The time shift factors can be obtained from the following:

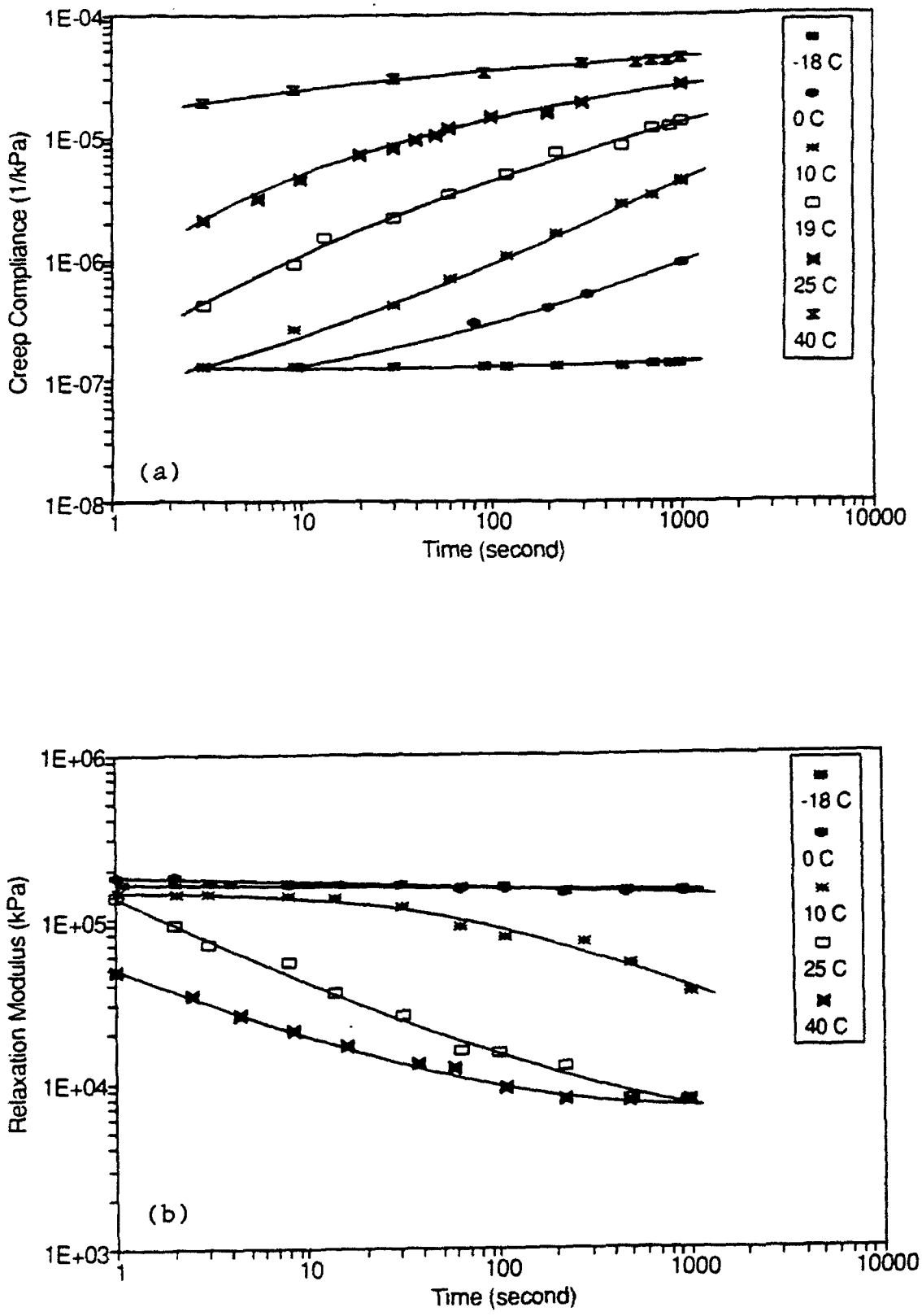

Fig. 4 (a) Creep compliance curves at a range of temperatures. (b) Relaxation modulus curves at a range of temperatures.

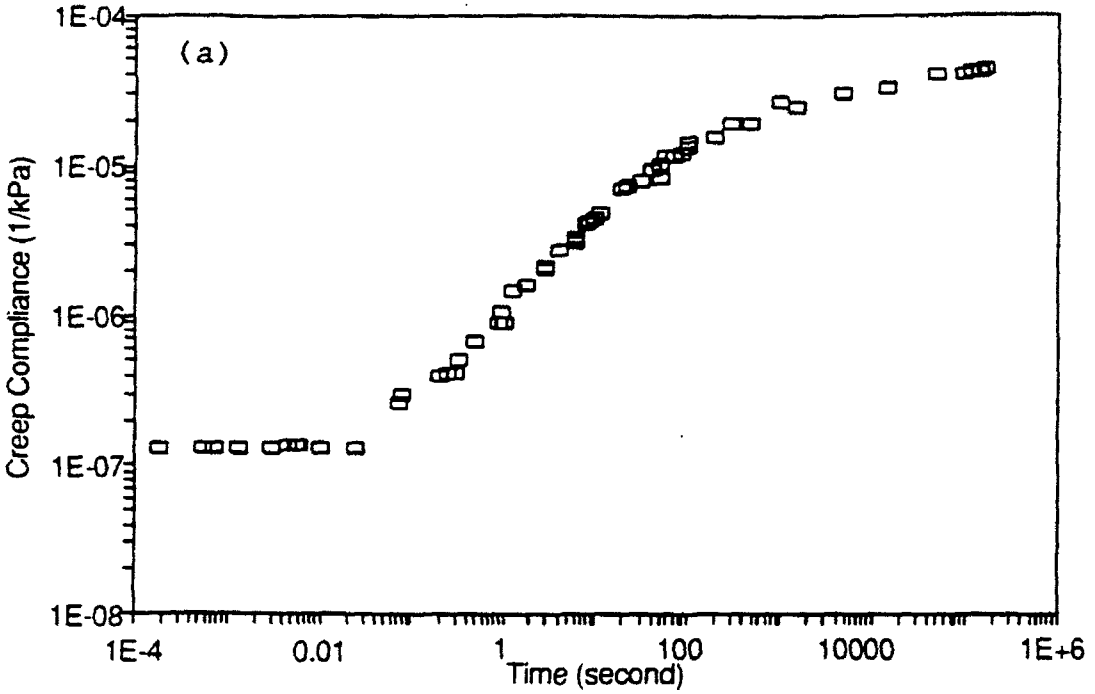

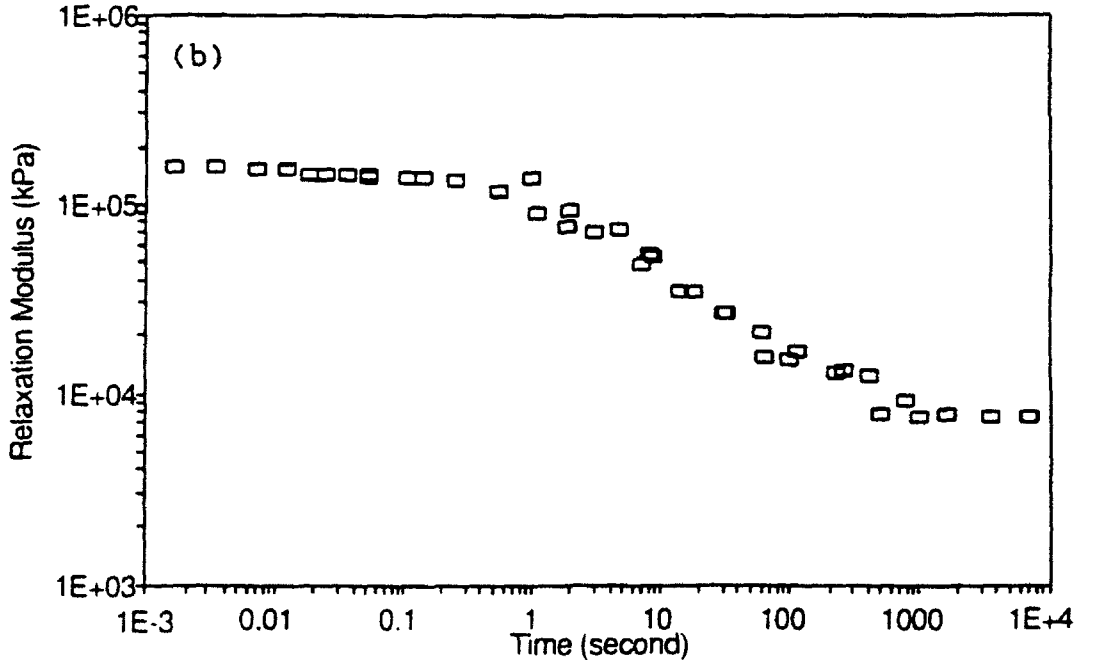

Fig. 5 Master curves: (a) Creep compliance and (b) Relaxation modulus.

$$\log a_T = \log \frac{t_T}{t_{T_0}}$$

where a_T = shift factor that is dependent on the difference between the reference temperature (T_0) and data temperature (T), and

t_T, t_{T0} = time required to reach a specific modulus value at temperatures T and T_0, respectively.

The shift factors for the relaxation modulus and creep compliance are plotted as a function of temperature in Fig. 6. The shift factors allow to express the relaxation modulus or creep compliance in terms of a single argument, ξ, where:

$$\xi = \frac{t}{a_T}$$

The variable ξ reflects both time and temperature dependence and is often called "reduced time" in the polymer literature and "temperature compensated time" in the metals literature.

This "thermorheologically simple" behavior with the definition of pseudo strain may allow to predict the linear viscoelastic stress-strain behavior of asphalt concrete at various temperatures from the stress-strain relationship at a reference temperature.

2. Uniaxial Constant-Strain-Rate Monotonic Testing

The concept of the correspondence principle was applied to uniaxial compressive constant-strain-rate monotonic tests with varying strain rates. Five different strain rates of 11.97, 11.13, 6.10, 3.19, and 1.61 mm/min. (0.4712, 0.4382, 0.2403,

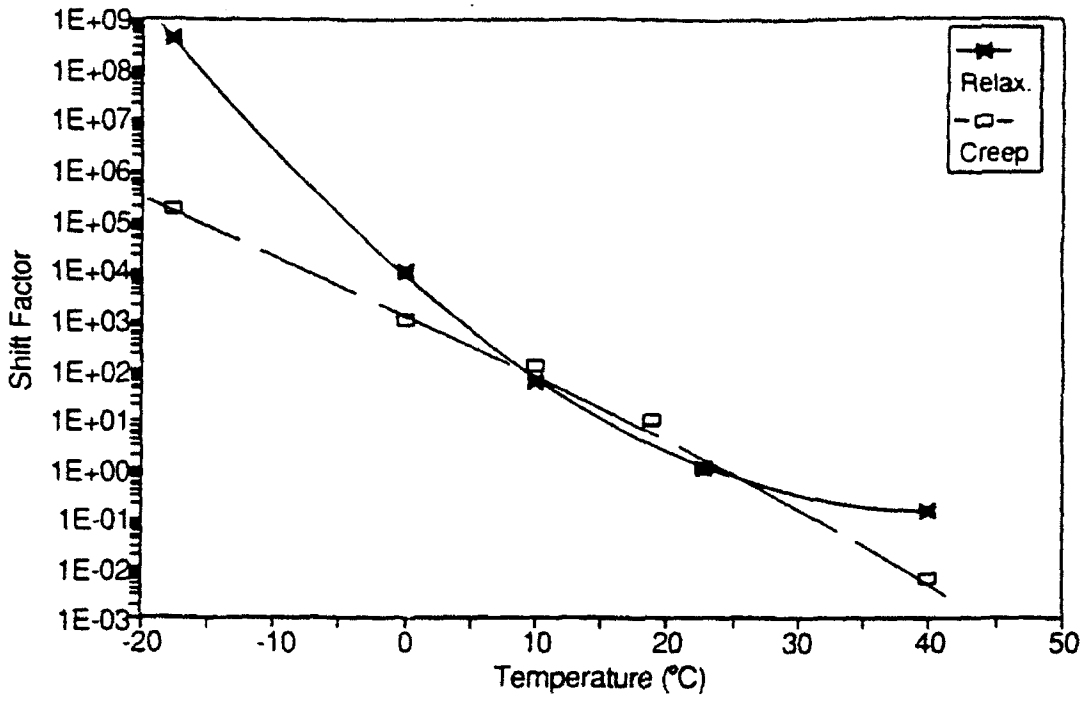

Fig. 6 Time-temperature shift factors for creep compliance and relaxation modulus (Reference temperature of 25°C).

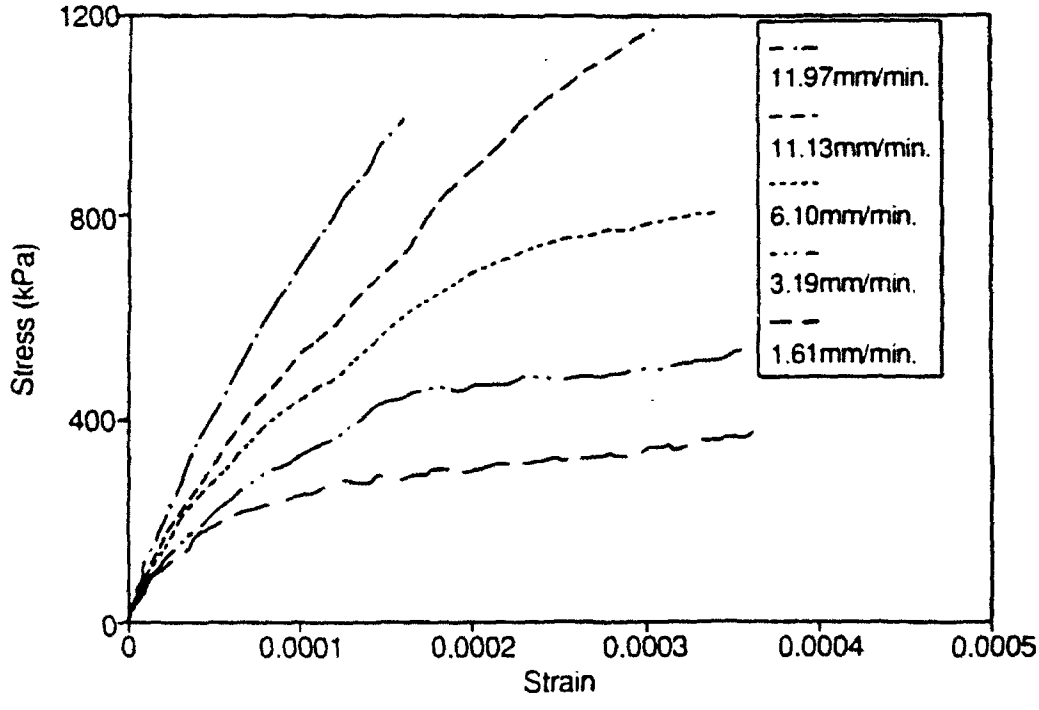

Fig. 7 Rate dependent stress-strain curves from uniaxial compressive constant-strain-rate monotonic testing.

0.1256, and 0.0632 in./min.) were used. All the five tests were performed on the same specimen with a 40-minute rest period between the individual tests. To ensure that the specimen was not damaged during the tests, the strain level was set up not to exceed 0.0375%. Fig. 7 shows the rate-dependent stress-strain behavior of asphalt concrete. As expected, the faster the rate, the higher the stiffness.

Pseudo strains were calculated from the predicted relaxation modulus and the first derivative of strain input, and the same data were plotted in terms of stress and pseudo strain in Fig. 8(a). The rate-dependency was eliminated therefore validating the applicability of the correspondence principle to the analysis of densely-graded asphalt concrete.

For linear viscoelastic media, either pseudo stress or pseudo strain can be used in the analysis without any difference because the boundary conditions do not change. To confirm this behavior, pseudo stresses were determined using the creep compliance and the first derivative of stress response and plotted against the strain in Fig. 8(b). Again, the curves from five strain rates were superimposed fairly well, and the linear behavior was observed between pseudo stress and strain.

The stress-strain data presented in Fig. 7 can be also used in predicting the time exponent of relaxation modulus (Kim 1988). This can be accomplished by constructing the isochronal curve at the reference time (t = 0.3 sec.) as in Fig. 9(a) and then shifting other curves horizontally to the reference curve. The shift factor was plotted against the time on a logarithmic scale

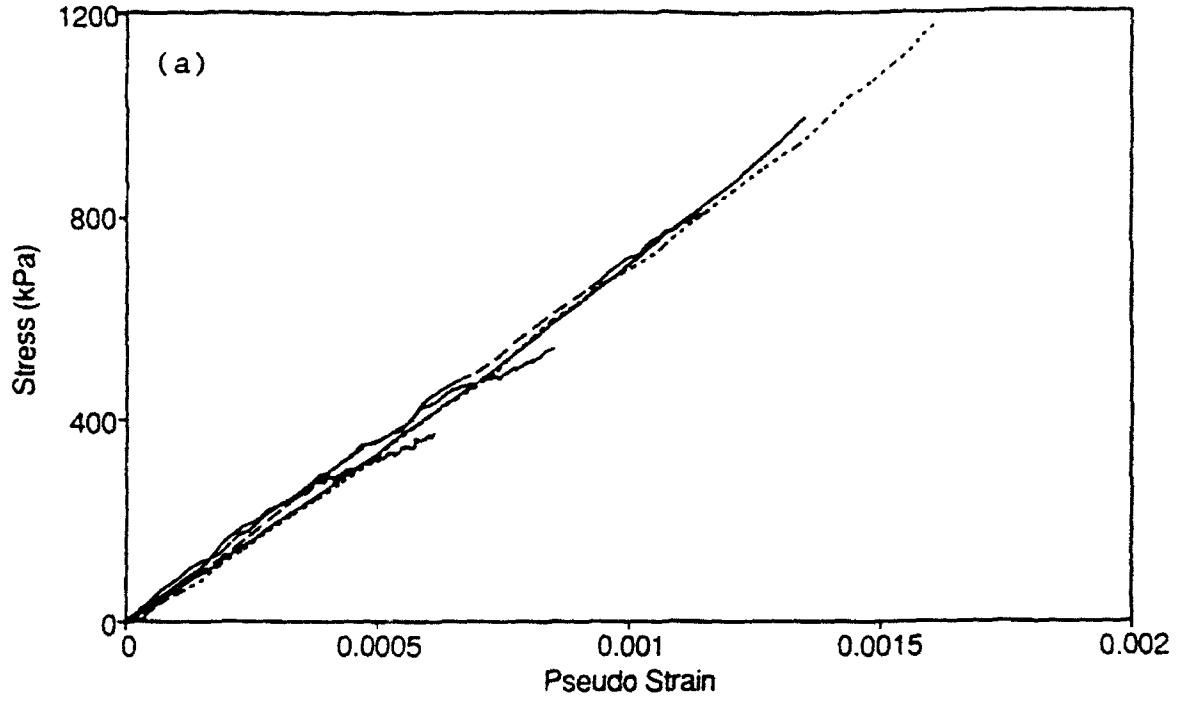

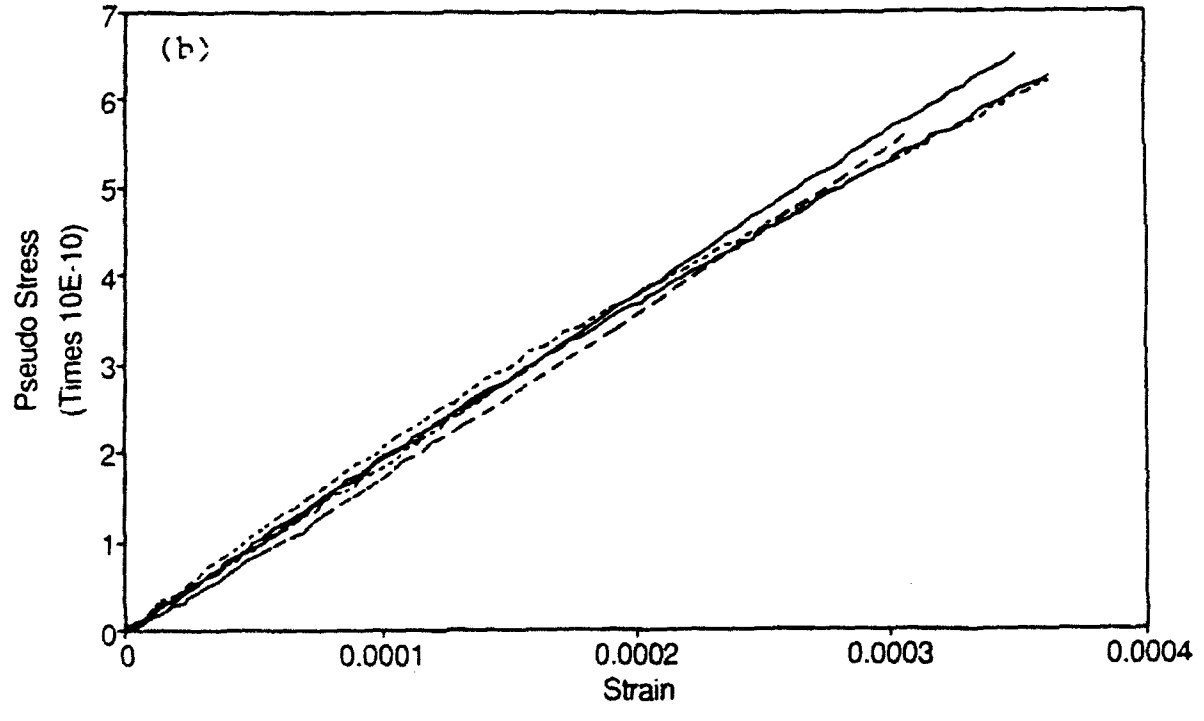

Fig. 8 Application of the elastic-viscoelastic correspondence principle through: (a) Pseudo strain and (b) Pseudo stress.

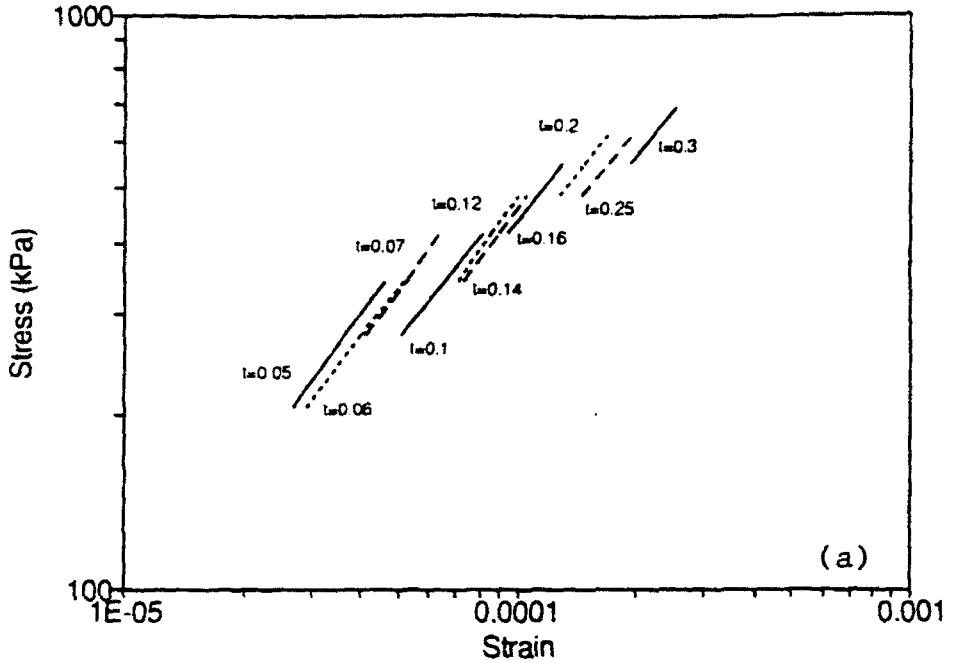

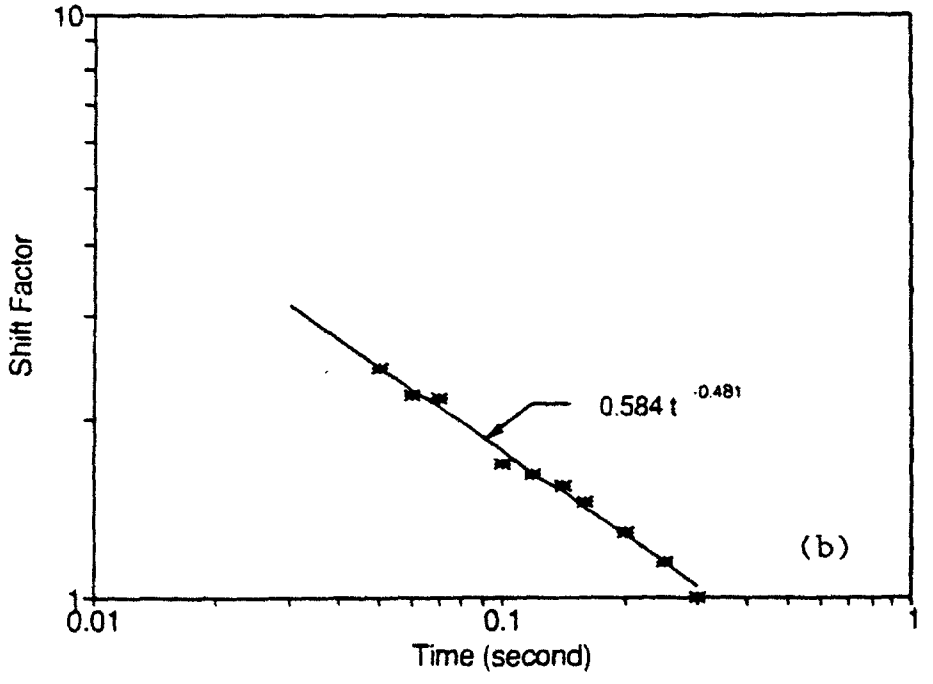

Fig. 9 (a) Isochronal curves from the constant-strain-rate monotonic testing and (b) Shift factor versus time.

in Fig. 9(b). The regression analysis between the shift factor and the time resulted in the exponent of -0.481 which happens to be exactly the same as the exponent from the predicted relaxation modulus.

3. Uniaxial Controlled-Stress Repetitive Testing

In an attempt to validate the applicability of the correspondence principle to cyclic loading conditions, uniaxial compressive cyclic testing was conducted on cylindrical specimens. Three load amplitudes were used to investigate the effect of damage growth on the hysteresis loops. The cyclic stress-strain behavior of asphalt concrete with loading amplitude of 0.556 kN (125 lbs) was presented in Fig. 10(a) at selected cycles.

In Fig. 10(b), stresses were plotted against pseudo strains that were calculated using the predicted relaxation modulus. The use of pseudo strain eliminated the change in the hysteresis loops at different cycles but was not able to account for the loading-unloading effect. Furthermore, in Fig. 10(b), the unloading paths were positioned higher than the loading paths. There are two possible explanations on these unexpected results. The first is that the time exponents in the creep compliance and relaxation modulus over-corrected the time-dependency of the material. Second reason is that the interlocking mechanisms between aggregate particles may have caused different time-dependent behaviors during loading and unloading periods. This difference can not be measured in the creep or relaxation tests

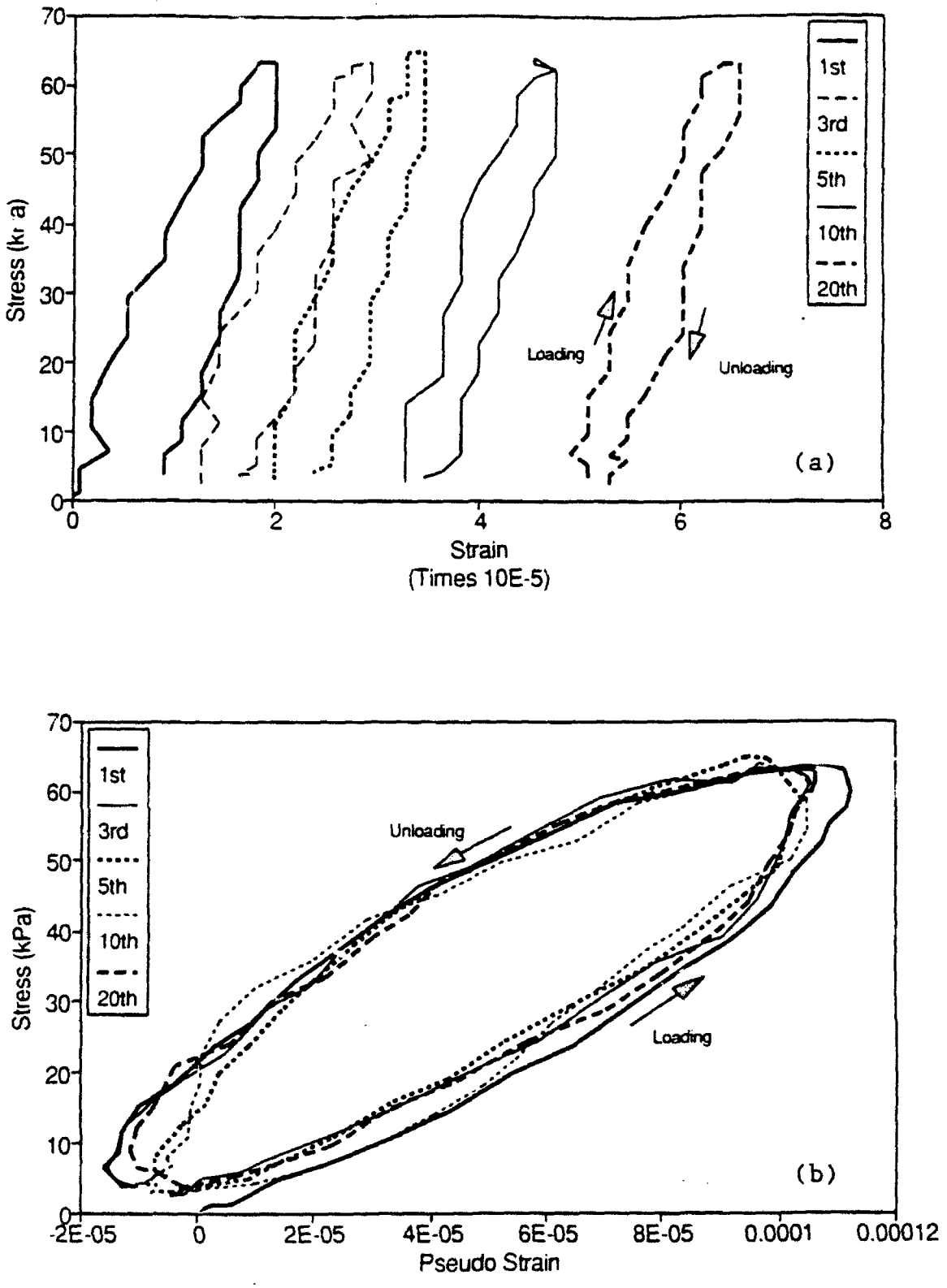

Fig. 10 Uniaxial controlled-stress cyclic test results with load amplitude of 0.556 kN (negligible damage): (a) Stress-strain and (b) Stress-pseudo strain.

because the unloading data are not utilized in determining the creep compliance or relaxation modulus. Further testing and analysis are recommended to identify the reason contributing to the reversed hysteresis loops in the stress-pseudo strain diagram.

The same approach was employed to investigate the applicability of the correspondence principle to accounting for the effect of rest period. Figs. 11(a) and 11(b) present the hysteresis loops before and after a rest period of 8 seconds. The use of pseudo strain successfully accounts for the change in strain due to the relaxation during the rest period. Different lengths of rest periods were applied after cyclic loading and yielded the same conclusion.

The loading amplitude was raised to 1.112 kN (250 lbs), and the same testing and analysis were performed (Figs. 12 and 13). It is noted here that the load amplitude of 1.112 kN (250 lbs) in the creep tests resulted in the same creep curve as the curve from 0.556 kN (125 lbs) loading amplitude (Fig. 2(a)) meaning that the load amplitude of 1.112 kN (250 lbs) in the creep loading condition did not induce significant damage to the specimen. However, as can be seen from Fig. 12(b), cyclic loading of 1.112 kN (250 lbs) resulted in shift of stress-pseudo strain loops implying some damage growth in the sample as cyclic loading continues. This observation draws a conclusion that cyclic loading induces more damage than a dead load does even with the same load amplitude.

The effect of rest period on a damaged specimen was also

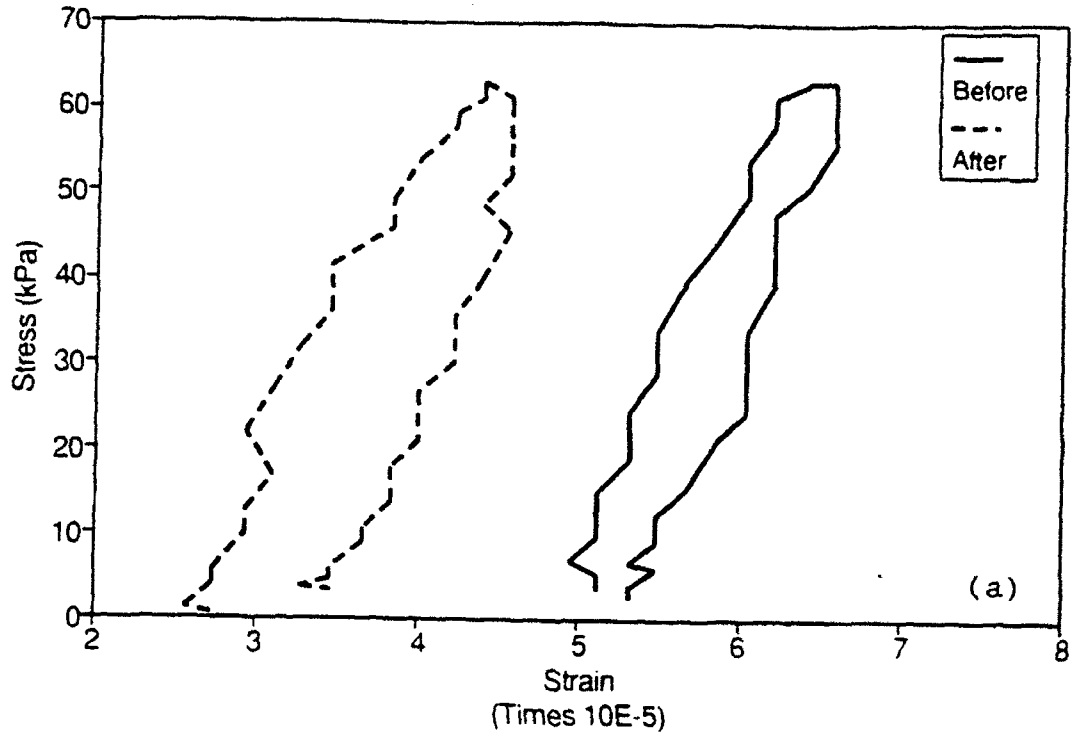

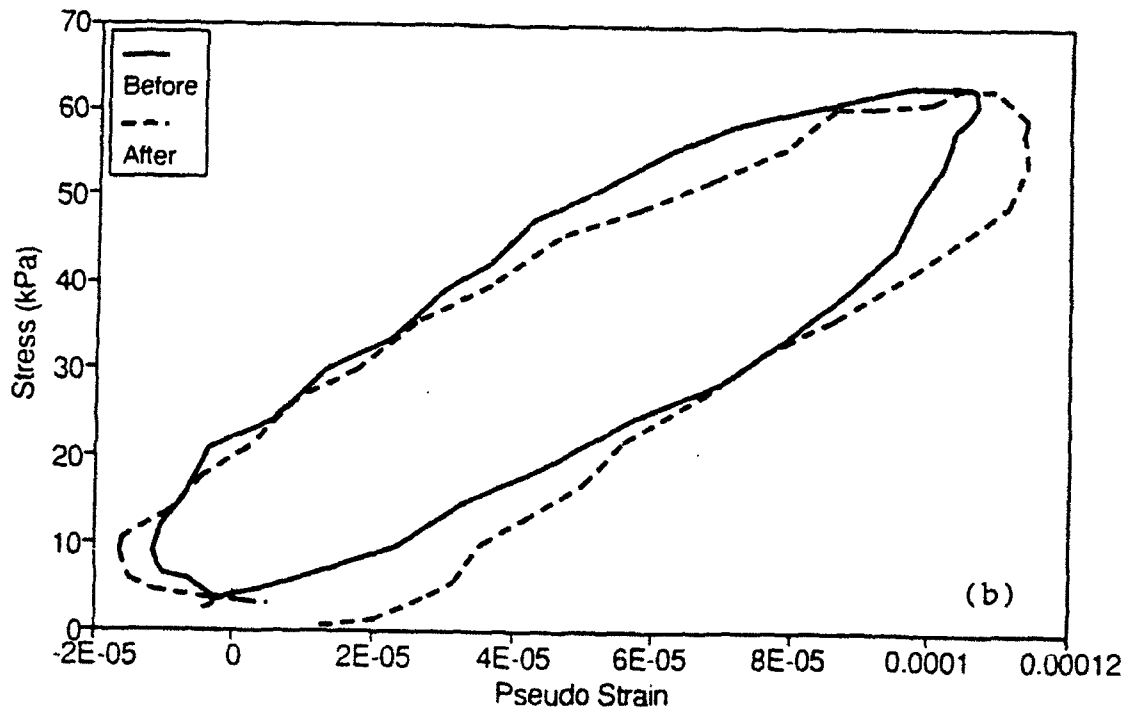

Fig. 11 Uniaxial controlled-stress cyclic test results before and after a 8-sec. rest period with load amplitude of 0.556 kN: (a) Stress-strain and (b) Stress-pseudo strain.

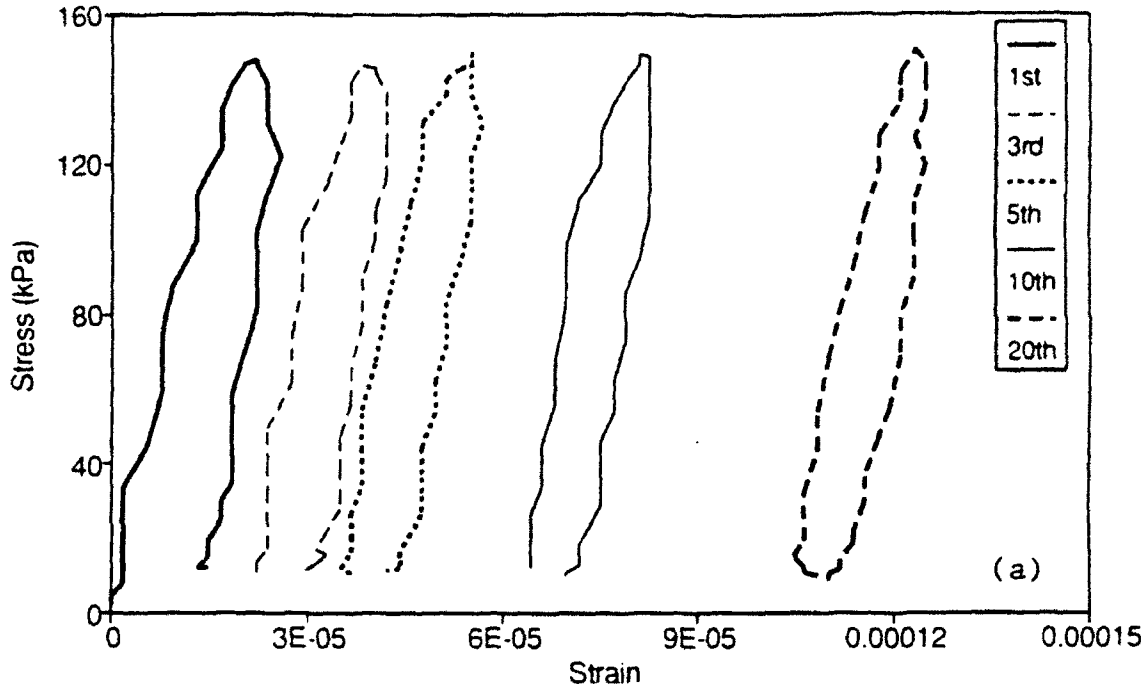

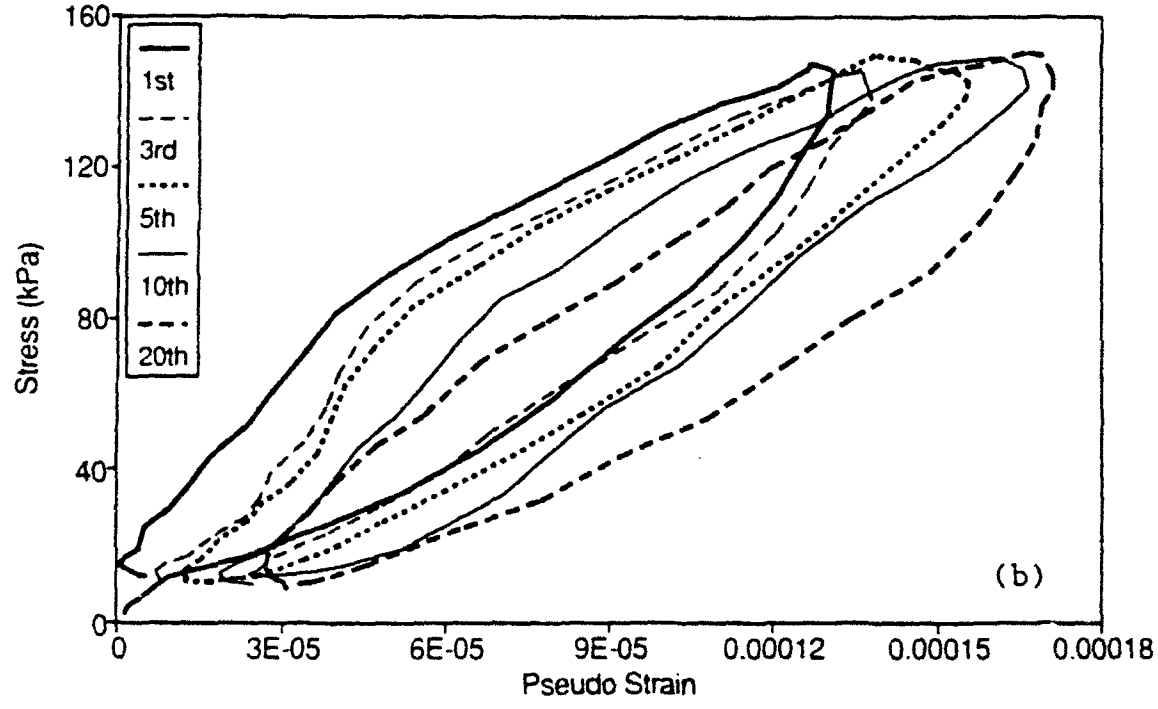

Fig. 12 Uniaxial controlled-stress cyclic test results with load amplitude of 1.112 kN (some damage growth): (a) Stress-strain and (b) Stress-pseudo strain.

investigated using the pseudo strain (Figs. 13(a) and 13(b)). Again, a different stress-pseudo strain behavior was observed in Fig. 13(b) compared to the behavior in Fig. 11(b) with negligible damage. The stress-pseudo strain curve after the rest period was positioned on the left side of the curve before the rest period. Since the beneficial effect of the time-dependent relaxation phenomenon has been accounted for by the use of the pseudo strain, the recovery observed in the stress-pseudo strain curve in Fig. 13(b) must be due to the fracture healing in micro-cracks.

Finally the load amplitude was increased to 11.12 kN (2500 lbs) with an expectation of severe damage growth (Figs. 14 and 15). The same conclusions were made as with 1.112 kN (250 lbs) except that the stress-pseudo strain curve is shifted further as cycle continues and that the stress and pseudo strain values are much higher than from the case of 1.112 kN (250 lbs).

CONCLUSIONS

With the given mixture tested in this study, it is clear that both the elastic-viscoelastic and time-temperature correspondence principles can be effectively applied to testing and analysis of asphalt concrete under the representative conditions of the in-service pavements. The use of pseudo strain eliminated the change in the hysteresis loops at different cycles although the effect of loading and unloading could not be accounted for. Additional testing and analysis are recommended to investigate the difference in the time-dependent behaviors

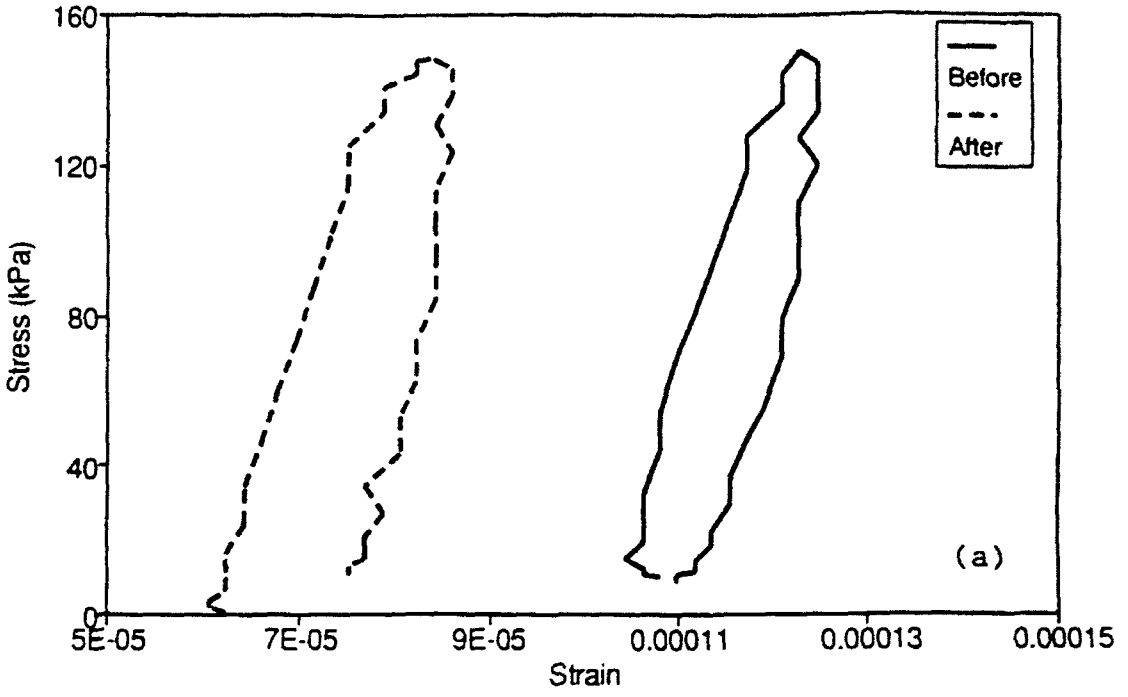

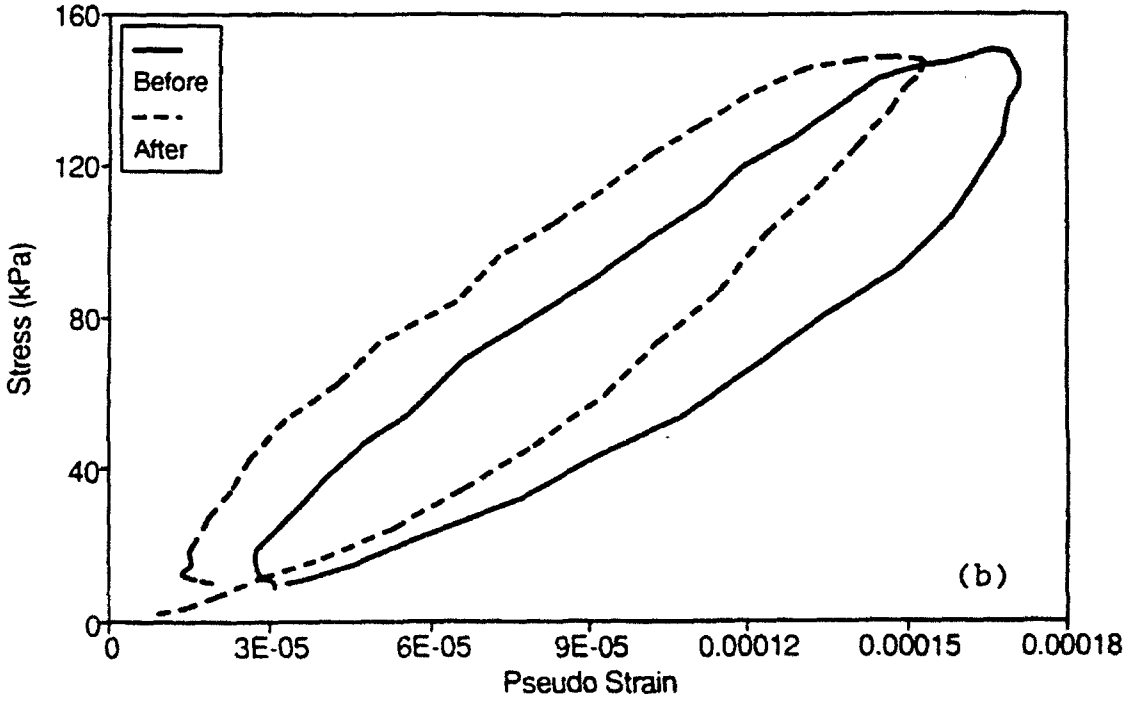

Fig. 13 Uniaxial controlled-stress cyclic test results before and after a 8-sec. rest period with load amplitude of 1.112 kN: (a) Stress-strain and (b) Stress-pseudo strain.

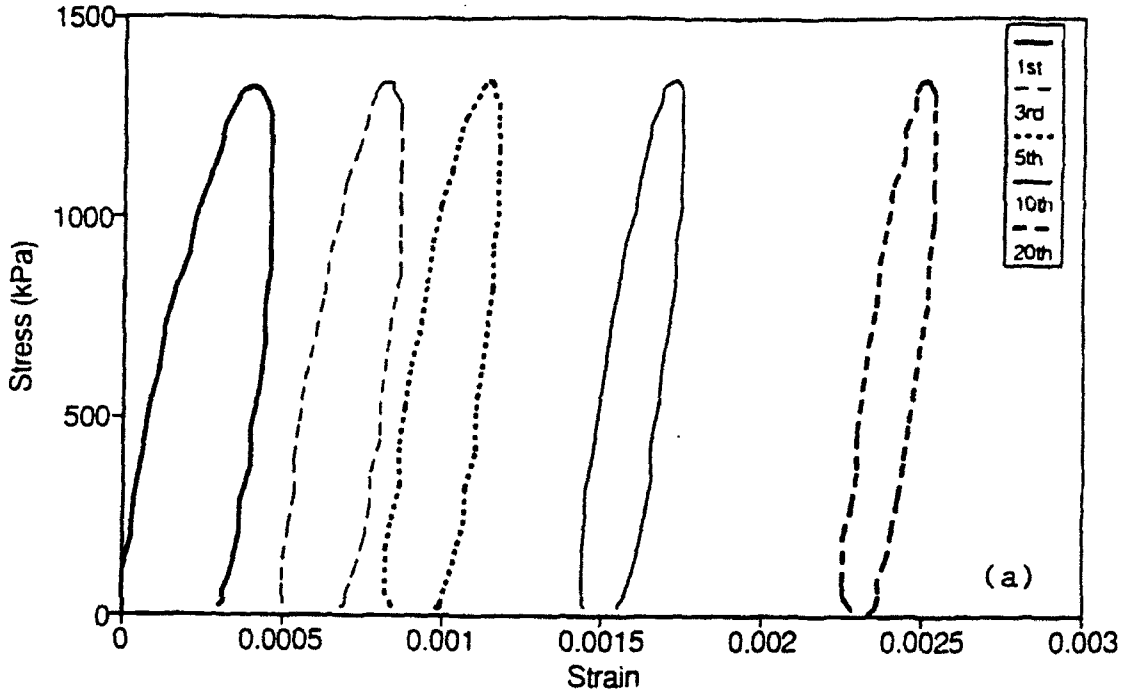

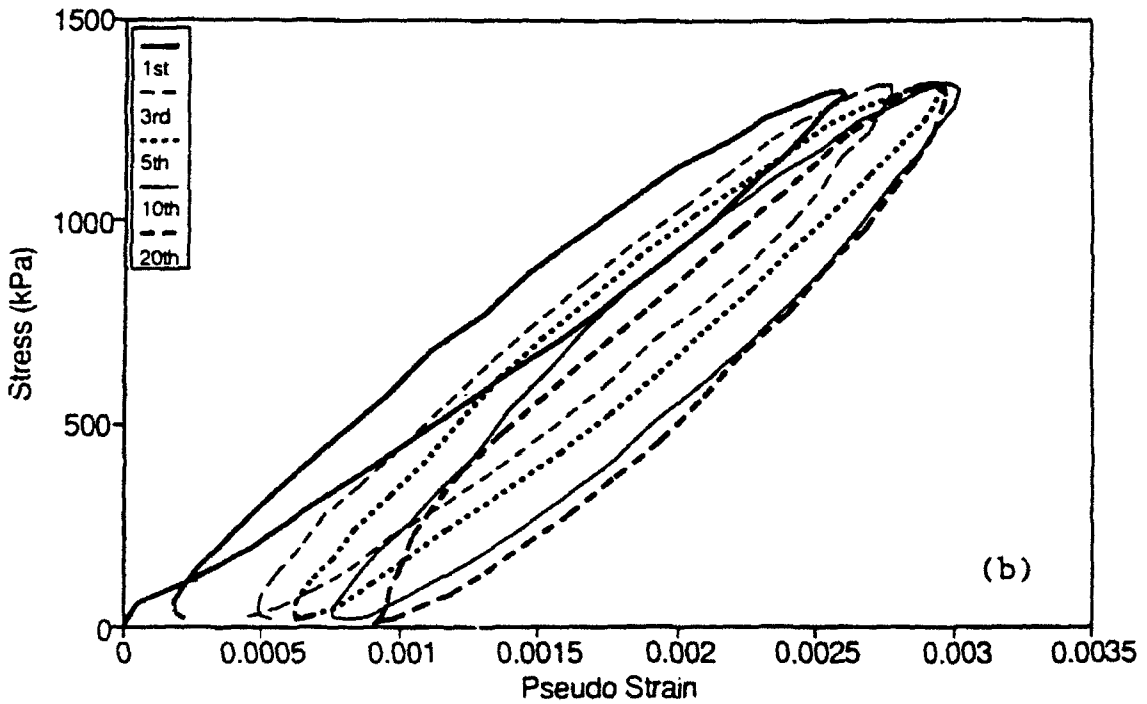

Fig. 14 Uniaxial controlled-stress cyclic test results with load amplitude of 11.12 kN (significant damage growth): (a) Stress-strain and (b) Stress-pseudo strain.

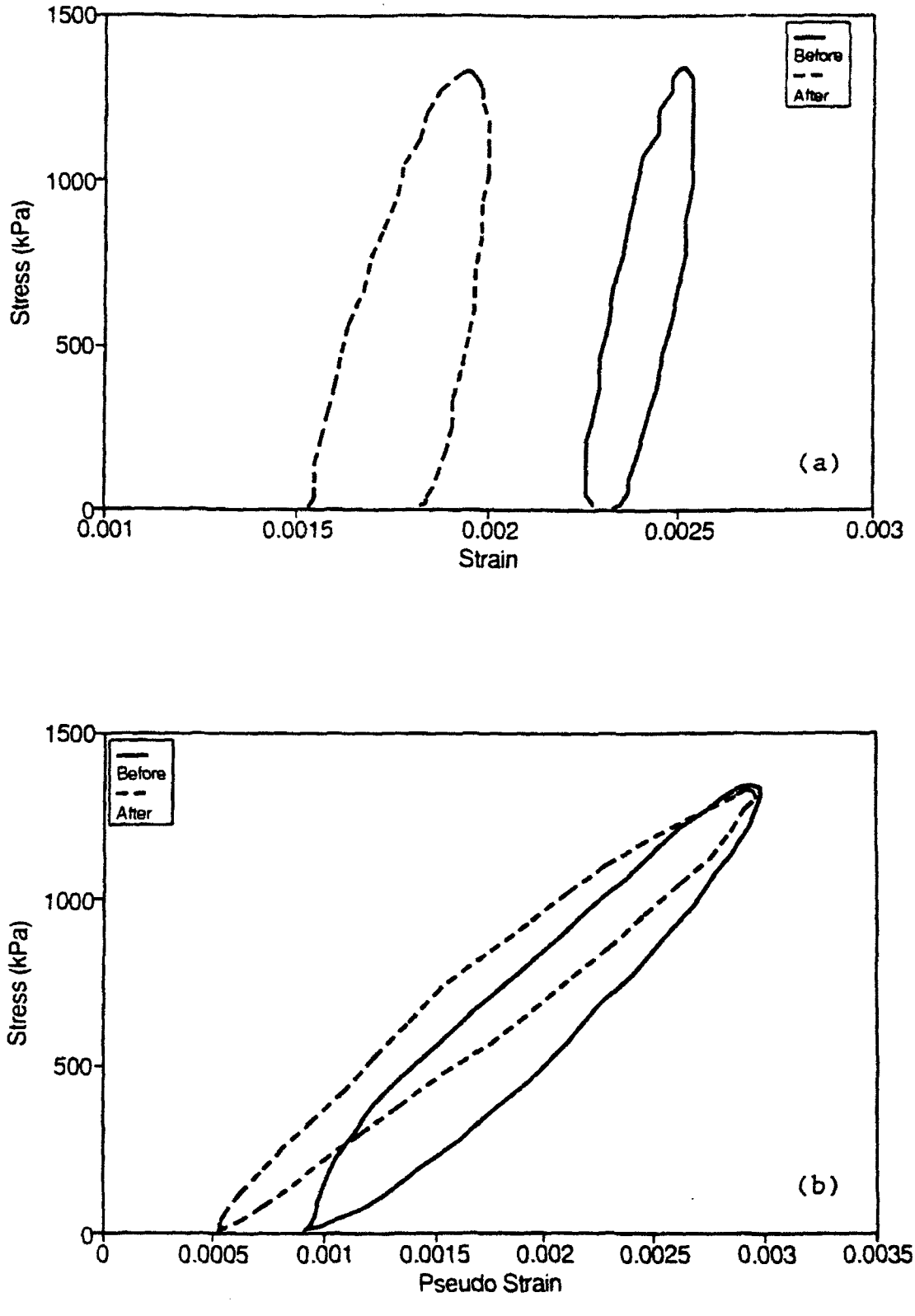

Fig. 15 Uniaxial controlled-stress cyclic test results before and after a 8-sec. rest period with load amplitude of 11.12 kN: (a) Stress-strain and (b) Stress-pseudo strain.

during loading and unloading periods due to the aggregate interlocking mechanism.

When the cyclic load level was low enough not to induce significant damage, the effect of rest period on the hysteretic behavior of asphalt mixture has been successfully eliminated using the pseudo strain. Also the stress-pseudo strain diagrams before and after rest periods at high load levels revealed that an additional beneficial phenomenon occurs during the rest periods which was concluded to be fracture healing of microcracks in asphalt mixtures.

REFERENCES

Dawley, C.B., B.L. Hogeweide, and K.O. Anderson (1990). "Mitigation of Instability Rutting of Asphalt Concrete Pavements in Lethbridge, Alberta, Canada." Proceedings, Association of Asphalt Paving Technologists, Vol. 59.

Harvey, J., Sousa, J.B., Deacon, J.A., and Monismith, C.L., "Effect of Sample Preparation and Air-void Measurement on Asphalt Concrete Properties," To be published in Transportation Research Record, Transportation Research Board, 1992.

Kim, Y.R. (1988). "Evaluation of Healing and Constitutive Modeling of Asphalt Concrete by Means of the Theory of Nonlinear Viscoelasticity and Damage Mechanics." Ph.D. Dissertation, Texas A&M University, College Station, Texas.

Kim, Y.R. and D.N. Little (1989). "Evaluation of Healing in Asphalt Concrete by Means of the Theory of Nonlinear Viscoelasticity." Transportation Research Record No. 1228, Transportation Research Board, pp. 198-210.

Kim, Y.R. and D.N. Little (1990). "One-Dimensional Constitutive Modeling of Asphalt Concrete." ASCE Journal of Engineering Mechanics, Vol. 116, No. 4.

Kim, Y.R., D.N. Little, and F.C. Benson (1990). "Chemical and Mechanical Evaluation on Healing Mechanism of Asphalt Concrete." Proceedings of Association of Asphalt Paving Technologists, Vol. 59, pp. 240-275.

Schapery, R. A. (1984). "Correspondence principles and a generalized J-integral for large deformation and fracture analysis of viscoelastic media." International Journal of Fracture, 25, 195-223.